



THÈSE

Présentée par

Melle KERMA S Nawel

**Pour l'obtention du diplôme de
DOCTORAT LMD en Technologie de la communication**

Filière : Télécommunication

Spécialité : Traitement du signal et télécommunication

THEME

Étude par simulation de l'amélioration des performances des transistors HEMT pour des applications en haute fréquences

Soutenu publiquement, le 25/06/2018 devant le jury composé de :

N°	Nom et prénom	Qualité	Grade	Etablissement
1	BENALLOU Yacine	Président	MCA	Université Dr. Tahar Moulay de Saida
2	DJELLOULI Bouaza	Rapporteur	Prof.	Université Dr. Tahar Moulay de Saida
3	ABID Hamza	Examineur	Prof.	Université Djillali Liabes, Sidi Belabbes
4	SOUDINI Belabbes	Examineur	Prof.	Université Djillali Liabes, Sidi Belabbes
5	ARBOUCHE Omar	Examineur	MCA	Université Dr. Tahar Moulay de Saida

Année Universitaire 2017-2018

Thèse préparée au Laboratoire de Modélisation et des Méthodes de Calcul – Université de Saida



THESIS

Presented by

Miss KERMAW Nawel

For obtain the degree of

DOCTOR in communications technology

Field: Telecommunication

Specialty: Signal treatment and telecommunication

TITLE

**Simulation study of the improvement of HEMT performance
for high frequency applications**

The jury members :

N°	Surname & name	Grad	Establishment
1	BENALLOU Yacine	MCA	University Dr. Tahar Moulay of Saida
2	DJELLOULI Bouaza	Prof.	University Dr. Tahar Moulay of Saida
3	ABID Hamza	Prof.	University Djillali Liabes, Sidi Belabbes
4	SOUDINI Belabbes	Prof.	University Djillali Liabes, Sidi Belabbes
5	ARBOUCHE Omar	MCA	University Dr. Tahar Moulay of Saida

Academic year : 2017-2018

Dedication

To my parents ...

Table of contents



Table of contents

Acknowledgements	i
Publications & Communications	iii
List of Figures	vi
List of Tables	xii
General introduction	01
Chapter I State-of-the-art of gallium-nitride technology and its promise for the future	04
I.1 Introduction.....	04
I.2 State-of-the-art of GaN-HEMTs in power electronics.....	07
I.3 State-of-the-art of GaN-HEMTs in RF-electronics.....	11
I.4 Challenges and future of scaling GaN technology.....	15
I.5 Motivations and contributions of this thesis.....	17
References.....	17
Chapter II AlGaN /GaN High Electron Mobility Transistors (HEMTs)	22
II.1 Introduction.....	22
II.2 Basic properties of GaN.....	22
II.2.1 Crystal structure.....	22
II.2.2 Electronic band structure.....	24

II.2.3	The III-nitride alloys.....	24
II.2.4	$\text{Al}_x\text{Ga}_{1-x}\text{N}/\text{GaN}$ heterostructure.....	26
II.3	Two Dimensional Electron Gas (2 DEG).....	27
II.3.1	Spontaneous polarization.....	28
II.3.2	Piezoelectric polarization.....	30
II.4	High Electron Mobility Transistors (HEMTs).....	32
II.4.1	Background.....	32
II.4.2	$\text{Al}_x\text{Ga}_{1-x}\text{N}/\text{GaN}$ HEMTs structure.....	34
II.4.3	Growth techniques and substrates choice	37
II.5	HEMTs operation.....	40
II.5.1	DC characteristics.....	41
II.5.2	Degradation of HEMT performance.....	43
II.5.3	Breakdown mechanisms.....	44
II.6	Summary.....	48
	References.....	49

Chapter III An analytical physics-based compact modeling of I–V and C–V characteristics in $\text{Al}_x\text{Ga}_{1-x}\text{N}/\text{GaN}$ HEMTs

III.1	Introduction.....	57
III.2	Physics-based device-models.....	58
III.2.1	Overview of compact models.....	58
III.2.2	Physics-based compact models	59
III.2.3	Fundamentals for physics-based compact models	63

III.2.4	Models development	66
III.3	Mole fraction effect	77
III.4	Drain-source current model.....	79
III.4.1	Derivative of the drain-source current.....	81
III.4.2	Self-heating effects and temperature dependencies.....	83
III.5	Analytical gate charge and capacitances model.....	84
III.5.1	Gate charge model	84
III.5.2	Gate capacitance models.....	85
III.5.3	Cut-off frequency f_T	87
III.6	Summary.....	88
	References.....	89

Chapter IV	Simulation results and discussion	94
IV.1	Introduction.....	94
IV.2	Silvaco simulation software.....	95
IV.2.1	Overview.....	95
IV.2.2	Silvaco semiconductor modeling equations	97
IV.3	Model definition.....	97
IV.4	AlGaIn/GaN HEMTs structure.....	97
IV.5	Mole fraction, gate length and self-heating effects.....	100
IV.5.1	Mole fraction effect.....	100
IV.5.2	Gate length effect.....	107

IV.5.3 Self-heating effect.....	111
IV.6 Summary.....	112
References.....	113
 V Conclusion and future work prospects	 114
V.1 General Conclusion	114
V.2 Future work prospects.....	115
 VI Appendix	 116
A Unified charge density model derivation.....	116
B ATLAS model for simulation.....	120
C Abbreviation.....	123
D Physical constants.....	124
E Symbols.....	125

Acknowledgements



Acknowledgements

Above all, I am thankful to Allah for giving me strength and will power to carry out this research.

First and foremost, I would like to express my sincere gratitude to my supervisor Mr. DJELLOULI Bouaza (Professor at University Dr. Moulay Tahar of Saida, Department of Electronics, Laboratory of Modelization and Calculation Methods, Saida), for giving me the benefit of his scientific knowledge and the opportunity to realize this work, for his time and patience it has given me and for accepting to judge this work as supervisor. He has treated me like his daughter and encouraged me in difficult research and also private situations. He was the best supervisor I could have.

I would like to express my sincere thanks to Dr. BENALLOU Yacine from University Dr. Moulay Tahar of Saida, who did me the honor of accepting to chair my thesis committee.

My respectful acknowledgments are also addressed to Mr. ABID Hamza and Mr. SOUDINI Belabbès (Professors at University of Sidi-Bel-Abbès), to have accepted to examine my work of this thesis.

My sincere thanks to Dr. ARBOUCHE Omar from University Dr. Moulay Tahar of Saida, who agreed to examine this work by taking part in my thesis committee.

I am also very grateful to all the members of my examination committee for realizing a thorough revision of the manuscript and providing me with important insights and remarks that improved the contents and quality of this final manuscript.

The work done in this thesis was carried out within both teams of Laboratory of Modelization and Calculation Methods, Department of Electronic, University of Saida & Laboratory of Materials, Applications and Environment, Faculty of Science and Technology, University Mustapha Stambouli of Mascara in collaboration with Research Group in Semiconductor Device Modeling and Simulation Consulting, Department of Electronic, Electrical and Automatic Control Engineering (DEEEIA) of the University Rovira I Virgili (URV), Tarragona, Catalonia, Spain.

I would like to express my thanks to all the people who supported me in realizing this dissertation. My special thanks go to:

- ☑ Dr. BOUGUENNA Driss from University Mustapha Stambouli of Mascara who provided assistance during my research and for many interesting scientific discussions. He taught me to approach problems keeping a clear head.
- ☑ Prof. BENJAMIN Iñiguez from URV, for hosting me in successive courses in his team research laboratory, as well for his good advice during all my stays at URV.
- ☑ The researchers of the teams: LPQ3M at the University Mustapha Stambouli of Mascara, LTC at the Dr. Moulay Tahar of Saida and to all my friends Miss. Adriana Degeanu, Miss. Oana Moldovan, Mr. Wondwosen Eshetu and Mr. Harould Cortes Ordonez PhD students from URV.

Finally, a special thanks to my parents and all my family for their unconditional love to me, for supporting me and for giving me guidance throughout my career. I wouldn't be who I am today if not for you.

Thank you so much everyone!!!

Miss Nawel KERMAS

Publications & Communications



Publications & Communications

Publications

1. Nawel Kermas, Bouaza Djellouli, Driss Bouguenna, Wondwosen Eshetu, and Benjamin Iñiguez, "Compact mole-fraction dependent modeling of I - V and C - V characteristics in $\text{Al}_x\text{Ga}_{1-x}\text{N}/\text{GaN}$ HEMTs", *J Comput Electron*, vol. **17**, n°.1, pp. 224–229, March 2018.
2. D. Bouguenna, T. Wecker, D. J. As, N. Kermas, A. Beloufa, "Numerical analysis of transmission coefficient, LDOS, and DOS in superlattice nanostructures of cubic $\text{Al}_x\text{Ga}_{1-x}\text{N}/\text{GaN}$ resonant tunneling MODFETs", *J Comput Electron*, vol. **15**, n°.4, pp.1269–1274, December 2016.
3. A. Douara, N. Kermas, B. Djellouli, "Capacitance models of AlGa N/GaN High Electron Mobility Transistors", *International Journal of Electrical, Computer, Energetic, Electronic and Communication Engineering*, vol. **111**, n°.3, pp.420-423, March 2016.
4. D. Bouguenna, N. Kermas, B. Djellouli, "High performance of cubic $\text{Al}_x\text{Ga}_{1-x}\text{N}/\text{GaN}$ Double Gate MOS-HEMTs", *IRJET*, vol. **2**, n°. 9, pp. 2072-2077, December 2015.

Communications

1. **N. Kermas**, D. Bouguenna, B. Djellouli and B. Iñiguez, “A Physics-Based Analytical model of Double Heterojunction AlGa_N/Ga_N HEMTs of *I-V* and *C-V* characteristics”, *POGP, Mascara*, 6 May 2018.
2. **N. Kermas**, D. Bouguenna, B. Djellouli and B. Iñiguez, “A Physics-Based Analytical model for two dimensional electron gas density (2DEG) in AlGa_N/Ga_N HEMTs”, *JPUMI, Mascara*, 2 May 2018.
3. **N. Kermas**, D. Bouguenna, B. Djellouli, A. Beloufa and B. Iñiguez, “Analysis modeling of threshold voltage and *I-V* characteristics of Double Channel AlGa_N/Ga_N HEMTs with polarization effects”, *DSDM, Mascara*, 25 April 2018.
4. D. Bouguenna, **N. Kermas**, B. Djellouli, A. Beloufa and B. Iñiguez, “ A physics-based compact model developed for *I-V* characteristics of AlGa_N/Al_N/Ga_N High Electron Mobility Transistors”, *DSDM, Mascara*, 25 April 2018.
5. B. Iñiguez, **N. Kermas** and W. Eshetu, “Physically-based compact modeling of *I-V* and *C-V* characteristics in AlGa_N/Ga_N HEMT”, *41st Workshop on Compound Semiconductor Devices and Integrated Circuit*, Las Palmas de Gran Canaria, Spain, pp. 77, 22 May 2017.
6. **N. Kermas**, D. Bouguenna, B. Djellouli, "Numerical analysis of *I-V* characteristics of Al_xGa_{1-x}N/Ga_N nanostructures HEMTs", Batena, Algeria, 02 Oct 2016.

7. **N. Kermas**, B. Djellouli, D. Bouguenna, "Study and Performance analysis of Electrical Characteristics of $\text{Al}_x\text{Ga}_{1-x}\text{N}/\text{GaN}$ High Electron Mobility Transistors HEMTs", *International Conference on Mechanics and Aeronautics*, Blida, Algeria, 19 Oct 2016.
8. **N. Kermas**, B. Djellouli, D. Bouguenna, " Simulation des caractéristiques I - V des transistors HEMTs à base de nanostructures de Nitrures III-V $\text{Al}_x\text{Ga}_{1-x}\text{N}/\text{GaN}$ ", *CIMA*, Blida, Algeria, 19 October 2016.
9. **N. Kermas**, B. Djellouli, D. Bouguenna, "Etude des Transistors à Effet de Champ Double Grille MOS-HEMTs à Base de Nanostructures de Nitrures III-V $\text{AlGaIn}/\text{GaIn}$ en phase cubique, Saida, Algeria, 19 April 2016.
10. **N. Kermas**, A. Douara, B. Djellouli, D. Bouguenna, "Study of the effect of the mole fraction of the ternary alloy $\text{Al}_x\text{Ga}_{1-x}\text{N}$ on the characteristics of Double Gate MOS-MODFET", *JEFE*, Annaba, Algeria, 27 May 2015

List of Figures



List of Figures

Figure I.1	Time evolution of GaN research, a patent family is set of patents filed in multiple countries by a common inventor(s) to protect a single invention, while a patent document is a patent filed in one country (1 st application or extensions).....	05
Figure I.2	The important loss components for a 12 V – 1.2 V buck converter operating at 1 MHz converter showing significantly lower switching loss due to lower gate charge in GaN switch (circuit board from EPC).....	08
Figure I.3	The theoretical BV and R_{dson} plots for GaN, Si and SiC showing improved characteristics of GaN compared to other technologies.....	09
Figure I.4	The number of patents families for industrials and non-profit organizations, 2010- 2015.....	09
Figure I.5	An overview on qualification status and a detailed packaging roadmap for power GaN.....	10
Figure I.6	(a) Comparison of power MOSFET in package with eGaN-FETs from EPC showing the size difference for the same device-metrics [9] and (b) the LMG5200- 10 A, 8 V GaN half-bridge power module with integrated driver from TI which satisfies the JEDEC standards demonstrating the arrival of GaN-HEMTs in the power market.....	11
Figure I.7	Comparison of RF-performance metrics among different technologies.....	12

Figure I.8	State-of-the-art demonstrations of GaN-HEMTs against of its competitors showing P_{max} vs f metric. GaN enables possibilities for both high-power and high-frequency.....	13
Figure I.9	(a) Triquint's TGS2354 GaN-on-SiC switch die compared against their GaAs-MMIC, (b) MACOM's MAGE-102425-300 GaN, Frequencies up to 2.45 GHz, (c) Cree (Wolfspeed) GaN-HEMTs offer higher bandwidth and power densities in the range of 10 MHz up to 18 GHz, (d) Infineon PG-DSO-20, 100V and 600V Enhancement (E) mode GaN HEMT.....	14
Figure I.10	Venture- Qs analysis of the positions of various technology companies in GaN technology ramp-up showing as many as 23 companies who are in advanced product development stage [2012 status].....	14
Figure I.11	Surface treatments by using SiN-passivation layers are shown to mitigate current collapse.....	15
Figure I.12	(a) Cascode-solution to obtain E-mode (positive threshold voltage) devices by using a low-voltage conventional Si-FET in series with a D-mode GaN-HEMT is currently provided by EPC and (b) an alternate solution to obtain E-mode devices is to use a p -GaN cap layer in the heterostructure under the gate to shift the threshold voltage to positive values and is provided by Panasonic.....	16
Figure II.1	Schematic diagram of wurtzite GaN structure. The blue atoms represent the Ga atoms and the red atoms represent the N atoms.....	23
Figure II.2	First Brillouin zones of the wurtzite GaN structure.....	23
Figure II.3	Schematic diagram of the band structure for GaN.....	24
Figure II.4	Band diagrams of the materials involved in the AlGaN/GaN heterostructure (Type I).....	26



Figure II.5	Schematic diagram showing the energy band structure in AlGaN/GaN heterostructure.....	27
Figure II.6	Schematic drawing of the crystal structure of wurtzite (a) Ga-face, (b) N-face.....	29
Figure II.7	Electric field and sheet charges due to piezoelectric polarization in $\text{Al}_x\text{Ga}_{1-x}\text{N}$ /GaN structure.....	29
Figure II.8	Spontaneous and piezoelectric polarization in $\text{Al}_{1-x}\text{In}_x\text{N}$ and $\text{Al}_x\text{Ga}_{1-x}\text{N}$ versus composition. The substrate lattice constant is taken as that of relaxed GaN.....	31
Figure II.9	Schematic diagram showing the energy band structure in $\text{Al}_x\text{Ga}_{1-x}\text{N}$ /GaN HEMT.....	33
Figure II.10	The schematic of a typical HEMT devices structure.....	34
Figure II.11	Description of I - V transistor characteristics, inset shows common source configuration for a HEMT.....	41
Figure II.12	Model (solid lines) and typical DC (dotted lines) I - V characteristics of a HEMT. Most of the common non idealities in GaN-based HEMTs are highlighted.....	42
Figure II.13	AlGaN/GaN HEMT structures with surface, interface and buffer layer traps.....	44
Figure II.14	Cross section of area beneath gate in AlGaN/GaN HEMT. Large electric field peak is shown at the drain-edge of the gate. Electrons from the gate leak into the semiconductor at $V_{GS} < V_{TH}$ which are given enough energy by the electric field to cause impact ionization and subsequent breakdown of the device.....	47
Figure III.1	(a) Comparison of accuracy of Fermi-potential (E_f) with numerical solution and (b) model comparison against	

	measurements.....	60
Figure III.2	(a) The workflow for terminal characteristics and (b) the surface-potential calculation approach in ASM-HEMT model.....	61
Figure III.3	The HSP model flow indicating the various effects incorporated in the model.....	62
Figure III.4	Band structure diagram at a hetero-junction for $\text{Al}_x\text{Ga}_{1-x}\text{N}/\text{GaN}$ HEMT.....	67
Figure III.5	E_f , E_0 and E_1 versus V_g calculated numerically reproduced from [16]. The regions defined for modeling are marked in the figure.....	73
Figure III.6	Numerical calculations of $E_f - E_0$ and $E_f - E_1$ versus gate voltage reproduced from [16] regions I and II are marked in the figure.....	74
Figure III.7	Comparison of the developed model of 2-DEG charge density with the numerical solution reproduced from [17] at $T = 300$ K. Typical value of $V_{off} = -3$ V is used.....	77
Figure III.8	GaN high electron mobility transistor small-signal equivalent circuit model.....	88
Figure IV.1	Silvaco Simulation Flowchart.....	96
Figure IV.2	Cross sectional view of $\text{Al}_x\text{Ga}_{1-x}\text{N}/\text{GaN}$ nanostructures HEMTs using for simulation.....	98
Figure IV.3	(a) Example of non-uniform mesh creation using ATLAS [1], (b) Structure and mesh of $\text{Al}_x\text{Ga}_{1-x}\text{N}/\text{GaN}$ nanostructures HEMTs using for simulation.....	99
Figure IV.4	Comparison of modeled I_d-V_d characteristics (solid line) with	

	Atlas TCAD data (symbols) for mole fraction x values of (25, 30, and 35) % at gate-to-source voltage $V_{gs} = -1$ V.....	101
Figure IV.5	The I_d-V_g characteristics plotted from the model simulation results (solid line) is validated by comparison against Atlas TCAD data (symbols), (a) in linear and (b) in logarithmic scale for different mole fractions x in $Al_xGa_{1-x}N/GaN$ HEMTs. Drain voltage was kept fixed at 7 V.....	102
Figure IV.6	Transconductance plots for different mole fractions x of our HEMT device, with drain-to-source voltage $V_{ds} = 7V$. Good agreement is achieved between the model (line) and Atlas TCAD data (symbols).....	103
Figure IV.7	Transfer characteristics for four samples of $Al_{0.25}Ga_{0.75}/GaN$ HEMT with gate width $W_g = 100$ μm , at $V_{ds} = 8$ V. The measurement direction was from negative to positive voltages.	104
Figure IV.8	Atlas TCAD data (symbols) and modeled (solid lines) gate-source capacitance, C_{gs} , of a device with a mole fraction value varies between (25 and 35)%. Drain voltage was kept fixed at 7 V	105
Figure IV.9	Comparison of modeled (solid line) with Atlas TCAD data (symbols) $C_{gd}-V_d$, for different Al mole fractions x in $Al_xGa_{1-x}N/GaN$ HEMT with $V_g = -1$ V.....	106
Figure IV.10	Influence of variation of the mole fraction (x) on the two frequencies: the cut-off frequency f_T (black) and the maximum oscillation frequency f_{max} (blue).....	106
Figure IV.11	Drain current plotted as a function of drain voltage. Plot used to show the gate length variation effect on the HEMT devices transfer characteristics of in both linear and saturation regions of operation.....	107
Figure IV.12	Comparison of modeled (solid line) with Atlas TCAD data (symbols) I_d-V_g in logarithmic scale, for different gate lengths	

	L_g in $\text{Al}_x\text{Ga}_{1-x}\text{N}/\text{GaN}$ HEMT with $x = 35\%$	108
Figure IV.13	I_d - V_g characteristics of $\text{Al}_x\text{Ga}_{1-x}\text{N}/\text{GaN}$ HEMTs for different gate lengths L_g at $x = 35\%$. The model simulation result (line) is validated by comparison against Atlas TCAD data (symbols).....	109
Figure IV.14	Comparison of modeled (solid line) with Atlas TCAD data (symbols) C_{gs} - V_g , for different gate lengths L_g in $\text{Al}_x\text{Ga}_{1-x}\text{N}/\text{GaN}$ HEMTs at $x = 35\%$	110
Figure IV.15	Gate length variation effect on the cut-off frequency f_T (black color) and the maximum oscillation frequency f_{\max} (blue color).....	110
Figure IV.16	Drain current as a function of drain voltage (with and without self-heating effect). Gate voltages of (-3, -2, -1 and 0) V, were used for the curves. At mole fraction of the $\text{Al}_x\text{Ga}_{1-x}\text{N}$ layer $x = 35\%$	111
Figure IV.17	$\text{Al}_x\text{Ga}_{1-x}\text{N}/\text{GaN}$ HEMTs drain current as a function of drain voltage with gate voltage as a parameter. Solid lines correspond to model simulations; symbols correspond to Atlas TCAD data.....	112

List of Tables



List of Tables

Table I.1	Electrical properties of different semiconductors. GaN shows a combination of large bandgap, high mobility and breakdown field.....	06
Table II.1	The bandgap energy of the group III-nitride ternary alloys by using Vegard's law.....	25
Table II.2	Comparison of different substrate materials used for GaN	38
Table III.1	Parameters used to plot the I - V and C - V characteristics for three different samples in relation with molar fraction.....	100
Table III.2	Extracted DC values for four different samples of $\text{Al}_{0.26}\text{Ga}_{0.74}\text{N}/\text{GaN}$ HEMT.....	100

General introduction



General introduction

General introduction

During the last three decades, miniaturization of microelectronic devices has revolutionized the electronics industry. Integrated circuits density increases exponentially, generating smaller devices that operate faster, consume less power and cost less. This miniaturization changed communications and information technology considerably. An important development of computing systems was closely followed by that of wireless and optical communications systems.

The increasing demand of the wireless communication market, military and space applications are the motivation behind the development of highly efficient microwave transistors. The personal next generation of cell phones, satellite communications and TV broadcasting requires higher frequencies and higher power to reduce the antenna size of terminal users. The same requirement holds for broadband wireless internet connection as well, because it requires high speed data transmission rate. Being the key component in the technical development, microwave transistors and amplifiers have attracted much attention in the recent years.

Silicon has been the dominant material in the fabrication of the power microwave devices. However this material is approaching its physical limits in terms of power density, breakdown voltage, and operating frequency. Instead, industry is turning to other superior material properties of wide bandgap (WBG) GaN and SiC devices that can better satisfy the requirements of tomorrow's high-efficiency and low-loss systems.

While SiC is undoubtedly the most mature WBG semiconductor, it still suffer from the several physical issues related to both surface and interfaces. Furthermore, the performance of SiC-based devices ultimately falls short at high frequencies because of its less than optimal transport properties; however this is not the case with GaN.

General introduction

As compared with SiC, GaN has a larger band gap and a higher breakdown voltage, which means that GaN-based transistors are the most suitable for microwave power applications. The ability of GaN to form heterojunctions makes it superior compared to SiC. GaN can be used to fabricate HEMTs whereas SiC can only be used to fabricate MESFETs. The advantage of the HEMT is its higher electron mobility due to reducing ionized impurity scattering, because the electrons in the channel remain separated from the dopants.

AlGaIn/GaN heterostructures are important materials for the fabrication of high electron mobility transistors (HEMTs). The first HEMT device on the basis of GaN appeared in 1993, and was followed by another device based on AlGaIn/GaN in the same year. In a HEMT, the two-dimensional sheet carrier density in the 2DEG channel is modulated by the gate voltage. Clearly, since the 2DEG is confined in the potential well arising from the band discontinuity of the two materials (AlGaIn and GaN) and the conductive channel is located very close to the surface, the physical problems affecting the operation of these devices must be investigated at a nanoscale level. Indeed, several fundamental issues related to both surfaces and interfaces in AlGaIn/GaN heterostructures are today object of deep scientific investigation in order to understand the physical phenomena related to the carrier transport in these nanometric systems and, ultimately, improve the performance of HEMT devices.

In this thesis, we aim to study the influence of the geometrical parameters, molar fraction of the AlGaIn barrier layer on the I - V and C - V characteristics of the HEMTs. The influence of the spontaneous and piezoelectric polarization charges is also studied.

This task includes the following objectives:

- ☑ To develop an analytical physics-based model for the two-dimensional electron gas density in AlGaIn/GaN HEMTs.
- ☑ To deduce the analytical expressions of the drain current as a function of the gate voltage and drain voltage and determine the I - V and C - V characteristics.

General introduction

- ☑ To determine the analytical expression of the gate and drain capacitances.
- ☑ To explore the I - V and C - V characteristics and study the influence of geometrical, compositional and polarization effects on the characteristics of the AlGaN/GaN HEMTs.

The rest of this thesis is organized as follows.

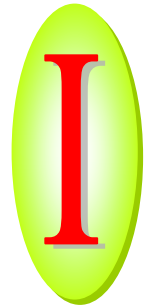
Chapter I gives an overview of the state-of-the-art of gallium-nitride technology and its promise for the future.

Chapter II presents an explanation of operation of AlGaN/GaN HEMTs. The properties of III-N materials are presented, in particular the polarization effects and the origin of the resulting 2DEG.

Chapter III describes the compact modeling compared to other types of modeling. The basic equations governing the simulations are described.

Chapter IV presents the numerical simulations and their comparison with experimental data. The results obtained are used to draw conclusions about the improvement of the performances of AlGaN/GaN HEMTs.

Chapter



State-of-the-art of gallium-nitride technology and its promise for the future

Chapter I

State-of-the-art of gallium-nitride technology and its promise for the future

I.1 Introduction

For decades now the dominant force in the semiconductor industry for electronics has been Si since the production of the first silicon transistor by Gordon Teal in 1954 [1]. Power MOSFETs on Si appeared in 1970s as an improved power device compared to the bipolar junction transistor (BJTs) developed in the 1960s. These devices were faster and more powerful due to the fact that they are majority carrier devices which give rise to the two most important characteristics of power devices: Power handling capabilities and switching speed. Silicon, however, has reached a stage where its material limitations now dominate its effectiveness.

Research is still ongoing into silicon device design and fabrication mainly due its low cost and it will still be used in power applications. It is felt however, that further research investment into Si devices will provide very little return in power electronics as the design and fabrication of them has already been very well established. A theoretical breakdown field of only 30 V/ μm can be reached in Si; it also suffers from high on-state resistance which leads to high conduction losses and it ceases to operate at temperatures above 150°C, meaning that large heat sinks are required to cool the devices. Therefore, it is clear that systems using silicon based power devices are extremely inefficient and alternative semiconductor materials would be desirable.

Chapter I: *State-of-the-art of gallium-nitride technology and its promise for the future*

Recently, new materials with superior properties are being investigated as potential replacements. In particular gallium nitride (GaN), silicon carbide (SiC) and C-diamond have emerged as attractive candidates for niche spaces within HV-market.

In areas like laser diodes, radio frequency and microwave power amplifiers, wide bandgap semiconductor materials like SiC and GaN overtake the limit of silicon since the discovery of the Gunn diode (TED) in 1962 [2]. Starting with Metal Semiconductor Field Effect Transistors (MESFETs) based on GaAs, Bipolar Junction Transistors (BJTs), Heterojunction Bipolar Transistors (HBTs), and High Electron Mobility Transistors (HEMTs), devices have been pushing the RF frontiers both in terms of the frequency bands (from HF band to mm-wave) and power density levels at any given band. Gallium nitride (GaN) has been a technology with so much promise for commercial RF applications, because of its potential to deliver high power levels of about 30 dBm even in high frequency W-band (75-110) GHz, due to its inherent high power-density properties [3].

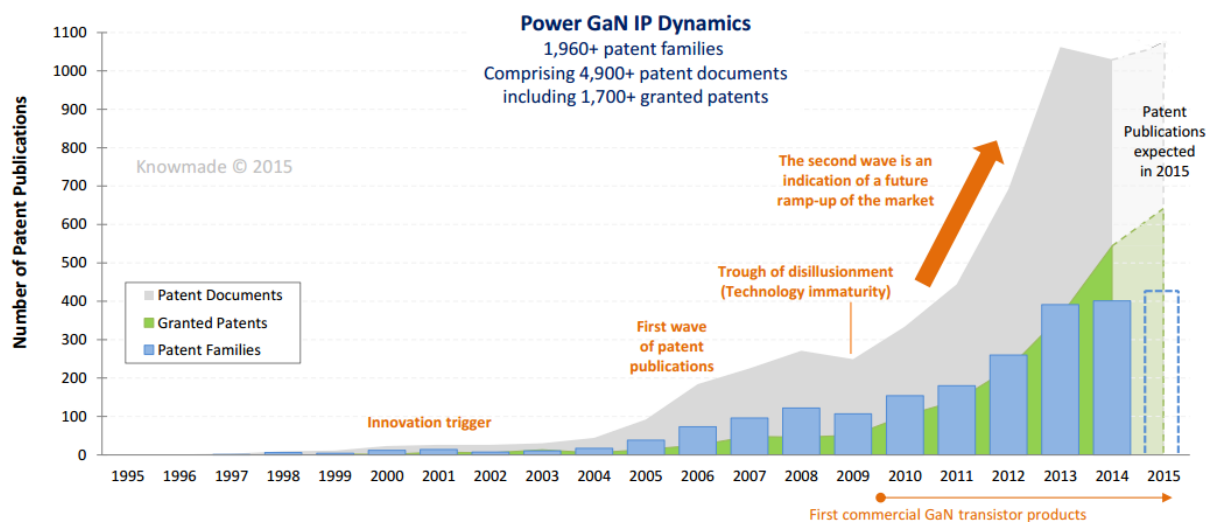


Figure I.1: Time evolution of GaN research, a patent family is set of patents filed in multiple countries by a common inventor(s) to protect a single invention, while a patent document is a patent filed in one country (1st application or extensions) [4].

Chapter I: *State-of-the-art of gallium-nitride technology and its promise for the future*

GaN based device technology has advanced a lot due to its excellent electrical properties in high-frequency, high-power, and high-temperature application fields. This is motivated by their wide bandgap, high thermal conductivity, high heat capacity together with low on-resistance and high carrier mobility in devices built with a heterostructure configuration using AlGaN and GaN (AlGaN/GaN). The first GaN material was produced by passing ammonia over hot Gallium by Jusa and Hahn in 1938. Since then numerous research breakthroughs and progress have been made in GaN based electronics [3]. Gallium nitride has also made a significant impact in the optoelectronic sector, particularly in light emitting diode (LED) lighting due to their unique properties such as direct tunable bandgap from 6.2 eV (AlN) to 0.7 eV (InN), and piezoelectric polarization. Large area GaN was grown by hydride vapor phase epitaxy (HVPE) directly on sapphire by Maruska and Tietjen in 1969 [5] and in 1993 high-brightness blue light-emitting-diodes (LEDs) was developed by Nichia. Since then this material system has become primary choice for blue LEDs, blue laser diodes and other optoelectronic devices. Figure (I-1) shows time Evolution of GaN research in the past few years. Note that the patent search was done in March 2015, thus the data corresponding to the year 2015 (and the years after) are not complete [4].

Table I.1: Electrical properties of different semiconductors. GaN shows a combination of large bandgap, high mobility and breakdown field [6].

Material	Mobility μ (cm ² /V.s)	Dielectric Constant (ϵ)	Bandgap E_g (eV)	Breakdown Field E_b (10 ⁶ V/cm)	T_{max} (°C)
Si	1300	11.90	1.12	0.30	300
GaAs	5000	12.50	1.42	0.40	300
4H-SiC	260	10.00	3.20	3.50	600
GaN	1500	9.50	3.44	2.00	700

The first GaN based transistors were realized in the early to mid-1990's [7] and since then GaN-HEMT have been extensively researched and developed for high-power and

Chapter I: *State-of-the-art of gallium-nitride technology and its promise for the future*

high frequency applications. As shown in Table (I.2) GaN falls into the category of wide bandgap semiconductors (bandgap energy, $E_g = 3.44$ eV) along with other materials such as diamond and SiC. A wide energy bandgap generally translates into an ability to support high internal electric fields before electronic breakdown occurs. Of these wide bandgap materials, GaN is particularly appealing due to its ability to form heterojunctions to wider bandgap semiconductors such as aluminium gallium nitride (AlGaN) or aluminium nitride (AlN) (up to 6.2 eV).

In doing so, a 2-dimensional-electron-gas (2DEG) forms at the interface due to large polarizations in the material which provides a highly dense, majority carrier channel with large electron mobility (usually and most preferably with undoped materials). These properties can be exploited to make devices which are capable of handling or providing high output power that can be operated as power switches or comfortably up to 10 GHz for power amplifier applications respectively. GaN power devices are expected to prevail in high end applications over more traditional semiconductors

I.2 State-of-the-art of GaN-HEMTs in power electronics

Today already 40% of the world wide used energy is provided by electric power. It is expected that this share is going to rise to about 60% until 2040. This enormous amount of energy not only needs to be produced environmentally friendly, but it also should be distributed and used efficiently [8]. Wide Bandgap semiconductors (WBG) such as SiC, GaN and AlN show superior material properties compared to silicon. Due to these unique characteristics (high maximum current, high breakdown voltage, and high switching frequency), these WBG represent the unique material of choice to help solving the energy problems of the future.

Over 50% of all consumed energy in the world is electrical, and about 60% of all electrical energy is lost due to the many (inefficient) conversion steps (AC do DC, different voltage levels) which are required to bring the electricity from its source to

Chapter I: *State-of-the-art of gallium-nitride technology and its promise for the future*

the consumer. Semiconductor devices in general can greatly help to increase the efficiency of the power converters. The adoption of WBG materials such as GaN in power electronics is a key factor to reach higher energy efficiency and reducing power management losses, we can see in Figure (I.2) that the conduction losses in GaN-switches are much lower compare to MOSFET.

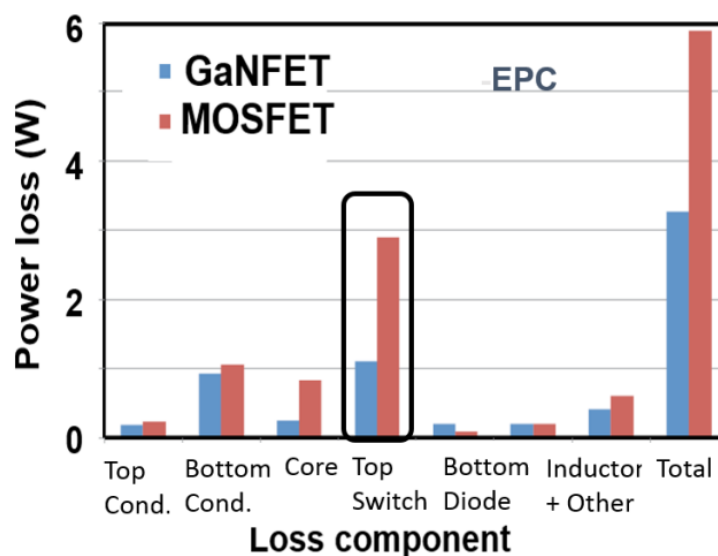


Figure I.2: The important loss components for a 12 V – 1.2 V buck converter operating at 1 MHz converter showing significantly lower switching loss due to lower gate charge in GaN switch (circuit board from EPC) [9].

GaN devices offer five key characteristics: high dielectric strength, high operating temperature, high current density, low on-resistance and high speed switching. The important areas in power conversion industry where GaN insertion is imminent are AC-DC switching power supplies, variable speed motor drives, fluorescent lights and DC-DC converters areas. In these applications, the key device performance metrics are breakdown voltage (BV), specific on-resistance (R_{dson}), and total-gate charge-capacitance (Q_g) and in all the three metrics GaN-technology fares better than its competitors as shown in Figure (I.3). The BV vs R_{dson} plot demonstrates that for a given BV the R_{dson} in GaN and GaN HEMT is lower compare their competitors.

Chapter I: *State-of-the-art of gallium-nitride technology and its promise for the future*

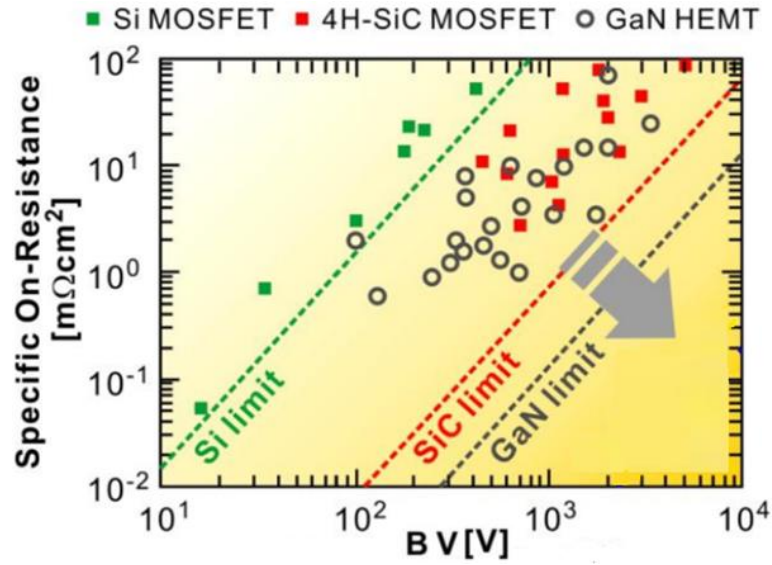


Figure I.3: The theoretical BV and $R_{ds(on)}$ plots for GaN, Si and SiC showing improved characteristics of GaN compared to other technologies [9]

These disruptive advantages have attracted some 15 technology manufacturers to invest in GaN-on-Si HEMT power device research and development. The full list can be found in [10] but includes IR, EPC, Transphorm, Fujitsu, Sanken, Toshiba, TI, and Freescale among others. Figure (I.4) shows the ranking of patent assignees of the

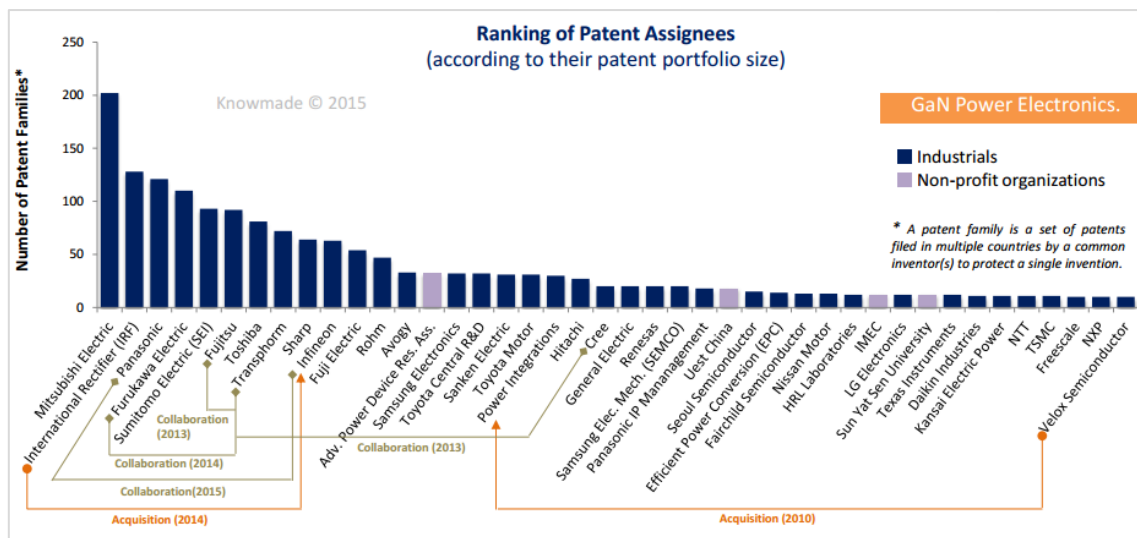


Figure I.4: The number of patents families for industrials and non-profit organizations, 2010- 2015[4].

Chapter I: *State-of-the-art of gallium-nitride technology and its promise for the future*

important industrials and non-profit organizations for GaN power electronics research investors according to their patent portfolio size over the last few years (A patent family is a set of patents filed in multiple countries by a common inventor(s) to protect a single invention).

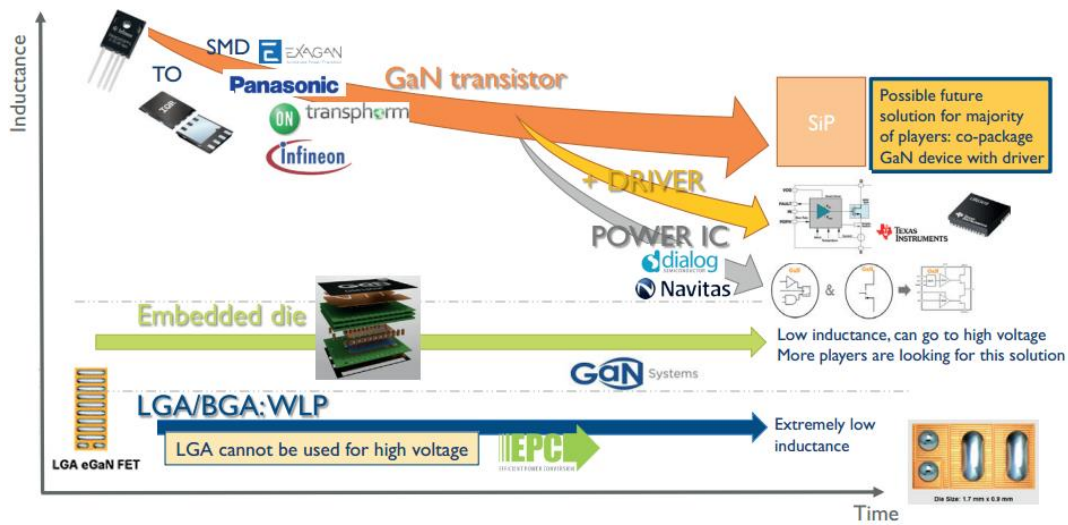


Figure I.5: An overview on qualification status and a detailed packaging roadmap for power GaN.

Studies into the suitability of the GaN material for power applications began in 2006, and coincide with the first wave of patent filings. The number of patent publications has sharply increased since 2010 with the commercialization of first power GaN devices. Currently, the second peak of patent filings combined to the increase of granted patents is a positive indication that GaN power market is ramping up. So far, there are only a few players selling power GaN products (Infineon/IR, EPC, GaN Systems and Transphorm) and the GaN device market is still small, estimated at \$10M in 2015. But the ramp-up became quite impressive since 2016. The market will multiply by 30 from now and reach more than \$300M in 2020 [11]. Yole Development has updated the technology section of the GaN report with an overview on qualification status and a detailed packaging roadmap as shown in Figure (I.5).

Chapter I: *State-of-the-art of gallium-nitride technology and its promise for the future*

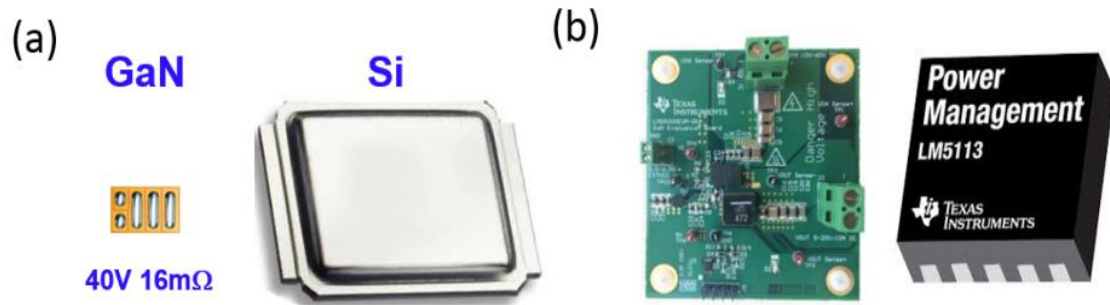


Figure I.6: (a) Comparison of power MOSFET in package with eGaN-FETs from EPC showing the size difference for the same device-metrics [9], (b) the LMG5200- 10 A, 8 V GaN half-bridge power module with integrated driver from TI which satisfies the JEDEC standards demonstrating the arrival of GaN-HEMTs in the power market.

GaN is anticipated to be a next generation power semiconductor. With a higher breakdown strength, faster switching speed, higher thermal conductivity and lower on-resistance (R_{on}), power devices based on this wide-bandgap semiconductor material can significantly outperform the traditional Si-based power chips. As such, GaN-based power devices will play a key role in the power conversion market within battery chargers, smartphones, computers, servers, automotive, lighting systems and photovoltaics. The advantages of GaN-technology can be visualized in Figure (I.6) by comparing these products against their competing solutions in Si in terms of form-factor and efficiency.

I.3 State-of-the-art of GaN-HEMTs in RF-electronics

GaN-based HEMTs were explored as candidates for outstanding high-power RF performance. In wireless communication, where high-power is required, GaAs transistors and Si-based laterally diffused transistors (LDMOS) have been challenged by the advancement of GaN-based technology [12, 13]. SiC based devices offer an alternative to Si-based transistors in applications where efficient heat dissipation and high breakdown voltage are required, thanks to the better thermal conductivity and

Chapter I: *State-of-the-art of gallium-nitride technology and its promise for the future*

breakdown field of SiC [14]. The performance of SiC-based devices ultimately falls short at high frequencies because of its less than optimal transport properties; however this is not the case with GaN.

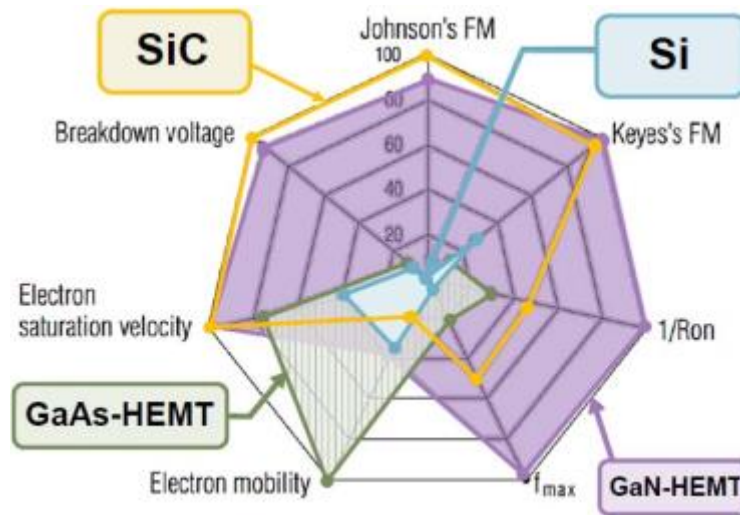


Figure I.7: Comparison of RF performance metrics among different technologies.

The superior breakdown field and saturated velocity make GaN-based devices capable of delivering higher RF power than GaAs and LDMOS based technologies [15]. Power densities of 41.4 W/mm and 30.5 W/mm were reported at 4 and 8 GHz, respectively [16, 17]. This is five to ten times more than what was achieved with GaAs HEMTs in the S-band [18]. In the Ka-band (26.5-40 GHz) AlGaN/GaN-based HEMTs devices have demonstrated powers up to 10 W/mm at 40 GHz [19]. The high mobility of GaN and its high critical field allows aggressive scaling of the transistor size, which makes it the leading technology for high-power applications at high frequency. In the W-band (75-110 GHz), some GaN-based MMIC have been demonstrated with 1-2 W/mm [20 - 22]. The application regimes that can take advantage of these benefits range from radar, CATV, space applications, SatCom, 3G/4G base-stations, and WIMAX/LTE PAs. Figure (I.7) shows the comparison of different technologies in terms of the figures-of-merit relevant to these RF applications.

Chapter I: *State-of-the-art of gallium-nitride technology and its promise for the future*

If we focus on RF applications, the material characteristics of GaN offer clear advantages. GaN RF transistors offer many times the theoretical maximum output power density of GaAs or silicon transistors. Additional key characteristics of GaN transistors include high cut-off frequency and good thermal conductivity. GaN devices offer the best solution for simultaneous high power, high frequency and high temperature operation. The chart below (Figure (I.8)) captures frequency versus output power capabilities for several compound semiconductor used in power amplifier applications [23].

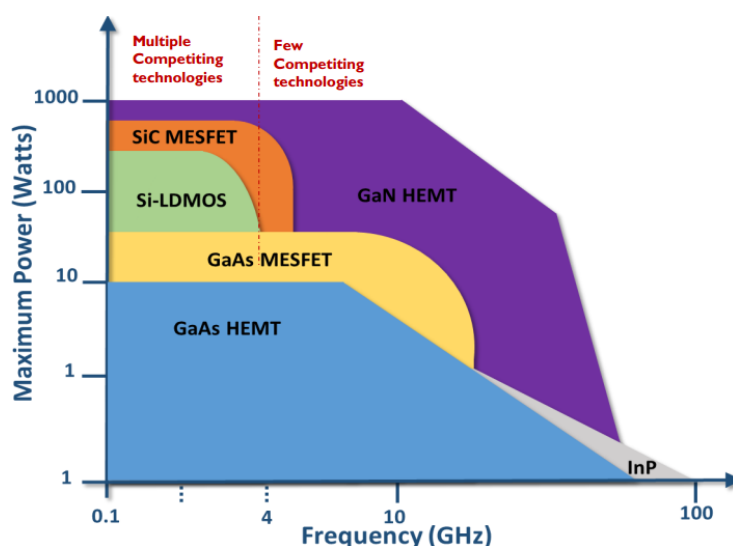


Figure I.8: state-of-the-art demonstrations of GaN-HEMTs against of its compitators showing P_{max} vs f metric. GaN enables possibilities for both high-power and high-frequency [24].

Initial concerns about reliability, substrate power-losses and thermal management have become moot as deployed systems build a compelling set of actual metrics. To take full advantage of the material advantages of GaN, just about every RF manufacturer uses a GaN-on-SiC wafer scheme. The GaN HEMT market has been dominated by many players such as HRL, Panasonic, STM, NXP, Cree [Wolfspeed], RFMD, Triquint [Qorvo] etc. in the RF market much earlier than in the power market [10]. Figure (I.9) shows a few products from leading companies showing improved form-factor and performance metrics when compared to earlier components.

Chapter I: *State-of-the-art of gallium-nitride technology and its promise for the future*

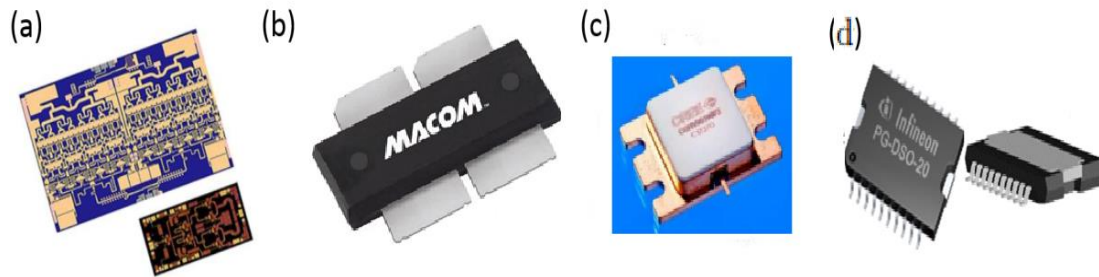


Figure I.9: (a) Triquint's TGS2354 GaN-on-SiC switch die compared against their GaAs-MMIC, (b) MACOM's MAGE-102425-300 GaN, frequencies up to 2.45 GHz, (c) Cree (Wolfspeed) GaN-HEMTs offer higher bandwidth and power densities in the range of 10 MHz up to 18 GHz and (d) Infineon PG-DSO-20, 100V and 600V Enhancement (E) mode GaN HEMT.

In the last couple of years, the radiofrequency (RF) GaN market experienced impressive growth and has reshaped the RF power industry landscape. The penetration rate in various markets, and in particular telecom and defense applications, had a breakout period in the last few years. The compound annual growth rate (CAGR) in these two markets is more than 20%. Another significant boost will occur around

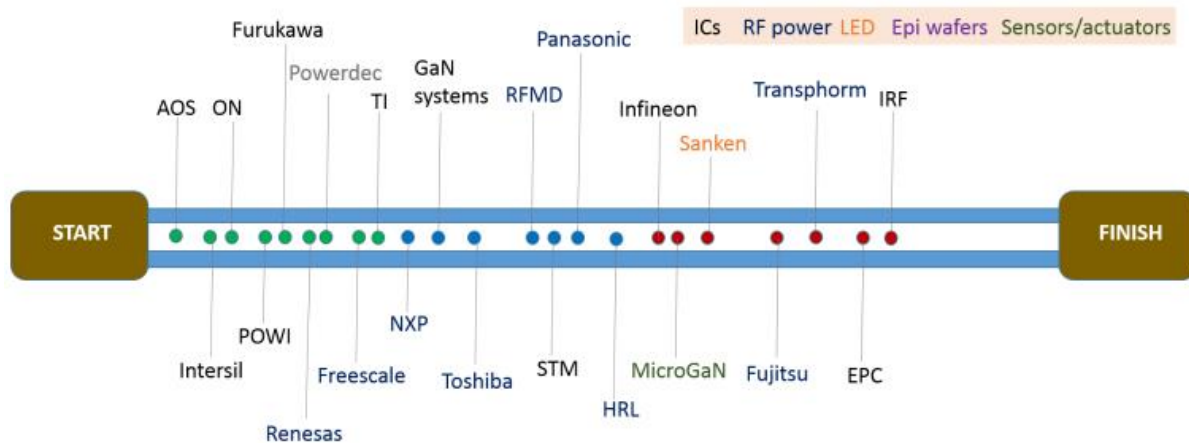


Figure I.10: Venture- Q_s [10] analysis of the positions of various technology companies in GaN technology ramp-up showing as many as 23 companies who are in advanced product development stage [2012 status]

Chapter I: *State-of-the-art of gallium-nitride technology and its promise for the future*

2019–2020, led by the implementation of 5G networks. The total RF GaN market size will be a factor of 3.4 larger by the end of 2023. The summary of the current status of GaN-HEMT in the semiconductor industry is highlighted in Figure (I.10). By looking at the position of industry players in the race for commercialization in GaN, it becomes clear that all the big players of both RF and power domains have invested resources in this technology indicating the widening adoption of GaN-HEMTs.

Further device scaling, however requires that the outstanding issues in the device technology and circuit design be addressed and mitigated and will be discussed in the following sub-section

I.4 Challenges and future of scaling GaN technology

In spite of the extraordinary material properties of AlGaN/GaN heterostructure systems, such as high mobility, high saturation velocity and high breakdown field, the main impediments to this technology are containing the current collapse phenomenon, developing technologies for enhancement mode (E-mode) HEMTs, and improving device reliability [10]. Conventional GaN-based HEMTs are of depletion mode (D-

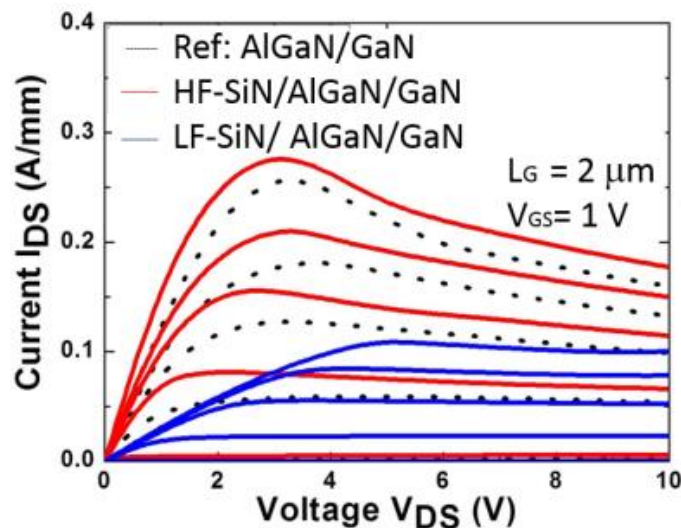


Figure I.11: Surface treatments by using SiN-passivation layers are shown to mitigate current collapse in [25].

Chapter I: *State-of-the-art of gallium-nitride technology and its promise for the future*

mode) type but enhancement mode (E-mode) or normally-off devices would be preferable for power electronics [26, 27]. Normally-off type (enhancement-mode) devices are highly desired for safe operations and low power consumptions in power switching applications. Wide variety of device structures has been proposed such as surface treatments and passivation layers along with field plate engineering. Figure (I.11) shows work in this direction [25] to mitigate the effects of current collapse with surface treatment and show promise in the front of device-reliability.

Recent work on Cascode shown in Figure (I.12 (a)) by EPC, and p-GaN or the so-called gate-injection-transistor (GIT) shown in Figure (I.12 (b)) by Panasonic along with recessed gate technologies are some of the answers to the E-mode HEMT requirement. With this background it can be seen that the GaN-devices are expected to dominate the modern era of power device technology for the foreseeable future.

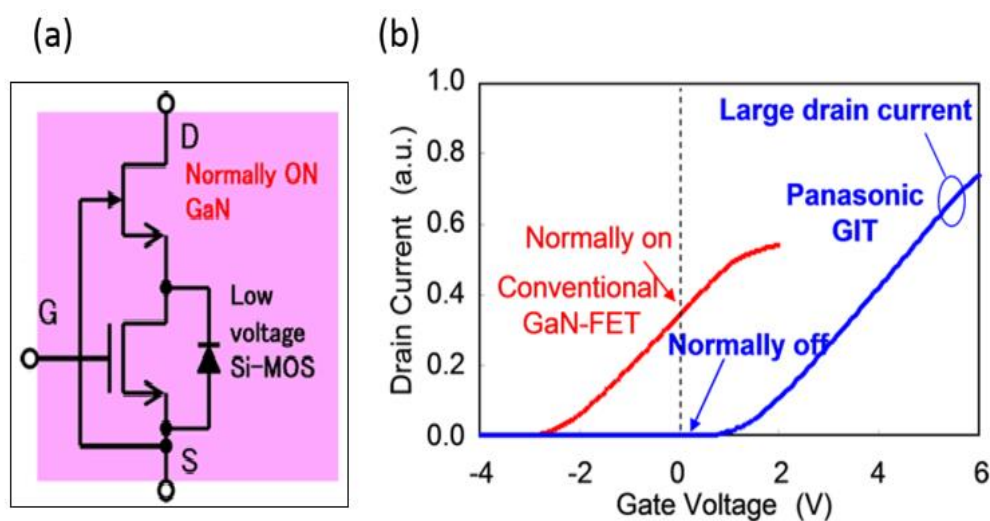


Figure I.12: (a) Cascode-solution to obtain E-mode (positive threshold voltage) devices by using a low-voltage conventional Si-FET in series with a D-mode GaN-HEMT is currently provided by EPC and (b) An alternate solution to obtain E-mode devices is to use a *p*-GaN cap layer in the heterostructure under the gate to shift the threshold voltage to positive values and is provided by Panasonic [28].

Chapter I: *State-of-the-art of gallium-nitride technology and its promise for the future*

I.5 Motivations and Contributions of this thesis

Realizing the greater of potential applications of GaN based devices; researchers have been trying to model the device from different perspectives in order to get a quick prediction of the characteristics of the devices or to optimize the performances before sending the device design for fabrication [29].

Device performance is dictated by the aluminum mole fraction of the barrier layer. This is because the mole fraction controls the amount of polarization at the hetero-interface and consequently the 2DEG density [30]. Spontaneous and piezoelectric polarizations at the hetero-interface are responsible for the high density of carriers in the channel and are accounted for in the model in the expression for the device threshold voltage which consider as one of the physical parameters that characterize the performance of transistor and has an impact in static and dynamic characteristics

In this work, we present a physics-based compact model for the I - V and C - V characteristics for $\text{Al}_x\text{Ga}_{1-x}\text{N}/\text{GaN}$ High Electron Mobility Transistors (HEMTs) in order to include a mole fraction-dependent threshold voltage. Thus, AlGaIn/GaN HEMTs with different Al mole-fractions and geometries is investigated to understand the impact of the 2DEG polarization dependence.

References

- [1] P. Siffert and E. Krimmel, "Silicon Evolution and future of a technology", *Springer*, 2004.
- [2] C. A. Barratt, "III-V semiconductors, a history in RF applications", *ECS Transactions*, vol. **19**, n° 3, pp.79–84, 2009.
- [3] S. Piotrowicz, E. Morvan, R. Aubry, G. Callet, E. Chartier, C. Dua, J. Dufraisse, D. Floriot, J.-C. Jacquet, O. Jardel, et al, "Overview of algan/gan hemt technology for l-to

Chapter I: *State-of-the-art of gallium-nitride technology and its promise for the future*

ku-band applications", *International Journal of Microwave and Wireless Technologies*, vol. **2**, n°.1, pp.105–114, 2010.

[4] Yole Development, "GaN Devices for Power Electronics", *Patent Investigation*, 2015.

[5] H. Pi. Maruska and J. J. Tietjen, "The preparation and properties of vapor-deposited single-crystal-line GaN", *Applied Physics Letters*, vol. **15**, n°.10, pp.327–329, 1969.

[6] M. Golio, "RF and Microwave Semiconductor Handbook", *Florida: CRC Press*, 2002.

[7] M.A. Khan, J.N. Kuznia, D. T. Olson, W. J. Schaff, J. W. Burm, and M. S. Shur, "Microwave performance of a 0.25 μ m gate AlGaIn/GaN heterostructure field effect transistor", *Applied Physics Letters*, vol. **65**, n°. 9, pp. 1121-1123, 1994.

[8] G. Meneghesso, "Gallium Nitride power devices: status, challenges and future opportunities", *University of Padova, Giornata IU.NET*, 2017.

[9] I. Akasaki, "Nitride semiconductors – impact on the future world", *Journal of crystal growth*, vol. **237**, n°.239, pp.905–911, 2002.

[10] S. Levin, "Vendor positions in the high voltage GaN commercialization race", *Technical report, Power Petrov group*, 2013.

[11] Yole Développement, "GaN and SiC for power electronics applications", 2015.


[12] F. van Rijs, "Status and trends of silicon LDMOS base station PA technologies to go beyond 2.5 GHz applications", in *Radio and Wireless Symposium, 2008 IEEE*, pp. 69–72, 2008.

[13] S. Theeuwens and H. Mollee, "LDMOS transistors in power microwave applications", *dec. white paper at Micr. Journ. web*, 2008.


Chapter I: *State-of-the-art of gallium-nitride technology and its promise for the future*

- [14] J. Casady and R. Johnson, "Status of silicon carbide (SiC) as a wide-bandgap semiconductor for high-temperature applications: A review", *Solid-State Electronics*, vol. **39**, n°.10, pp.1409–1422, 1996.
- [15] D. Fanning, A. Balistreri, E. Beam III, K. Decker, S. Evans, R. Eye, W. Gaiewski, T. Nagle, P. Saunier, and H.-Q. Tserng, "High voltage GaAs pHEMT technology for S-band high power amplifiers", in *Proc. Int. Conf. CS-Mantech*, 2007.
- [16] Y. F. Wu, A. Saxler, M. Moore, R. Smith, S. Sheppard, P. Chavarkar, T. Wisleder, U. Mishra, and P. Parikh, "30-W/mm GaN HEMTs by field plate optimization", *Electron Device Letters, IEEE*, vol. **25**, n°.3, pp.117–119, 2004.
- [17] Y.-F. Wu, M. Moore, A. Saxler, T. Wisleder, and P. Parikh, "40-W/mm double field-plated GaN HEMTs", in *Device Research Conference, 64th*, pp.151–152, 2006.
- [18] A. Katz and M. Franco, "GaN comes of age", *Microwave Magazine, IEEE*, vol. **11**, n°.7, pp.S24–S34, 2010.
- [19] T. Palacios, A. Chakraborty, S. Rajan, C. Poblenz, S. Keller, S. P. DenBaars, J. S. Speck, and U. K. Mishra, "High-power AlGaN/GaN HEMTs for Ka-band applications", *Electron Device Letters, IEEE*, vol. **26**, n°.11, pp.781–783, 2005.
- [20] M. Micovic, A. Kurdoghlian, K. Shinohara, S. Burnham, I. Milosavljevic, M. Hu, A. Corrion, A. Fung, R. Lin, L. Samoska, P. Kangaslahti, B. Lambrigtsen, P. Goldsmith, W. S. Wong, A. Schmitz, P. Hashimoto, P. J. Willadsen, and D. H. Chow, "W-band GaN MMIC with 842 mW output power at 88 GHz", in *Microwave Symposium Digest (MTT), 2010 IEEE MTT-S International*, pp.237–239, 2010.
- [21] M. Micovic, A. Kurdoghlian, P. Hashimoto, M. Hu, M. Antcliffe, P. J. Willadsen, W. S. Wong, R. Bowen, I. Milosavljevic, Y. Yoon, A. Schmitz, M. Wetzel, and D. H. Chow, "GaN MMICs for RF power applications in the 50 GHz to 110 GHz frequency range", *Physica Status Solidi (c)*, vol. **5**, n°.6, pp.2044–2046, 2008.

Chapter I: *State-of-the-art of gallium-nitride technology and its promise for the future*

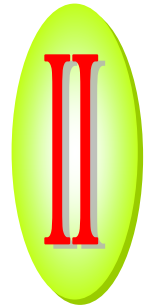
- 
- [22] M. Micovic, A. Kurdoghlian, A. Margomenos, D. Brown, K. Shinohara, S. Burnham, I. Milosavljevic, R. Bowen, A. Williams, P. Hashimoto, R. Grabar, C. Butler, A. Schmitz, P. Willadsen, and D. H. Chow, "92–96 GHz GaN power amplifiers", in *Microwave Symposium Digest (MTT), 2012 IEEE MTT-S International*, pp.1–3, 2012.
- [23] E. Higham, "GaN is Finally Here for Commercial RF Applications", *GaAs & Compound Semiconductor Technologies*, 2017.
- [24] Yole Development, "Market, technology and strategy consulting ", www.yole.fr, 2016.
- [25] S. Joglekar, M. Azize, E.J Jones, D. Piedra, S. Gradecak, and T. Palacios, "Impact of Al₂O₃ passivation on AlGaIn/GaN nanoribbon high-electron-mobility transistors", *Electron Devices, IEEE Transactions on*, vol. **63**, n°.1, pp.318–325, 2016.
- [26] J. Millan, P. Godignon, X. Perpina, A. Perez-Tomas, and J. Rebollo, "A survey of wide bandgap power semiconductor devices", *IEEE Transactions on Power Electronics*, vol. **29**, n°.5, pp.2155-2163, 2014.
- [27] T. Kachi, D. Kikuta, and T. Uesugi, "GaN power device and reliability for automotive applications", in *IEEE International Reliability Physics Symposium (IRPS)*, pp. 3D.1.1-3D.1.4, 2012.
- [28] U. Radhakrishna, "Modeling Gallium-Nitride based High Electron Mobility Transistors: Linking Device Physics to High Voltage and High Frequency Circuit Design", *PhD thesis, Massachusetts Institute of Technology*, 2016.
- [29] E. Sazia Afreen, "Modeling of AlGaIn/GaN High Electron Mobility Transistor for Sensors and High-Temperature Circuit Applications", *PhD thesis, University of Tennessee*, 2008.

Chapter I: *State-of-the-art of gallium-nitride technology and its promise for the future*



[30] S. Jonathan, "A physics-based analytical model of an AlGaN/GaN high electron mobility transistor", *PhD thesis, Rochester Institute of Technology*, 2004.

Chapter



AlGa_N/Ga_N High Electron Mobility Transistors (HEMTs)

Chapter II

AlGaN/GaN High Electron Mobility Transistors (HEMTs)

II.1 Introduction

This chapter will give an overview of the physical properties and the working mechanisms of AlGaN/GaN based HEMTs. To begin with, the basic properties of gallium nitride GaN and the development of heterostructures will be highlighted. The strong polarizations which occur in the material will be covered which will lead onto a description of how the two dimensional electron gas (2DEG) is formed. Basic device structure will then be covered with the various substrates on which it can be grown. The various substrates on which they can be grown will be outlined and commented on, also the device operation and breakdown mechanisms concluding the chapter. This chapter is essentially a theoretical overview about AlGaN/GaN HEMTs.

II.2 Basic properties of gallium nitride GaN

II.2.1 Crystal structure

The crystallographic structure of the group III-nitride semiconductor materials can be of a wurtzite, zinc-blende, or rock-salt structures. Under ambient conditions, the wurtzite structure is thermodynamically the most stable crystalline structure for the III-nitride semiconductors compared to the zinc-blende and rock-salt structures [1]. The

Chapter II: *AlGaN/GaN High Electron Mobility Transistors (HEMTs)*

schematic diagram for wurtzite GaN is shown in Figure (II.1). The blue atoms representing Ga atoms and the red atoms representing N atoms form the hexagonal close packed layers. The Ga atoms can also be replaced by other atoms such as Al in the wurtzite crystal structures. The two parameters a and c satisfies: $c/a = (8/3)^{1/2} = 1.633$.

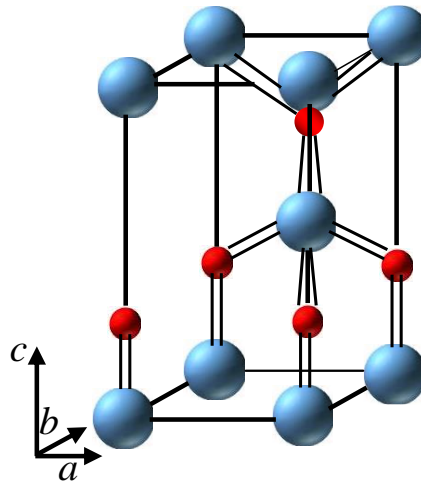


Figure II.1: Schematic diagram of wurtzite GaN structure. The blue and red atoms represent the Ga atoms and the N atoms, respectively.

In the crystal structure of GaN, different planes of the lattice exhibit different electrical and symmetry properties. Figure (II.2) provides the schematic diagrams of the first Brillouin zones of the wurtzite GaN structure [2].

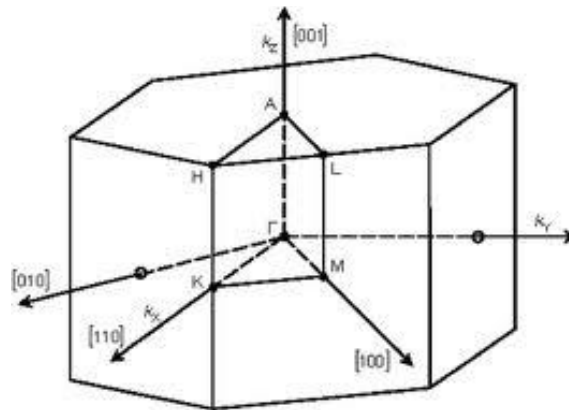


Figure II.2: First Brillouin zones of the wurtzite GaN structure.

Chapter II: AlGaN/GaN High Electron Mobility Transistors (HEMTs)

II.2.2 Electronic band structure

In the typical wurtzite GaN structure, the band structure is composed of one conduction band and three valence bands, namely, the heavy hole (*hh*) band, light hole (*lh*) band and the split-off (*so*) band.

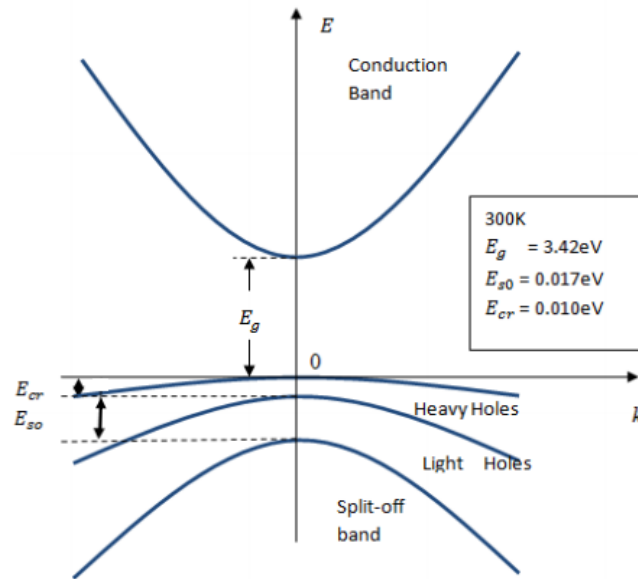


Figure II.3: Schematic diagram of the band structure for GaN.

The schematic diagram of GaN band structure is provided in Figure (II.3). The band energy E_g is normally regarded as the energy gap between the bottom of the conduction band and the top of the *hh* valence band. The band energy for GaN is 3.42 eV [1]. The energy gap between the *hh* band and *lh* band at $k = 0$, and the energy between the *lh* band and the *so* band at $k = 0$ have been given in Figure (II.4) [3].

II.2.3 III-nitride material alloys

The strong ionic bonding in the group III-nitride semiconductors is resulted from the large differences in the electron negativity between the group III metal cations and nitrogen anions [4]. The large differences in the ionic radii and bonding energies of the group III atoms (cations) lead to different lattice constants, bandgap energies, and electron affinities of the III-nitride semiconductors. Furthermore, the superior thermal

Chapter II: *AlGaN/GaN High Electron Mobility Transistors (HEMTs)*

and chemical stability of the wurtzite III-nitride semiconductors is also contributed by their strong bond strength. These characteristics of III-nitride semiconductors play an important role to be a promising candidate for photonic and electronic devices used for the device operation under high power and high-temperature environment.

The wurtzite III-nitride alloys are direct bandgap semiconductor having wide bandgap energy. The bandgaps of III-nitride binary alloys are known as (0.7 ± 0.05) eV [5, 10], (3.52 ± 0.1) eV [4], and (6.1 ± 0.1) eV [4] for InN, GaN, and AlN, respectively. In addition, the bandgap energy can be further engineered by controlling the mole fraction of each binary component in the ternary or quaternary alloys. The ternary combinations, such as $\text{In}_x\text{Ga}_{1-x}\text{N}$, $\text{In}_x\text{Al}_{1-x}\text{N}$, and $\text{Al}_x\text{Ga}_{1-x}\text{N}$, can be determined by the Vegard's law with the mole fraction of the binary alloys and their fundamental bandgap energies, as expressed in Eq. (II.1), is given by

$$E_g(A_xC_{1-x}N) = xE_g(A) + (1 - x)E_g(C) - bx(1 - x). \quad (\text{II.1})$$

where $E_g(A_xC_{1-x}N)$ is the bandgap energy of a ternary alloy, $E_g(A)$ and $E_g(C)$ are the bandgap energies of binary alloy A and C , respectively. x is the alloy mole fraction in a $A_xC_{1-x}N$ alloy, and b is the bandgap bowing parameter that is specific to each compound and determined experimentally. The band gap energies of each binary alloy and the bowing parameters for III-nitride ternary alloys are shown in the Table (II.1).

Table II.1: The bandgap energy of the group III-nitride ternary alloys by using Vegard's law [4, 5].

$A_xC_{1-x}N$	E_g of A (eV)	E_g of C (eV)	b (eV)
$\text{Al}_x\text{Ga}_{1-x}\text{N}$	6.1 ± 0.1	3.52 ± 0.1	0.7 ± 0.1
$\text{In}_x\text{Ga}_{1-x}\text{N}$	0.7 ± 0.05	3.52 ± 0.1	1.6 ± 0.2
$\text{In}_x\text{Al}_{1-x}\text{N}$	0.7 ± 0.05	6.10 ± 0.1	$3.4x \pm 1.2$

Chapter II: *AlGa_xN/GaN High Electron Mobility Transistors (HEMTs)*

II.2.4 *Al_xGa_{1-x}N/GaN heterostructure*

In 1992, the development of Al_xGa_{1-x}N/GaN heterostructure offered the opportunity of tremendous progress in the performance of microwave and high power transistors. Such structures are now a key component in modern high-performance microwave and high power devices such as HEMTs (High Electron Mobility Transistors) and HBTs (Heterostructure Bipolar Transistors).

Figure (II.4) shows typical band diagrams and bandgap values for commonly used heterostructure systems. The bandgap difference and the band offsets are extremely important factors for the performance and operation of heterostructure devices such as HBTs and HEMTs [6].

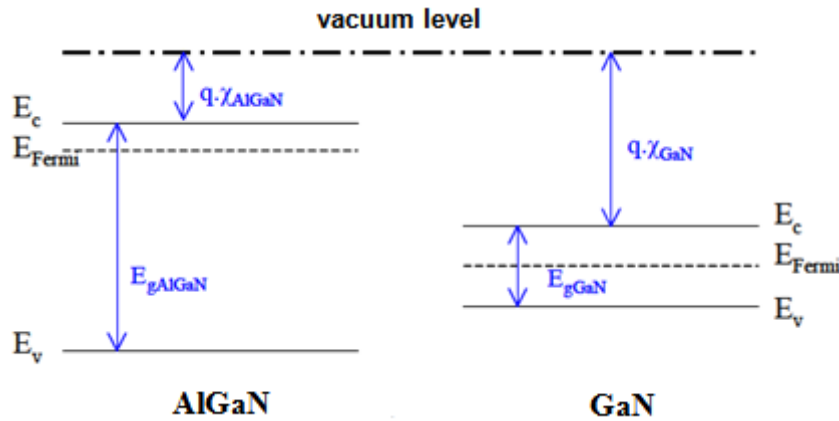


Figure II.4: Band diagrams of the materials involved in the Al_xGa_{1-x}N/GaN heterostructure (type I) [7].

At the beginning of heterostructure research it was believed that only materials with nearly the same lattice constant could result in heterostructures useful for electron devices. However it was later realized that it is also possible to grow good quality heterostructures from materials with different lattice constants provided the thickness of the grown layer does not exceed a certain critical value t_c .

Chapter II: *AlGaN/GaN High Electron Mobility Transistors (HEMTs)*

When a narrow bandgap semiconductor is put into contact with a wide bandgap semiconductor layer, in case of thermal equilibrium the Fermi level (E_f) of the semiconductors equilibrate resulting in a discontinuity in the conduction (E_c) and valence (E_v) bands. GaN-heterostructure is formed between two materials: AlGaN and GaN with different bandgaps that allow the formation of a quantum-well at their interface. Parallel to the heterojunction, near the boundary at the bottom, electrons can move freely and a two dimensional electron gas (2DEG) is formed as shown in Figure (II.5). An overview of how the two dimensional electron gas (2DEG) is formed is given in the following section.

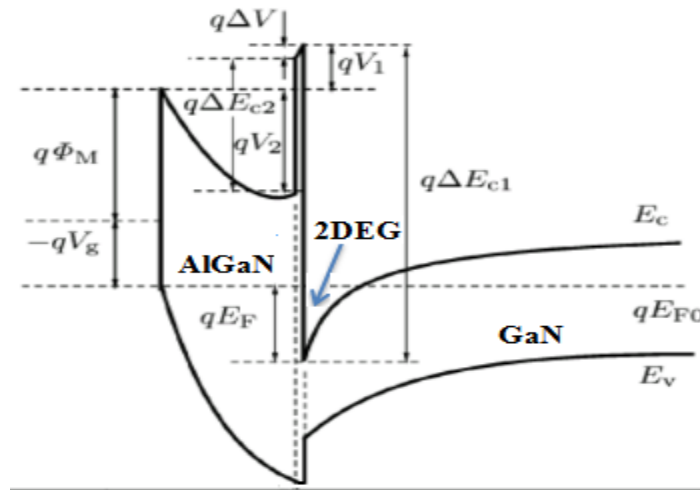


Figure II.5: Schematic diagram showing the energy band structure in AlGaN/GaN heterostructure.

II.3 Two Dimensional Electron Gas (2DEG)

The knowledge of the electron density in the 2DEG is essential for the description of the currents in a HEMT. The 2DEG is formed without any externally applied field and hence is naturally occurring at all times (under the correct growth parameters). For this reason when an AlGaN/GaN HEMT is fabricated i.e. with gate, source and drain contacts, the device will give large current flows at zero gate bias and will require a

Chapter II: *AlGaN/GaN High Electron Mobility Transistors (HEMTs)*

negative voltage to switch it off. These devices are known as depletion mode (D-mode) transistors in contrast to the enhancement mode (E-mode) transistor which requires a gate voltage of above zero volts to switch on.

There are two types of polarization contributing to the total polarization in the $\text{Al}_x\text{Ga}_{1-x}\text{N}/\text{GaN}$ compound structure, namely spontaneous and piezoelectric polarizations. The *spontaneous polarization* P_{sp} refers to the built-in polarization field present in an unstrained crystal. The *piezoelectric polarization* P_{pz} is the polarization field resulting from distortions of the crystal lattice. Due to the large difference in lattice constant between $\text{Al}_x\text{Ga}_{1-x}\text{N}$ and GaN materials, the $\text{Al}_x\text{Ga}_{1-x}\text{N}$ layer, which is grown on the buffer layer GaN is strained. Due to the large value of the piezoelectric coefficients of these materials, this strain results in a sheet charge at the two faces of $\text{Al}_x\text{Ga}_{1-x}\text{N}$ layer [8].

The spontaneous and piezoelectric polarization fields of the nitrides in $\text{Al}_x\text{Ga}_{1-x}\text{N}/\text{GaN}$ based HEMT induced the 2DEG in the devices channel. Ambacher *et al.*, utilizing piezoelectric constants obtained from previous research, calculated the induced sheet charge bound at the heterojunction interface. His conclusion was that the formation of the 2DEG in $\text{Al}_x\text{Ga}_{1-x}\text{N}/\text{GaN}$ structures was the result of both spontaneous polarization P_{sp} and the strain induced piezoelectric effects P_{pz} [9].

II.3.1 Spontaneous polarization

The two distinct polarization mechanisms found in GaN HEMTs enable a high carrier concentration even though there may be no intentional doping. Spontaneous polarization is the effect that is present at the heterojunction even though there is no strain present. The spontaneous polarization P_{sp} is developed due to the wurtzite group III-nitrides being tetrahedrally coordinated with a lack of symmetry along the [0001] axis or c-direction [7]. The polarization effects vary according to the how the structure

Chapter II: *AlGaN/GaN High Electron Mobility Transistors (HEMTs)*

was formed. The structure will have either N-face or Ga-face surfaces. Figure (II.6) shows the crystal structure of a wurtzite (a) for Ga-face, and (b) for N-face.

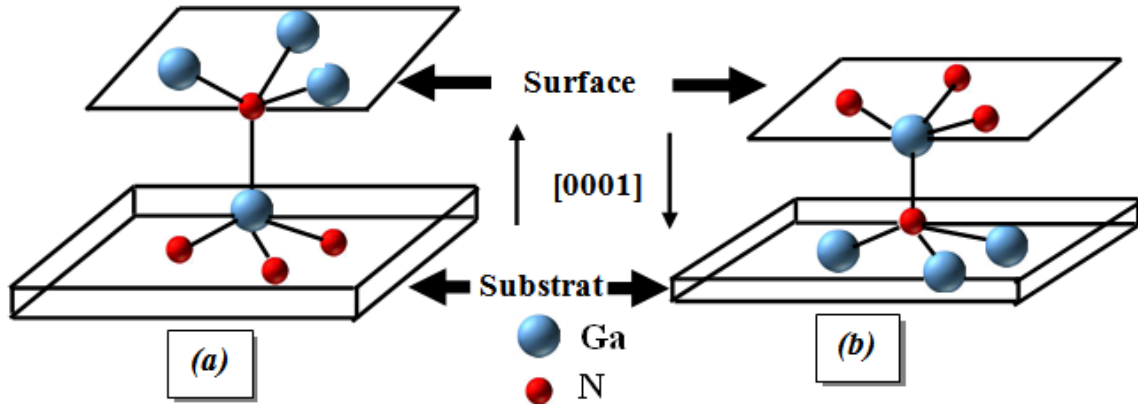


Figure II.6: Schematic drawing of the wurtzite structure: (a) Ga-face, (b) N-face [7].

The ability to reach a high carrier concentration at the 2DEG is determined by the ability of the structure to confine carriers through the polarization effects. To achieve a high carrier confinement, the polarization directions should be the same. The polarization induced sheet charge density (n_s) must be positive. This positive sheet charge attracts electrons and forms the 2DEG. Figure (II.7) illustrates the polarization charge effects for strained $\text{Al}_x\text{Ga}_{1-x}\text{N}$ over GaN which resulted in all polarization effects acting in the same direction. This also results in a positive sheet charge at the interface.

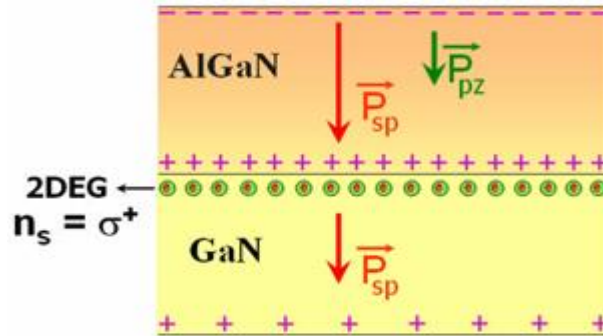


Figure II.7: Electric field and sheet charges due to piezoelectric polarization in $\text{Al}_x\text{Ga}_{1-x}\text{N}/\text{GaN}$ structure [8].

Chapter II: AlGaN/ GaN High Electron Mobility Transistors (HEMTs)

II.3.2 Piezoelectric polarization

The total polarization in the structure is given by $P_{total} = P_{sp} + P_{pz}$. The piezoelectric polarization can be calculated by the following Eq. (II.2) [9]

$$P_{pz} = e_{33} \varepsilon_z + e_{31} (\varepsilon_x + \varepsilon_y). \quad (II.2)$$

Where $\varepsilon_z = \left(\frac{c - c_0}{c_0} \right)$ is the strain along the c-axis, and the in-plane strain $\varepsilon_x = \varepsilon_y = \left(\frac{a - a_0}{a_0} \right)$, is assumed to be isotropic, with a_0 and c_0 are the equilibrium values of the lattice parameters, The third independent component of the piezoelectric tensor e_{31} is related to the polarization induced by shear strain, which is not applicable in this device. The relation between the lattice constants of the hexagonal GaN is given by Ambacher *et al.* [9] it can be expressed by Eq. (II.3)

$$\left(\frac{c - c_0}{c_0} \right) = -2 \left(\frac{C_{13}}{C_{33}} \right) \left(\frac{a - a_0}{a_0} \right). \quad (II.3)$$

where C_{13} and C_{33} are elastic constants.

The total piezoelectric polarization in the direction of the c-axis can be determined by Eqs. (II.2) and (II.3) [9]

$$P_{pz} = 2 \left(\frac{a - a_0}{a_0} \right) \left(e_{31} - e_{33} \left(\frac{C_{13}}{C_{33}} \right) \right). \quad (II.4)$$

Since the value of $\left[e_{31} - e_{33} \left(\frac{C_{13}}{C_{33}} \right) \right] < 0$ for AlGaN over the entire range of compositions, the piezoelectric polarization is negative for tensile and positive for compressive strained barriers, respectively [9].

Figure (II.8) shows the trend of the different polarization components. The different magnitudes of P_{sp} and P_{pz} highlight the importance of the choice of a barrier material and of its composition. While large lattice mismatch gives rise to intense piezoelectric

Chapter II: *AlGaN/GaN High Electron Mobility Transistors (HEMTs)*

polarization, its dependence on the stress in the layer makes the 2DEG density sensitive to all stress-releasing processes such as dislocation formation and post-growth annealing. This proves to be a reliability concern and source of process variability. Therefore, barrier materials like $\text{Al}_{1-x}\text{In}_x\text{N}$ which attain a stronger total polarization fields even in close-to-lattice-matched compositions thanks to the spontaneous polarization P_{sp} component, are increasingly employed as better alternatives for the fabrication of rugged HEMTs [10].

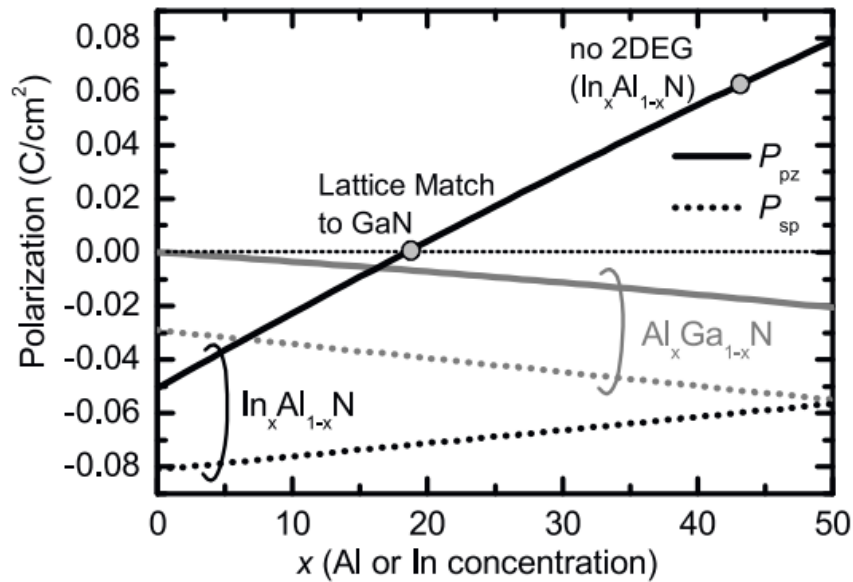


Figure II.8: Spontaneous and piezoelectric polarizations in $\text{Al}_{1-x}\text{In}_x\text{N}$ and $\text{Al}_x\text{Ga}_{1-x}\text{N}$ versus Al mole fraction. The substrate lattice constant is taken as that of relaxed GaN.

GaN based semiconductors are attractive in HEMT designs due to the high piezoelectric constants. The piezoelectric fields developed in GaN devices can create a vertical electric field in the MV/cm range which increases the channel conductivity.

Chapter II: *AlGaN/GaN High Electron Mobility Transistors (HEMTs)*

II.4 High Electron Mobility Transistors (HEMTs)

II.4.1 Background

A transistor is a semiconductor device containing three or more terminals, the main functions of which are to switch electronic signals, or to amplify, owing to the fact that the controlled (output) power can be higher than the controlling (input) power.

In a Field Effect Transistor (FET), there are three terminals, including source (S), through which the carriers enter the channel, Drain (D), through which the carriers leave the channel and Gate (G) the terminal that modulates the channel conductivity. Conventionally, current entering the channel at S is designated by I_s , current entering the channel at D is designated by I_d , Drain-to-source voltage is V_{ds} . By applying voltage to G, one can control I_d [11]. The device consists of an active channel through which charge carriers, electrons or holes, flow from the source to the drain. Source and drain terminal conductors are connected to the semiconductor through ohmic contacts, and the gate terminal through Schottky contact. The conductivity of the channel is a function of the potential applied across the gate and source terminals.

The gate can be separated from the channel by an insulator (as in a MOSFET), can form a p - n junction (JFET), or a Schottky barrier junction with the channel [Metal Semiconductor FET (MESFET)]. The **High Electron Mobility Transistor (HEMT)** is a modification of FET, also known as heterostructure FET (**HFET**), which is a FET incorporating a junction between two materials with different bandgaps as the channel instead of utilizing a doped region. The **HEMT** has other "aliases" such as **TEGFET** (**T**wo-**D**imensional **E**lectron **G**as **F**ield **E**ffect **T**ransistor), **SDFET** (**S**electively **D**oped **F**ield **E**ffect **T**ransistor), and **MODFET** (**M**ODulation **D**oped **F**ield **E**ffect **T**ransistor) [12]. Currently, commonly used material combinations are AlGaN, InAlN and AlN with GaN.

Chapter II: AlGaN/GaN High Electron Mobility Transistors (HEMTs)

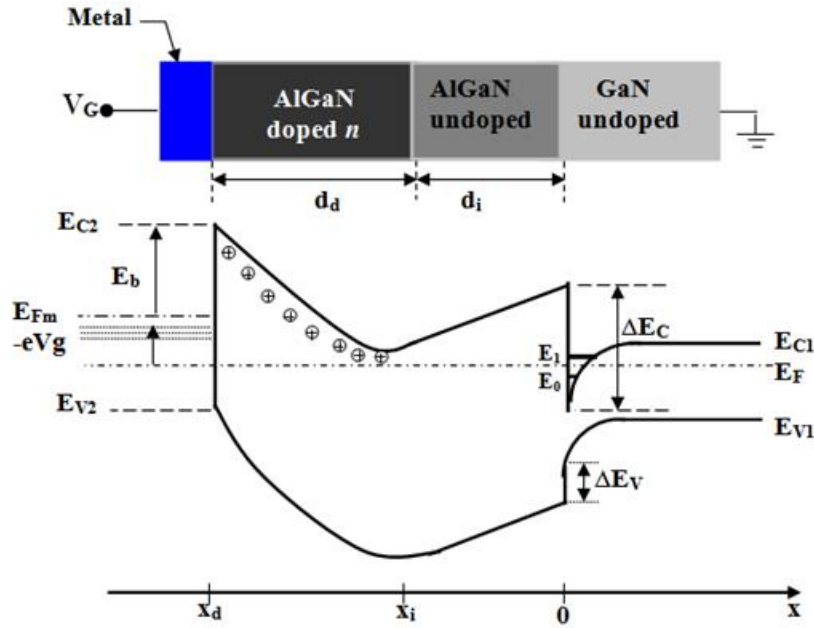


Figure II.9: Schematic diagram showing the energy band structure in $\text{Al}_x\text{Ga}_{1-x}\text{N}/\text{GaN}$ HEMT [13].

The fundamental characteristic of the HEMT structure is the conduction band offset between the materials which construct the barrier and channel layers (see Figure (II.9)).

The barrier layer has a higher conduction band than the channel layer. Due to the large conduction band offset, the electrons diffusing from the large bandgap $\text{Al}_x\text{Ga}_{1-x}\text{N}$ into the smaller bandgap GaN form a Two-Dimensional Electron Gas (2DEG) in the triangular quantum well at the interface which is the Hallmark of a HEMT. In a HEMT, by placing a Schottky barrier gate on the barrier layer, the 2DEG sheet charge concentration can be controlled by applying an appropriate bias.

In 1993, Khan *et al.* demonstrated the first $\text{Al}_x\text{Ga}_{1-x}\text{N}/\text{GaN}$ MODFET (with n-doped barrier layers), with a transconductance of 23 mS/mm and 2DEG mobility of 563 cm^2/Vs at 300 K [14]. They also reported the first microwave results with current gain cut-off frequency (f_t) of 11 GHz and maximum frequency of oscillation (f_{max}) of 14

Chapter II: *AlGaN/GaN High Electron Mobility Transistors (HEMTs)*

GHz [15]. In the early stages, the MODFETs exhibited very low transconductance and relatively poor frequency response. With improvements in the materials quality, however, the transconductance, current capacity and drain breakdown voltage were all increased to the point that GaN based MODFETs were used in the arena of high-power *RF* devices. One of the highest power density achieved for $0.45 \times 125 \mu\text{m}$ GaN MODFET was 6.8 W/mm at 10 GHz and associated gain of 10.65 dB [16]. The operation temperature was pushed to 750 °C by using a thermally stable Pt/Au gate contact [17].

II.4.2 $\text{Al}_x\text{Ga}_{1-x}\text{N}/\text{GaN}$ HEMT devices structure

Typical $\text{Al}_x\text{Ga}_{1-x}\text{N}/\text{GaN}$ HEMT devices structure is schematically provided in Figure (II.10). HEMT operates on the basis of charge accumulation. HEMT similar to other FETs is a three terminal device containing source, drain and gate contacts as shown in Figure (II.10). The current between source and drain can be controlled by the gate voltage and flows through the two dimensional conducting channel formed by 2DEG.

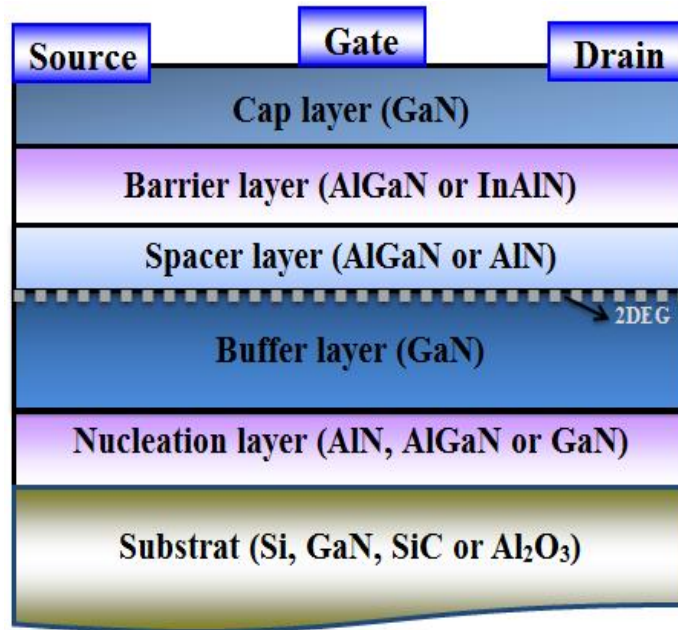


Figure II.10: The schematic of a typical HEMT devices structure.

Chapter II: *AlGaN/GaN High Electron Mobility Transistors (HEMTs)*

If gate voltage is increased more towards to negative values (threshold voltage, V_{th}), 2DEG region is depleted under gate and the flow of current between source and drain is decreased until the channel is pinched-off, this $Al_xGa_{1-x}N/GaN$ HEMT operates in the depletion mode (normally-on). When the threshold voltage is adjusted to be positive values, HEMT operates in the enhancement mode (normally-off). Changing the mode of operation depends on both epitaxial structure and fabrication technique [18].

The typical layers are from top to bottom as follows:

- ☑ **Cap layer:** is used to reduce the gate leakage, increase the ohmic contact resistance and increase the Schottky barrier height. It also prevents surface from oxidation.
- ☑ **Barrier layer:** is the most crucial layer of the HEMT structures. It is the wider bandgap material forming the 2DEG at the channel interface. Thickness and Al fraction affects the 2DEG properties. Increasing Al mole fraction up to a certain level results in an increase in the 2DEG sheet carrier concentration. In addition, the thickness should be above a critical thickness on the other hand it should be below where the relaxation occurs [19, 20].
- ☑ **Spacer layer:** is a very thin layer placed between buffer and barrier layers, to increase the sheet carrier concentration through the elimination of alloy disorder scattering and the reduction of interface roughness scattering. Moreover, the spacer layer decreases the Coulomb scattering between 2DEG electrons and their ionized parent atoms in the supply layer resulting in an increase in the 2DEG mobility [21 - 23].
- ☑ **Buffer layer:** is the layer consists of a material with a lower bandgap than barrier layer. Highly resistive GaN or semi-insulating GaN can be used for this purpose. This layer should have low defect density and a smooth surface. Besides, it determines the

Chapter II: *AlGaN/GaN High Electron Mobility Transistors (HEMTs)*

properties of HEMT device such as buffer leakage, drain current collapse, output power reduction, pinch-off voltage and breakdown voltage values. [24, 25].

Highly resistive or semi-insulating GaN buffer layer is necessary to obtain HEMT devices with a good performance. Typically unintentionally doped GaN grown by MOCVD shows *n*-type conductivity due to the residual donors. These residual donors have to be compensated to achieve highly resistive or semi-insulating GaN. Widely used method for this purpose is creating deep acceptor states by intentional doping the GaN layers with Iron (Fe), Chromium (Cr) and Carbon (C). The other approach is introducing dislocations or carbon impurities to achieve highly resistive GaN buffer layer [26-28].

☑ **Nucleation layer:** is depends on the choice of the substrate. Very thin AlN, $\text{Al}_x\text{Ga}_{1-x}\text{N}$ or GaN layers can be used. Generally, low temperature GaN or two step AlN layers are used for SiC substrates. Nucleation layer acts as a template between GaN buffer layer and SiC substrate releasing strain due to the lattice mismatch in between. There are different routes for the deposition of nucleation layers [29].

☑ **Substrate:** Si, GaN, SiC and Al_2O_3 can be used as epitaxial substrates for the deposition of GaN. 6H-SiC is preferred due to the small lattice mismatch and its high thermal conductivity.

☑ **Schottky contact (Gate):** is the main transport mechanism in rectifying contacts is thermionic emission which allows electrons to move over the Schottky barrier. For wide bandgap materials such as GaN, the barrier height is strongly influenced by the work function of the contact metal. For GaN based semiconductors, metals with high work functions are generally used to fabricate Schottky contacts [30, 31]. In HEMT, the gate contact is a Schottky contact. A voltage applied to the gate modulates the 2DEG carrier density at the $\text{Al}_x\text{Ga}_{1-x}\text{N}/\text{GaN}$ interface, and so modulates the drain to

Chapter II: *AlGaN/ GaN High Electron Mobility Transistors (HEMTs)*

source current. For conventional HEMTs, the gate has a negative bias (is not forward biased).

☑ **Ohmic contact (Source/Drain):** is defined as one in which there is unimpeded transfer of majority carriers from one material to another, i.e., the contacts do not limit the current. The contact resistance between the metal and semiconductor is dependent on the doping concentration of the semiconductor, engineering of the interface structures and unintentionally formed interface states. It is very important to form very low contact resistance, R_c , for Field-Effect Transistors (FETs) in order to achieve excellent DC and RF performances. It is generally very difficult to realize Ohmic contacts with very low R_c in wide bandgap materials due to the low work functions and hence small electron affinity of such materials; meaning that the barrier height (Φ_B) of the metal/semiconductor is generally higher [32]. In general, there are two ways of overcoming the Ohmic contact issues on $\text{Al}_x\text{Ga}_{1-x}\text{N}/\text{GaN}$:

1. Forming a low barrier height at the metal/semiconductor interface in order to allow the thermionic emission effect, and/or
2. Forming a very thin barrier at or near the bottom of the conduction band to allow thermally excited electrons to be tunneled directly.

II.4.3 Growth techniques and substrates choice

A°) Growth techniques of GaN based epilayers

The growth of good quality GaN based binary and ternary heterostructures is important for the production of high performance HEMT devices. III-nitrides can be grown by metal organic chemical vapor deposition (MOCVD) or molecular beam epitaxy (MBE). MOCVD has been the most commonly used technique for developing GaN based epilayers and is carried out at temperatures in excess of 1000°C and involves gaseous reactants (such as trim-ethyl-gallium and NH_3) passing over a heated substrate which react to form a condensed layer or film on the substrate. Growth rates

Chapter II: *AlGaN/GaN High Electron Mobility Transistors (HEMTs)*

are typically between $(1 - 2) \mu\text{m}$ per hour. MBE on the other hand, is a slower process with growth rates typically between $(0.5 - 1) \mu\text{m}$ per hour and is carried out at lower temperatures compared to MOCVD ($(500 - 900)^\circ\text{C}$). MBE uses solid Ga and Al sources along with NH_3 and occurs via reactions between thermal-energy molecular, atomic, or ionized beams of the constituent elements on a heated substrate in an ultra-high vacuum. MBE also offers the advantage of precise definition at the interfaces and also flexibility of the polarity of the GaN [33].

B°) Substrate choice for AlGaN/GaN HEMTs

One of the key challenges in the development of GaN HEMT technology is the selection of substrate materials which provide high-quality GaN epitaxy with low density of impurities and excellent thermal conductivity in order to dissipate heat generated during device operation.

Table II.1: Comparison of different substrate materials used for GaN [34].

Material	Symmetry	Lattice mismatch to GaN	Thermal Conductivity at 300K (W/cm K)	Thermal Expansion Coefficient mismatch	Wafer Size and Cost
GaN	Wurtzite	0%	1.3	0%	2" Very Expensive
Sapphire	Hexagonal	14%	0.3	34%	Up to 8" Moderate Cost
6H-SiC	Wurtzite	3.5%	4.9	25%	Up to 6" Expensive
Si	Cubic	-17%	1.3	56%	Up to 12" Low Cost

AlGaN/GaN epilayers are usually heteroepitaxially grown, most commonly on sapphire, SiC and Si due to the difficulty and significant cost involved in producing

Chapter II: *AlGaN/GaN High Electron Mobility Transistors (HEMTs)*

large amounts of stand-alone GaN. Gallium nitride would be the preferred substrate as it would reduce the density of defects and there would be no lattice mismatch. Table (II.1) lists some of the properties of the substrates which are relevant and important when designing high power electronic devices. These substrates will be discussed below.

Silicon (Si)

Si has a reasonable cost and an acceptable thermal conductivity which is similar to bulk crystalline GaN, but is inferior to that of SiC and sapphire. In order to achieve the growth of high quality GaN on Si (111), the lattice misfit (~17%) and thermal expansion coefficient (TEC) mismatch between Si and GaN must be overcome. In addition, the thermal stability of Si at typical GaN growth temperature is also inferior to SiC and sapphire. GaN grows on Si substrate with a tensile stress since Si has a larger lattice constant than GaN, which leads to the creation of crystal defects, degrading the performance of the device. In order to overcome the impact of the inherent properties in Si on epitaxial crystal quality, a nucleation layer is applied to ensure good GaN-on-Si crystal quality [35,36].

Silicon carbide (SiC)

Of the three foreign substrate materials, SiC is the most mature and best lattice matched to GaN. It has the appealing property of high thermal conductivity (4.9 W/cm K) which is particularly useful for high power electronics, and relatively low thermal expansion coefficient (TEC) mismatch (25%). Although the lattice mismatch is small (3.5%), it is still significant enough to create a large number of defects in the GaN layers ($10^8 - 10^{10} \text{ cm}^{-2}$), which can lead to reduced performance of fabricated devices [33]. Of the three substrate materials it is by far the most expensive but despite this, SiC is generally regarded as the best material on which to grow GaN and produce powerful electronic devices. It is the substrate of choice for most commercial RF GaN devices.

Chapter II: *AlGaN/GaN High Electron Mobility Transistors (HEMTs)*

Sapphire (Al_2O_3)

Sapphire is cheap and available in wafers with large diameters, so it is one of the more commonly employed substrates. However, it has the largest lattice misfit (~14%) and thermal expansion coefficient mismatch with GaN (the thermal mismatch varies from 14 to 26%, depending on the their relative orientation of the crystals). Another main drawback of this substrate is its poor thermal conductivity (0.3 W/cm K) compared to SiC (4.9 W/cm K), which severely limits its use in applications where efficient dissipation of heat is required. The exceptionally high current in 2DEG channel of GaN power devices produces significant amount of heat during device operation. Poor thermal conductivity can cause device overheating and degrade the device performance, even during I-V sweeps. With the development of GaN epitaxy technology, GaN-on-sapphire is being replaced by GaN-on-Si and GaN-on-SiC for HEMTs fabrication.

II.5 HEMTs operation

The main purpose of a HEMT is to either switch electronic signals or to amplify them (as a standalone device or part of a larger amplifier circuit). Figure (II.11) shows the output current vs. voltage characteristic for a depletion mode HEMT. This figure is for illustrative purposes only and will be used as an aid for describing the operation of the device.

The most common way to bias a HEMT is in the common source configuration as shown in the inset of Figure (II.11). The gate electrode is the input whilst the drain electrode is the output and the source is the common terminal. The gate input signal acts as the control signal of the device and has the ability to switch the device on and off. In a depletion mode device the switching off requires the application of a negative voltage to deplete the channel of electrons which will result in a highly resistive channel where no current will flow, this is known as “*pinch-off*”.

Chapter II: AlGaN/GaN High Electron Mobility Transistors (HEMTs)

The expression which relates the number of carriers in the channel to the applied bias voltage is given by modeling the 2DEG - metal gate as a capacitor [37].

$$n_s = \frac{\epsilon_{AlGaN}}{q(d_{AlGaN} + \Delta d)} (V_{gs} + V_{th}). \quad (II.5)$$

Where n_s is the charge density per unit area of the 2DEG, d_{AlGaN} is the thickness of the $Al_xGa_{1-x}N$ barrier layer, Δd is the effective distance of the 2DEG from the hetero-interface, V_{gs} is the gate bias voltage and V_{th} , known as the threshold voltage, is some negative value of gate voltage at which the device begins to conduct current.

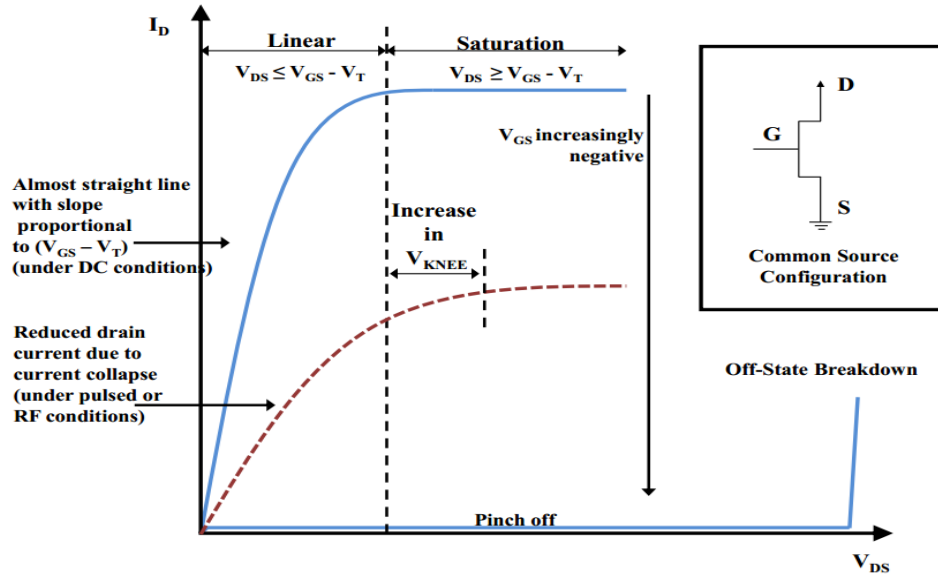


Figure II.11: Description of I - V transistor characteristics, inset shows common source configuration for a HEMT [34].

II.5.1 DC characteristics

The regimes of operation where the HEMTs can provide an advantage over other technologies are high-current, high-voltage RF operation modes. Drain current densities can exceed 2 A/mm, at drain voltages higher than 10 V. With significant DC powers being dissipated, the strong electric field and the high local temperatures

Chapter II: AlGaN/GaN High Electron Mobility Transistors (HEMTs)

involved create several non-idealities which can be identified in the I - V characteristics of a device. Figure (II.12) shows drain current *vs.* drain voltage ($I_D - V_{DS}$) curves for different values of gate-source voltage (V_{GS}) in the ideal case (solid lines) compared to some real measurements (dotted lines). The main differences between the standard saturated current model and real measurements are highlighted.

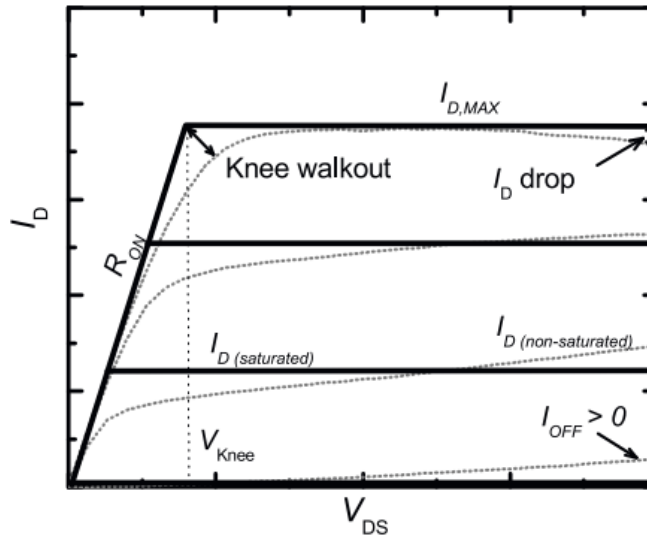


Figure II.12: Model (solid lines) and typical DC (dotted lines) I - V characteristics of a HEMT. Most of the common non idealities in GaN-based HEMTs are highlighted [38].

Heating due to the significant DC currents can generate a drop in the maximum drain current ($I_{D,MAX}$). Trapping can lead to a non-sharp transition from the linear to the saturation regime (knee walkout), making the knee voltage (V_{Knee}) loosely defined. Short-channel effects can produce finite output conductance, and prevent a complete turn off of the transistor ($I_{OFF} > 0$). Loss of channel control can also produce non saturating I_D with increasing drain-source voltages (V_{DS}) for V_{GS} values close to pinch-off. In the saturated velocity (v_{sat}) approximation, one can write $I_{D,MAX} = q \cdot v_{sat} \cdot n_s$: it follows that achieving high maximum currents require high 2DEG densities which are attained with stronger polarization field and thicker barriers. Besides driving high

Chapter II: AlGaN/GaN High Electron Mobility Transistors (HEMTs)

currents, a high-performance HEMT should provide high gain both in RF and DC mode of operation. In DC, the gain is represented by the transconductance (g_m). The saturated velocity model tells us that

$$g_{m,int} = \frac{v_{sat} \cdot C_{gs}}{L_g}. \quad (II.5)$$

where C_{gs} is the gate-source capacitance, and L_g is the gate length. Because C_{gs} becomes smaller with decreasing L_g , scaling down the gate lengths does not produce an increase in transconductance. In deeply scaled gate lengths the proportionality between C_{gs} and L_g become dominated by fringing capacitances [38].

Thinner barrier layers lead to higher transconductance, but then to provide reduced 2DEG densities. The loss of electron density can be avoided by increasing the polarization sheet charge density (σ_{pol}), which is mostly a material-dependent parameter. This is one of the main reasons why research on GaN-HEMTs has increasingly focused on materials with strong total polarization fields even in thinner layers, shifting from AlGaN based barrier layers to other nitrides like AlInN and AlN.

II.5.2 Degradation of HEMT performances

A°) Current collapse

The theoretical maximum output power that can be given by a HEMT can be estimated from its $I-V$ output characteristics (for a sinusoidal current about a quiescent DC bias) by [45]

$$P_{Out} = \frac{1}{8} I_{D,MAX} \times (V_{BR} - V_{Knee}). \quad (II.6)$$

where $I_{D,MAX}$ is the maximum drain current, V_{BR} is the breakdown voltage of the device and V_{Knee} is the voltage at which the I-V curves transitions from the linear to the

Chapter II: *AlGa_xN/GaN High Electron Mobility Transistors (HEMTs)*

saturation region. It has been shown experimentally, however, that under RF or pulsed conditions, the drain current is temporarily reduced [39] (see Figure II.13).

This decrease in output current is a direct result of traps which exist at the surface and in deep levels (see Figure II.13) which reduce the number of electrons available in the channel [40]. This effect also has the consequence of increasing the knee voltage of the device since the effective on-resistance is increasing in the channel (whilst the current is decreasing). This phenomenon is often referred to as dispersion, current collapse and/or current slump/compression.

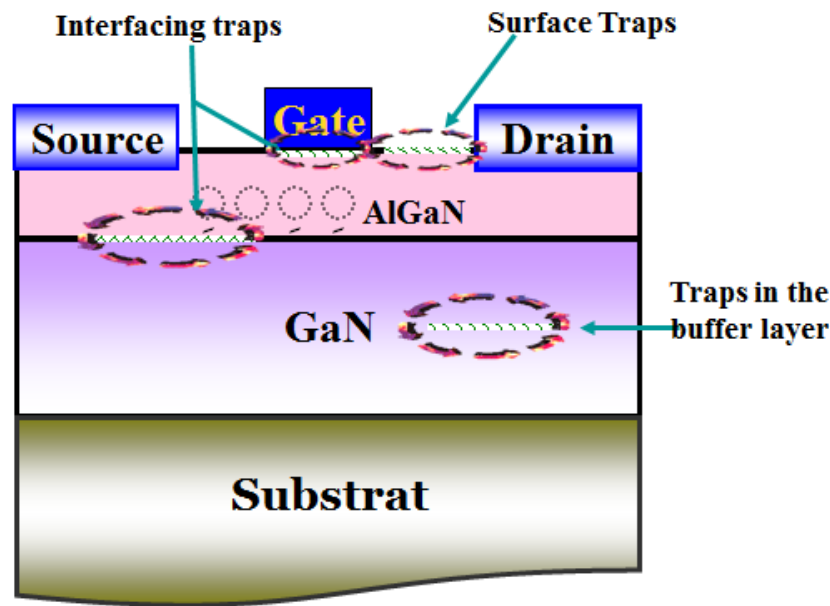


Figure II.13: Al_xGa_{1-x}N/GaN HEMTs structure with surface, interface and buffer layer traps [13].

B^o) Gate leakage

The gate leakage is an important effect parameter that the off-state leakage current can be kept to a minimum in any transistor configuration, particularly when they are incorporated into circuits and systems where low (negligible) off-state power consumption is desirable. Gate leakage is generally measured between the gate and the

Chapter II: *AlGaN/GaN High Electron Mobility Transistors (HEMTs)*

drain and it has been proposed that there are two possible tunneling leakage paths in $\text{Al}_x\text{Ga}_{1-x}\text{N}/\text{GaN}$ HEMTs: vertical through the main gate area and lateral from the edge of the gate [41]. Techniques such as surface passivation using SiO_2 [42] or Si_3N_4 [43], a GaN cap layer [41] and a post gate anneal [44] have all shown to be effective in suppressing the gate leakage current from these devices.

C°) Frequency dispersion

The reduction in device output power due to current collapse is enhanced during high frequency operation and is further exacerbated when a large input signal is applied at the gate in order to increase power added efficiency (PAE) of the power transistor. This effect, named as frequency dispersion, is another mechanism that limits the device output power [45]. The measured output power of the device would be smaller than that predicted by DC I - V characteristic. Such a mechanism is also one of the main reasons that cause the discrepancy between the measured DC I - V and pulsed I - V characteristics since pulsed I - V characteristic is usually measured with large pulse amplitudes and pulse width smaller than μ_s range.

D°) Hot-electron effect

One well-known failure mechanism of early GaAs-based devices was hot electron-induced degradation [46 - 48]. Under higher drain bias, the accelerated electrons gain a great deal of enough energy in the channel and may be trapped on the device surface, in the AlGaN barrier layer or in the GaN buffer layer. This can lead to a shift in threshold voltage, an increase in drain resistance and a reduction in drain saturation current [49, 50]. Hot-electron induced degradation has been observed in AlGaN/GaN HEMTs with SiN_x and SiO_2 passivation on sapphire and SiC substrates under DC and RF stress conditions. With high drain bias and high input drive, hot electrons are created in the region between the gate and drain, and generate permanent traps which cause increased surface depletion, increased series resistance, and reduced

Chapter II: AlGaN/GaN High Electron Mobility Transistors (HEMTs)

gate-drain electric field. Not only can hot-electrons be trapped but they can also induce trap formation at surface region between gate and drain. In a 3000-hour test on AlGaN/GaN HEMTs under on-state and off-state conditions, a decrease of the drain current and transconductance, and an increase of the channel resistance were observed by Sozza *et al.* Through the use of low frequency techniques, they were able to attribute the increase in traps density at the surface between the gate and drain to hot-electrons present in the channel [51]. To avoid degradation by hot-electrons caused by the presence of high electric field in the gate-drain region, proper solutions are needed such as by adopting surface passivation and field plate.

E°) Inverse piezoelectric effect

Recently, another degradation mechanism was proposed by Joh and del Alamo [52,53], crystallographic defects formed through inverse piezoelectric effect in GaN-based HEMTs. Due to the lattice mismatch between AlGaN and GaN, there is a great deal of elastic energy stored in AlGaN/GaN heterostructure even in absence of bias. Typically, AlGaN on GaN is under tensile strain [54]. When tensile mechanical strain was applied on devices intentionally during electrical stress, a 1 to 3V lower value of critical voltage was found compared to control samples [55]. During device operation under high drain bias, a large electric field appears around the drain-side of the gate edge across barrier layer. This induces a large amount of mechanical stress, which would trigger the formation of crystallographic defects and relaxation of the strain when the electric field reaches a certain value. Those defects behave as traps, which degrade carrier transport properties and carrier concentration in the channel, resulting in increasing of drain resistance and decreasing of saturation drain current and transconductance. The gate leakage current is increased as well through trap-assisted tunneling in the barrier layer.

II.5.3 Breakdown mechanisms

The mechanisms causing breakdown in $\text{Al}_x\text{Ga}_{1-x}\text{N}/\text{GaN}$ HEMTs is a complex issue and one in which there is no unified theory in the literature. Ideally, for a gate-to-drain separation of $1\text{ }\mu\text{m}$, a drain voltage of around 300 V could be applied for breakdown to occur. In reality though, a three terminal $\text{Al}_x\text{Ga}_{1-x}\text{N}/\text{GaN}$ HEMTs does not reach this theoretical limit. The most common theory in the literature which explains breakdown is attributed to impact ionization although thermal runaway has also been suggested in [56]. The impact ionization stems from electrons leaking from the gate into the semiconductor which then gain enough energy from a high electric field at the drain-edge of the gate to cause ionization of surrounding atoms.

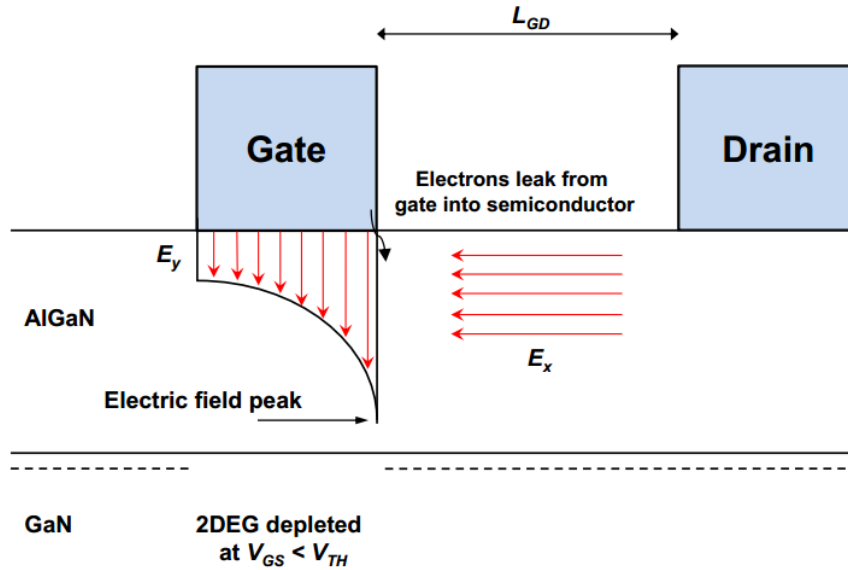


Figure II.14: Cross section of area beneath gate in AlGaN/GaN HEMT. Large electric field peak is shown at the drain-edge of the gate. Electrons from the gate leak into the semiconductor at $V_{GS} < V_{TH}$ which are given enough energy by the electric field to cause impact ionization and subsequent breakdown of the device.

In the off-state, the gate of the HEMT is reverse biased such that $V_{GS} < V_{TH}$ and consequently the channel directly beneath the gate should be fully depleted of

Chapter II: *AlGaN/GaN High Electron Mobility Transistors (HEMTs)*



electrons. At this point the channel of the device will be highly resistive and no current shall flow from the source to the drain. As the drain voltage is increased, the depletion region expands laterally from the gate edge towards the drain and the depleted charge from this region is imaged on the gate [57]. The resulting charge distribution is such that the electric field peaks at the drain-edge of the gate as is shown in Figure (II.14). It is widely accepted that this electric field at the drain-edge of the gate causes electrical degradation to AlGaN/GaN HEMTs [57-61].

The off-state breakdown mechanisms can be summarized in the following way:

1. Leakage electrons tunnel from the gate electrode to the channel at gate pinch off and positive drain bias.
2. By increasing the drain bias voltage, the electric field at the drain-edge of the gate increases and so the electrons (which have leaked from the gate) will acquire enough energy to cause impact ionization which leads to an avalanche effect and a sharp rise in drain current.
3. An increase in temperature results in a higher breakdown voltage since impact ionization requires higher energy due to a reduced electron mean free time.

The off-state breakdown voltage is commonly defined as when the gate current reaches 1 mA/mm which happens to be a strong function of the electric field at the gate [57].

II.6 Summary

Gallium nitride (GaN) is recognized as the key for next-generation amplifier technology applications. This is motivated by their potential in commercial and military applications. The factors that limit GaN transistors performance are primarily current collapse and gate leakage.

Chapter II: *AlGa_xN/GaN High Electron Mobility Transistors (HEMTs)*

In order to obtain devices with high performance for both high power and high frequency applications, following parameters must be adjusted accordingly:

- ☑ Buffer leakage; highly resistive buffer layers with low leakage and low defect density.
- ☑ Breakdown voltage (V_{BR}); high quality material, proper surface passivation, low buffer leakage.
- ☑ Carriers sheet density (n_s); high Al mole fraction of the barrier layer $\text{Al}_x\text{Ga}_{1-x}\text{N}$ without strain relaxation to maximize the polarizations (both P_{sp} and P_{pz}).
- ☑ Electron velocity (v); reducing effective gate length (L_g) and gate length extension.
- ☑ Electron mobility (μ); reducing of scattering centers due to dislocations, interface roughness and alloy disordering at the heterojunction.
- ☑ Thermal conductivity; proper substrate to remove the generated heat during operation.
- ☑ Minimizing short-channel effect.
- ☑ Conductivity; maximizing $n_s \times \mu$ product.

$\text{Al}_x\text{Ga}_{1-x}\text{N}/\text{GaN}$ HEMT devices are most promising for the integrated high-speed, high-efficiently, high-power and high-temperature operations. Moreover, $\text{Al}_x\text{Ga}_{1-x}\text{N}/\text{GaN}$ HEMT devices show great potential in commercial and military applications, e.g., the area of communication and telecommunication systems, base stations market, as well as radar, W-CDMA mobile-phone applications and sensor applications.

References

- [1] C. Y. Yeh et al., "Zinc-blende- wurtzite polytypism in semiconductors", *Phys. Rev. B*, vol. **46**, n°.16, pp.10086-10097, 1992.

Chapter II: *AlGaN/GaN High Electron Mobility Transistors (HEMTs)*

- [2] T. Zhu and R.A. Oliver, "Unintentional doping in GaN", *Phys. Chem. Chem. Phys.*, vol. **14**, n°.10, pp.9558-9573, 2012.
- [3] J. Wu et al., "Superior radiation resistance of InGaN alloys: Full-solar-spectrum photovoltaic material system", *J. Appl. Phys.*, vol. **94**, n°.10, pp.6477-6480, 2003.
- [4] H. Morkoc, W. Verlag, "Unintentional doping in GaN Handbook of Nitride Semiconductors and Devices", vol.1, ISBN: 978-3-527-40837-5, pp.1–1311, 2008.
- [5] A. Belabbes et al., "Electronic properties of polar and nonpolar InN surfaces: A quasiparticle picture", *Phys. Rev. B*, vol. **85**, n°.11, p.115121, 2012.
- [6] F. Schwier, Liou, J. Juin, "Modern Microwave Transistors: Theory, Design, and Performance", *John Wiley & Sons*, 2002.
- [7] S. De Meyer, "Étude d'une nouvelle filière de composants HEMTs sur technologie nitrure de gallium, conception d'une architecture flip-chip d'amplificateur distribué de puissance à très large bande", *PhD thesis in electrical engineering, University of Limoges*, p.216, 2005.
- [8] A.H. Jardndal, "Large Signal Modelling of GaN Device for High Power Amplifier Design", *PhD thesis, University of Kassel: Kassel*, 2007.
- [9]. O. Ambacher, B. Foutz, J. Smart, J. R. Shealy, N. G. Weimann, K. Chu, M. Murphy, A. J. Sierakowski, W. J. Schaff, L. F. Eastman, R. Dimitrov, A. Mitchell and M. Stutzmann, "Two dimensional electron gases induced by spontaneous and piezoelectric polarization in undoped and doped AlGa_N/Ga_N heterostructures", *J. Appl. Phys.*, vol. **87**, n°.1, pp.334-344, 2000.
- [10] D. Maier, M. Alomari, N. Grandjean, J.F. Carlin, M. Dufort-Poisson, C. Dua, S. Delage, and E. Kohn, "InAlN/GaN HEMTs for operation in the 1000 °C regime: A first experiment", *Electron Device Letter. IEEE*, vol. **33**, n°.7, pp. 985–987, 2012.

Chapter II: *AlGaN/GaN High Electron Mobility Transistors (HEMTs)*

- [11] J. Millman, "Electronic devices and circuits", *Singapore : McGraw-Hill international book company*, p.384, 1985
- [12] W. Liu, "Fundamentals of III-V Devices: HBTs. MESFETs. and FETs/HEMTs", *John Wiley and Sons, New York*, 1999.
- [13] D. Bouguenna, " Etude Comparative et Modélisation des Transistors à Effet de Champ MODFETs et MOS-MODFETs à base de Nanostructure de Nitrures III-V $\text{Al}_x\text{Ga}_{1-x}\text{N}/\text{GaN}$ Cubique", *PhD thesis, University of Oran*, 2014.
- [14] M.A. Khan, J. Kuznia, D.T. Olson, W. Schaff, J. Burm, and M. Shur, "Microwave performance of a 0.25 μm gate AlGaN/GaN heterostructure field effect transistor", *Appl. Phys. Lett*, vol. **65**, n°.9, pp.1121–1123, 1994.
- [15] J.N.K. M. Asif Khan, A. Bhattarai and D.T. Olson, "High electron mobility transistor based on a GaN/ $\text{Al}_x\text{Ga}_{1-x}\text{N}$ heterojunction", *Appl. Phys. Lett*, vol. **63**, n°.9, p.1214, 1993.
- [16] S. Sheppard, K. Doverspike, W. Pribble, S. Allen, J. Palmour, L. Kehias, and T. Jenkins, "High-power microwave GaN/AlGaN HEMTs on semi-insulating silicon carbide substrates", *IEEE Electron Device Letters*, vol. **20**, n°.4, pp.161–163, 1999.
- [17] I. Daumiller, C. Kirchner, K. Kamp, K. Ebeling, L. Pond, C. Weitzel, and E. Kohn, "Evaluation of AlGaN-GaN HFETs up to 750 °C", *56th Annual Device Research Conference Digest*, pp.114 –115, 1998.
- [18]. R. Wang, "Enhancement/depletion-mode HEMT technology for III-nitride mixed-signal RF applications", *PhD thesis, The Hong Kong University of Science and Technology*, 2008.
- [19] H. Morkoc, "Nitride Semiconductors Devices", *Springer Berlin Heidelberg*, vol. **32**, 1999.

Chapter II: AlGaN/GaN High Electron Mobility Transistors (HEMTs)

- [20] Y. Koide, H. Itoh, M.R.H. Khan, K. Hiramatu, N. Sawaki, and I. Akasaki, "Energy bandgap bowing parameter in an $\text{Al}_x\text{Ga}_{1-x}\text{N}$ alloy", *J. Appl. Phys.*, vol. **61**, n°.9, p.4540, 1987.
- [21] L. Guo, X.X. Wang, C. Wang, H. Xiao, J. Ran, W. Luo, B. Wang, C. Fang, and G. Hu, "The influence of 1nm AlN interlayer on properties of the $\text{Al}_{0.3}\text{Ga}_{0.7}\text{N}/\text{AlN}/\text{GaN}$ HEMT structure", *Microelectronics J*, vol. **39**, n°.5, pp.777–781, 2008.
- [22] Z.Y. Ma, Z.L. Wang, G.X. Hu, J.X. Ram, H.L. Xiao, W.J. Luo, J. Tang, J.P. Li, and J.M. Li, "Growth and characterization of AlGaN/AlN/GaN HEMT structures with a compositionally step-graded AlGaN barrier layer", *Chinese Phys. Lett*, vol. **24**, n°.6, pp.1705–1708, 2007.
- [23] L. Shen, S. Heikman, B. Moran, R. Coffie, N.Q. Zhang, D. Buttari, I. Smorchkova, S. Keller, S. DenBaars, and U. Mishra, "AlGaN/AlN/GaN high-power microwave HEMT", *IEEE Electron Device Lett*, vol. **22**, pp.457–459, 2001.
- [24] X. Wu, P. Fini, S. Keller, E. Tarsa, B. Heying, U. Mishra, S. DenBaars, and J. Speck, "Morphological and structural transitions in GaN films grown on sapphire by metal-organic chemical vapor deposition", *Jpn. J. Appl. Phys.*, vol. **35**, n°.12B, pp.1648–1651, 1996.
- [25] L. Eastman, V. Tilak, J. Smart, B. Green, E. Chumbes, R. Dimitrov, O. Ambacher, N. Weimann, T. Prunty, M. Murphy, W. Schaff, and J. Shealy, "Undoped AlGaN/GaN HEMTs for microwave power amplification", *IEEE Trans. Electron Devices*, vol. **48**, n°.3, pp.479–485, 2001.
- [26] I. Akasaki and H. Amano, "Crystal growth and conductivity control of group III nitride semiconductors and their application of short wavelength emitters", *Japan*, vol. **36**, n°.9A, pp.5393-5408, 1997.

Chapter II: AlGaN/GaN High Electron Mobility Transistors (HEMTs)

- [27] S. Heikman, S. Keller, S.P. Den Baars, and U.K. Mishra, "Growth of Fe doped semi-insulating GaN by metalorganic chemical vapor deposition", *Appl. Phys. Lett.*, vol. **81**, n°.3, p.439, 2002.
- [28] A. Grzegorzczuk, L. Macht, P. Hageman, J. Weyher, and P. Larsen, "Influence of the nucleation layer morphology and epilayer structure on the resistivity of GaN films grown on c-plane sapphire by MOCVD", *J. Cryst. Growth*, vol. **273**, n°.3-4, pp.424–430, 2005.
- [29] M. Rudzinski, "GaN grown on SiC by MOCVD", *PhD thesis, Radboud University Nijmegen*, 2008.
- [30] S. Kolluri, S. Keller, S. P. DenBaars, and U.K. Mishra, "Microwave power performance N-polar GaN MIS-HEMTs grown by MOCVD on SiC substrates using an etch-stop technology", *IEEE Electron Device Letters*, vol. **33**, n°.1, pp.44–46, 2012.
- [31] A. Stocker, E. Schubert, and J. Redwing, "Crystallographic wet chemical etching of GaN", *Appl. Phys. Lett.*, vol. **73**, n°.18, pp.2654–2656, 1998.
- [32] C.H. Chen and S. Keller, "Cl₂ reactive ion etching for gate recessing of AlGaIn/GaN field effect transistors", *Journal of Vacuum Science and Technology B*, vol. **17**, n°.6, pp.2755–2758, 1999.
- [33] R. Quay, "Gallium Nitride Electronics". *Springer*, 2008.
- [34] D.J. Macfarlane, "Design and fabrication of AlGaIn/GaN HEMTs with high breakdown voltages", *PhD thesis, School of Engineering, University of Glasgow*, 2014.
- [35] E. Feltin, B. Beaumont, M. Laugt, P. de Mierry, P. Vennéguès, H. Lahrechè, M. Leroux, and P. Gibart, "Stress control in GaN grown on silicon (111) by metalorganic vapor phase epitaxy", *Appl. Phys. Lett.* vol. **79**, n°.20, p.3230, 2001.

Chapter II: AlGaN/GaN High Electron Mobility Transistors (HEMTs)

- [36] A. Dadgar, M. Poschenrieder, J. Blasing, K. Fehse, A. Diez, and A. Krost, "The origin of stress reduction by low-temperature AlN interlayers", *Appl. Phys. Lett*, vol. **80**, n°.15, p.3670, 2002.
- [37] S. Taking, "AlN/GaN MOS-HEMTs Technology", *PhD thesis, School of Engineering, University of Glasgow*, 2012.
- [38] S. Tirelli, "GaN-based HEMTs for High Power RF Applications", *PhD thesis, University of Pisa*, 2014.
- [39] R. Vetury, N.Q. Zhang, S. Keller, and U.K. Mishra, "The impact of surface states on the DC and RF characteristics of AlGaN/GaN HFETs", *IEEE Transactions on Electron Devices*, vol. **48**, n°.3, pp.560–566, 2001.
- [40] L.F. Eastman, "Results, potential and challenges of high power GaN-based transistors", *Solid State Physics*, vol. **176**, n°.1, pp.175–178, 1999
- [41] E.J. Miller, X.Z. Dang, and E.T. Yu, "Gate leakage current mechanisms in AlGaN/GaN heterostructure field effect transistors", *Journal of Applied Physics*, vol. **88**, n°.10, pp.5951–5958, 2000.
- [42] C. Kirkpatrick, B. Lee, R. Suri, X. Yang, and V. Misra, "Atomic layer deposition of SiO₂ for AlGaN/GaN MOS-HFETs", *IEEE Electron Device Letters*, vol. **33**, n°.9, pp.1240–1242, 2012.
- [43] M. Kuroda, T. Murata, S. Nakazawa, T. Takizawa, M. Nishijima, M. Yanagihara, T. Ueda, and T. Tanaka, "High f_{\max} with high breakdown voltage in AlGaN/GaN MIS-HFETs using in-situ SiN as gate insulators", *IEEE Compound Semiconductor Integrated Circuits Symposium*, pp.1–4, 2008.
- [44] H. Kim, J. Lee, D. Liu, and W. Lu, "Gate current leakage and breakdown mechanism in unpassivated AlGaN/GaN high electron mobility transistors by post-gate annealing", *Appl. Phys. Lett*, vol. **86**, n°.14, pp.143505, 2005.

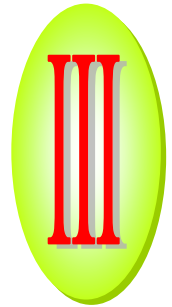
Chapter II: AlGa_N/Ga_N High Electron Mobility Transistors (HEMTs)

- [45] E. Kohn, I. Daumiller, P. Schmid, N.X. Nguyen, and C.N. Nguyen, "Large signal frequency dispersion of AlGa_N/Ga_N heterostructure field effect transistors", *Electron. Lett*, vol. **35**, n°.12, pp.1022-1024, 1999.
- [46] G. Meneghesso, G. Verzellesi, F. Danesin, F. Rampazzo, F. Zanon and A. Tazzoli, et al., "Reliability of Ga_N high-electron-mobility transistors: state of the art and perspectives", *IEEE Trans. Dev. Mater. Reliab.* vol. **8**, n°.2, p.332, 2008.
- [47] A. Watanabe, K. Fujimoto, M. Oda, T. Nakatsuka and A. Tamura, "Rapid Degradation of Wsi Self-Aligned Gate MESFET by Hot Carrier Effect", *IEEE Int. Rel. Phys. Symp*, pp.127-130, 1992.
- [48] C. Tedesco, C. Canali, F. Magistrali, A. Paccagnella and E. Zanoni, "Hot-electron induced degradation in AlGaAs/GaAs HEMTs", *Microelectron. Eng*, vol. **19**, n°.1-4, pp.405-408, 1992.
- [49] H. Kim, V. Tilak, B. M. Green, J. A. Smart, W. J. Schaff, J. R. Shealy, and L. F. Eastman, *Phys. Stat. Sol. (A)*, vol. **188**, n°.1, p.203, 2001.
- [50] H. Kim, V. Tilak, B. M. Green, H. Cha, J. A. Smart, J. R. Shealy and L. F. Eastman, *IEEE International Reliability Physics Symposium 'IEEE IRPS', Orlando, Florida*, p.214, 2001.
- [51] A. Sozza, C. Dua, E. Morvan, M. A. diForte-Poisson, S. Delage, F. Rampazzo, A. Tazzoli, F. Danesin, G. Meneghesso, E. Zanoni, A. Curutchet, N. Malbert, N. Labat, B. Grimbert and J. C. De Jaeger, *IEEE IDRM*, p.593, 2005.
- [52] J. A. del Alamo, and J. Joh, "Ga_N HEMT reliability", *Microelectron. Reliab.* vol. **49**, n°.9-11, pp.1200-1206, 2009.
- [53] J. Joh, and J. A. del Alamo, "Mechanisms for electrical degradation of Ga_N high-electron mobility transistors", *IEDM Tech. Dig.*, pp.415-418, 2006.

Chapter II: AlGaN/GaN High Electron Mobility Transistors (HEMTs)

- [54] S. R. Lee, D. D. Koleske, K. C. Cross, J. A. Floro and K. E. Waldrip, "In situ measurements of the critical thickness for strain relaxation in AlGaN/GaN heterostructures", *Appl. Phys. Lett.*, vol. **85**, n°.25, p.6164, 2004.
- [55] J. Joh, L. Xia, and J. A. del Alamo, *IEEE Int. Electron Devices Meet, Washington (DC), USA*, p.385, 2007.
- [56] W.S. Tan, P.A. Houston, P.J. Parbrook, D.A. Wood, G. Hill, and C R. Whitehouse, "Gate leakage effects and breakdown voltage in metalorganic vapor phase epitaxy AlGaN/GaN heterostructure field-effect transistors", *Appl. Phys. Lett.*, vol. **84**, n°.17, pp.3207–3209, 2002.
- [57] M. H. Somerville and J. A. del Alamo, "A model for tunneling-limited breakdown in high-power HEMTs", in *International Electron Devices Meeting*, pp.35-38, 1996.
- [58] M. Faqir, G. Verzellesi, G. Meneghesso, E. Zanoni, and F. Fantini, "Investigation of high-electric-field degradation effects in AlGaN/GaN HEMTs", *IEEE Transactions on Electron Devices*, vol. **55**, pp.1592-1602, 2008.
- [59] S. Selvaraj, T. Suzue, and T. Egawa, "Breakdown enhancement of AlGaN/GaN HEMTs on 4-in silicon by improving the GaN quality on thick buffer layers", *IEEE Electron Device Letters*, vol. **30**, n°.6, pp.587-589, 2009.
- [60] M. Faqir, G. Verzellesi, A. Chini, F. Fantini, F. Danesin, G. Meneghesso, E. Zanoni, and C. Dua, "Mechanisms of RF current collapse in AlGaN-GaN high electron mobility transistors", *IEEE Transactions on Device and Materials Reliability*, vol. **8**, n°.2, pp.240-247, 2008.
- [61] J. Joh, L. Xia, and J. del Alamo, "Gate current degradation mechanisms of GaN high electron mobility transistors", in *IEEE 2007 International Electron Devices Meeting*, pp.385-388, 2007.

Chapter



An analytical physics-based compact modeling of I-V and C-V

characteristics in $\text{Al}_x\text{Ga}_{1-x}\text{N}/\text{GaN}$ HEMT devices

Chapter III

An analytical physics-based compact modeling of I–V and C–V characteristics in $\text{Al}_x\text{Ga}_{1-x}\text{N}/\text{GaN}$ HEMT devices

III.1 Introduction

Physics-based modeling of semiconductor devices is a very active area of research. In this chapter we discuss the classification of physics-based device-models. Then we present a physics-based analytical model for two dimensional electron gas (2DEG) density n_s which is derived from a consistent solution of Schrodinger's and Poisson's equations. Based on this analytical models is derived for the I – V and C – V characteristics for $\text{Al}_x\text{Ga}_{1-x}\text{N}/\text{GaN}$ High Electron Mobility Transistor (HEMT) devices in order to include a mole fraction-dependent threshold voltage. We incorporate this new threshold model for the drain current, carrier sheet density and gate capacitances physics-based compact models. The drain current model includes an important effect of the physical parameters like velocity saturation and threshold voltage.

Chapter III: *An analytical physics-based compact modeling of I-V and C-V characteristics in $Al_xGa_{1-x}N/GaN$ HEMTs*

III.2 Physics-based device models

Physics-based device models are of two variants: ‘analytical-models’ and ‘compact models’, both of which are based on analytical expressions obtained from solutions to the laws governing relevant physical phenomena. However, the key distinction between the two is that the analytical-models lays emphasis on physical-rigor and may be regional, and have clearly stated-assumptions on approximations and they are broader in scope and targeted to evaluate and study any new device/system. While the compact models are based on simplified equations and are reserved particularly to circuit-simulations. Moreover, compact models are robust for complex circuit-simulations with ease of computational efficiency and the hope is that the compromise in physics is minimal with the use of minimum extent of empirical factors such as expressions and/or parameters. Developing such compact models is the aim of this thesis work.

III.2.1 Overview of compact models

Compact models are essentially mathematical description of the terminal characteristics of devices. For accurate circuit simulation various physical quantities at the device terminal are required. A simple DC simulation requires the terminal current whereas device charge is required for transient and AC simulations. More advanced simulation like harmonic balance, need accurate first and higher order derivatives of device currents and charges. A compact model should calculate all these quantities in a fast, accurate and reliable way.

There are many types of compact modeling techniques with their own merit and drawbacks. In general sense, compact models can be divided in four different types such as: empirical models, table-based models, artificial neural network based models and physics-based models.

Chapter III: *An analytical physics-based compact modeling of I-V and C-V characteristics in $Al_xGa_{1-x}N/GaN$ HEMTs*

In the following we introduce the physics-compact models which are used in this thesis.

III.2.2 Physics-based compact models

Physics-based compact models are derived from solving the fundamental physical equation in the device. The device geometry, material properties, electrostatics in the device etc... are applied to derive these models. All the physical quantities of interest are expressed in terms of analytical functions of input variables like device geometry, material properties, voltage, and temperature. A typical model development flow for these models starts with solution of the electrostatics in the device to calculate the number of charge carriers. Charge transport is then used to derive expressions of current at the device terminals. These models provide insight into the device operation, valuable information about parameters affecting the device performance and have well defined scaling rules with respect to device geometry and temperature.

To precise for “*non-idealities*” in the device and improve agreement with experimental data, some parameters are introduced in these models. As the parameters introduced in the model are physically meaningful, these models can be used for statistics analysis of device performance. One drawback of physics-based models is their complexity. The complicated behavior of advanced semiconductor devices makes the mathematical formulations in the model very complex. This increases simulation time. However, engineering approximations are made in the model developments to reduce complexity and keep simulation time within useful limits. It is due to all of the above advantages that the physics-based models are the most popular ones. BSIM [1, 2], EKV [3] and PSP [4] which are widely used models for silicon MOSFETs are examples of such compact models. The focus of this study is to developing the physics-based compact models for advanced III-V and silicon devices.

Chapter III: *An analytical physics-based compact modeling of I-V and C-V characteristics in $Al_xGa_{1-x}N/GaN$ HEMTs*

Three well known physical compact models namely, the Tsinghua, the ASMHEMT and the HSP-LETI models for GaN-HEMTs are briefly discussed and their performance is analyzed in this section.

A°) Tsinghua model

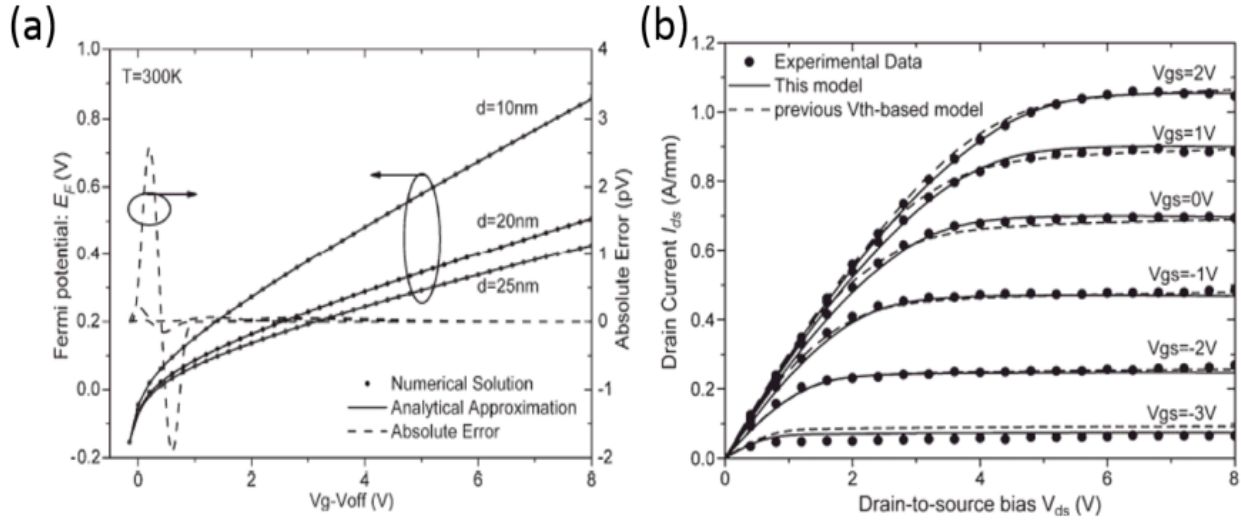


Figure III.1: (a) Comparison of accuracy of Fermi-potential (E_f) with numerical solution and (b) Model comparison against measurements [5].

The Tsinghua model is a surface-potential-based approach to capture terminal characteristics in GaN-HEMTs in which the Fermi-potential (E_f) is obtained in the form of closed-form analytical approximations to the charge-density-of-states (DOS) and Poisson equations. The formulation of terminal currents and charges is based on this calculation and is found to be valid over a wide bias and temperature range as shown in Figure (III-1) and in detail in [5]. Unlike constant-threshold voltage based models in which the E_f is pinned, this methodology ensures improved accuracy even in moderate-accumulation regimes in the operation of the device as it self-consistently solves for E_f and the charge-density in the potential-well (n_s). Explicit approximations to the

Chapter III: *An analytical physics-based compact modeling of I-V and C-V characteristics in $Al_xGa_{1-x}N/GaN$ HEMTs*

implicit-transcendental functions ensure fast and reduced computational requirements. The detailed model formulation can be found in [5] and the model equations are not reproduced here, but it is clear that the model is capable of including several second-order effects in the channel and is symmetric with respect to source and drain terminals (Gummel Symmetry).

However the model does not include the effect of access regions and field plates, channel-noise, small and large-signal validation which is the main priority for RF designers is not demonstrated. The number of parameters in the model seems to be large with several fitting parameters to combine linear-to-saturation regions.

B°) ASM-HEMT model

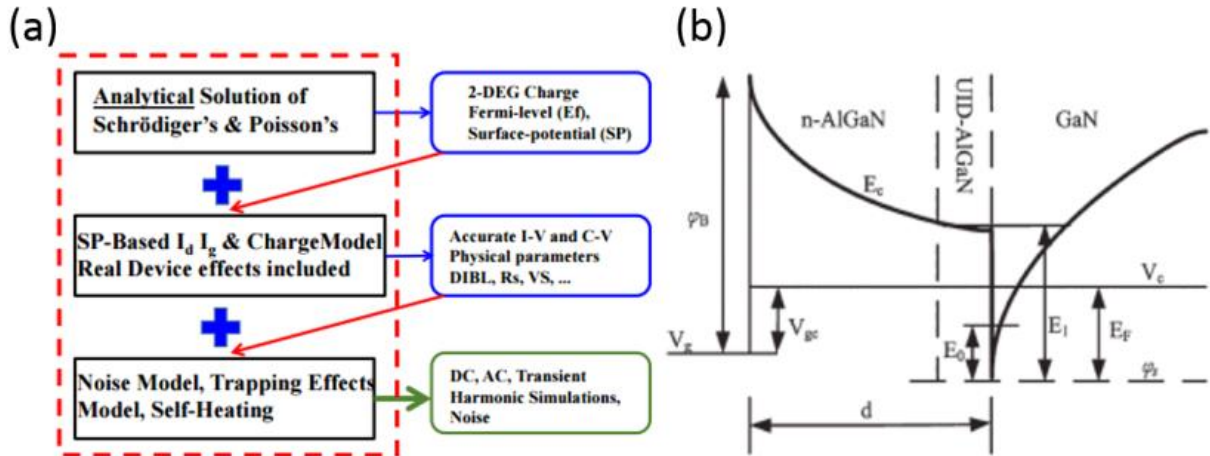


Figure III.2: (a) The workflow for terminal characteristics and (b) the surface-potential calculation approach in ASM-HEMT model [6].

The ASM-HEMT model is also a surface-potential model which incorporates most of the requirements for an industry-standard model by computing a solution to the surface potential in the channel from Schrodinger-Poisson coupled equations making reasonable assumption on band occupation. The work-flow of the model is highlighted in Figure (III.2) which shows a complete flow of the model formulation. The ASMHEMT

Chapter III: *An analytical physics-based compact modeling of I-V and C-V characteristics in $Al_xGa_{1-x}N/GaN$ HEMTs*

model captures most of the device-level terminal characteristics [6] but is not tested for robustness at the circuit-simulation level which is another key cornerstone that must be achieved by any successful model. It is found to accurately model the RF-device characteristics (both small- and large-signal characteristics) but not the characteristics of HV-GaN-HEMT including non-linear capacitances.

C°) HSP-LETI model

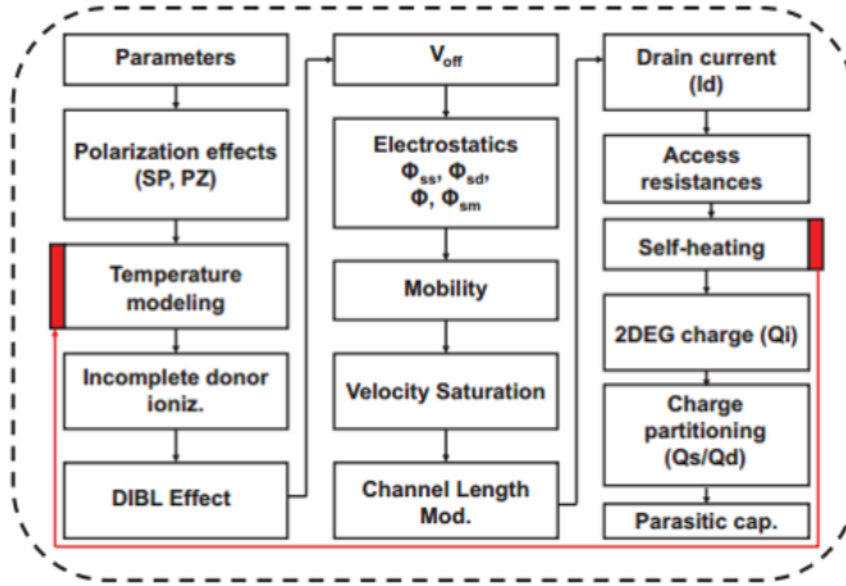


Figure III.3: The HSP model flow indicating the various effects incorporated in the model [7].

The HSP model (acronym for HEMT Surface-Potential model) claims to include: the effects of the spontaneous and piezoelectric polarizations, incomplete donor activation, temperature dependence of different parameters and self-heating effect. Other effects, like series resistances, velocity saturation and channel length modulation also appears to be incorporated in the model. Figure (III.3) shows the model flow with the various effects included. Resulting accuracy of the model fits against actual measurement data is however

Chapter III: *An analytical physics-based compact modeling of I-V and C-V characteristics in $Al_xGa_{1-x}N/GaN$ HEMTs*

not quite clear from [7] and these device- and circuit-level validation steps are critical in gauging any model's usability in circuit design.

III.2.3 Fundamentals for physics-based compact models

The Poisson's equation is one of the basic equations governing the charge formation in field-effect transistors. This equation related the electric potential V to the total charge in the channel and is expressed as

$$\nabla^2 V = -\frac{\rho}{\varepsilon} \quad (\text{III.1})$$

where ∇^2 is the Laplacian operator, ρ is the charge density and ε is the dielectric permittivity of the channel material.

Eq. (III.1) is a three dimensional equation, however, with justifiable assumptions it's typically reduces to one dimension for development of compact models. To model the terminal behavior of the device charge density in the channel ρ needs to be calculated. ρ consist of both mobile and fixed charges in the channel. For terminal current calculation mobile charges are of interest. The calculation of mobile charges in the channel almost always results in transcendental equation. Eq. (III.2) is an example of such a transcendental function, which is the Poisson in case of HEMT,

$$n_s = DV_{th} \left[\ln \left(e^{\left(\frac{E_f - E_0}{V_{th}} \right)} + 1 \right) + \ln \left(e^{\left(\frac{E_f - E_1}{V_{th}} \right)} + 1 \right) \right]. \quad (\text{III.2})$$

where n_s is the sheet carrier density, V_{th} is the threshold voltage, E_f is the Fermi level position, E_0 and E_1 are first and the second sub-band position respectively.

From a compact modeling point of view explicit solution is desired, this is much faster to calculate. The method of deriving explicit solution from intricate transcendental equations like Eq. (III.2) in this a very important part of compact model development. Appropriate

Chapter III: *An analytical physics-based compact modeling of I-V and C-V characteristics in $Al_xGa_{1-x}N/GaN$ HEMTs*

approximations, algorithms and/or mathematical conditioning of equations are used to develop such solution. Poisson's equation being a fundamental device physics equation is valid irrespective of the device technology.

a) Schrodinger's equation

A complete description of the charge carriers confinement is given by their particle as well as wave-nature. The wave-function of the carriers is the solution of the three-dimensional Schrodinger's equation [8]

$$-\frac{\hbar^2}{2m}\nabla^2\varphi + U(x, y, z)\varphi = E \quad (\text{III.3})$$

where \hbar is the reduced Planck's constant, m is the mass of the particle, φ is the wave-function, U is the potential energy of the system and E is the energy of the particle. This is the time-independent form of Schrodinger's equation. By applying appropriate boundary conditions in Eq. (III.3) the positions of allowed energy-levels can be obtained. Eq. (III.3) along with Poisson's equation and carrier statistics need to be solved to calculate the carrier sheet density in the channel. A consistent solution of these equations is quite complex and to develop explicit solutions justifiable approximations are made.

b) Charge transport

The current flow is transport of charge carries. Semi-classical carrier transport is described by Boltzmann transport equation. However, it is not possible to get an analytical solution of the Boltzmann equation and approximations are made to develop analytical model. The drift-diffusion framework is an approximation of Boltzmann transport equation which is widely used in development of compact models. We describe drift and diffusion mechanisms in brief from a compact modeling point of view below.

Chapter III: *An analytical physics-based compact modeling of I-V and C-V characteristics in $Al_xGa_{1-x}N/GaN$ HEMTs*

Drift is the carrier motion in the presence of an electric field. The application of electric field to a semiconductor focuses charge carriers to accelerate in one direction. Holes move in the direction of the electric field, while the electrons in the opposite direction. As the charge carriers move they get scattered by impurities, crystal defects and/or lattice vibrations. The microscopic drifting motion of carriers is complex and it consists of a large number of acceleration and deceleration events. However, the quantity of interest from a compact modeling point of view is the overall drift current.

The drift current is macroscopic observable quantity which reflects the average motion of all charge carriers. The average charge carriers velocity v in presence of an electric field ξ is expressed as

$$v = \mu\xi \quad (III.4)$$

where μ is the carriers mobility and is a very important device parameter which needs to be modelled accurately for correct prediction of the current and ξ is the electric field. The drift current density J_{drift} is then expressed as [9]

$$J_{drift} = nqv = nq\mu\xi \quad (III.5)$$

where n is the charge carriers density and q is the charge carriers.

Diffusion is the process in which the carriers tend to spread-out or redistribute as a result of their random thermal motion, moving from region of high charge carriers density to lower density. The diffusion current density J_{diff} depends on the gradient of the charge carriers density dn/dx and it's can be expressed as [9]

$$J_{diff} = qD \frac{dn}{dx} \quad (III.6)$$

where D is the diffusion constant which is related to the carrier mobility via the Einstein's relation. Eq. (III.6) is a generic equation for the diffusion current of both electrons and

Chapter III: *An analytical physics-based compact modeling of I-V and C-V characteristics in $Al_xGa_{1-x}N/GaN$ HEMTs*

holes and proper values of D should be used for correct calculation of J_{diff} . The total current density is given as the sum of the drift and diffusion components J_{diff} and J_{drift} [9].

III.2.4 Models development

As mentioned earlier, our focus is on physics-based compact models due to the discussed advantages of this type of models. The formation of the 2DEG is the core of the HEMT devices operation and we focused first on developing a physics-based model for the 2DEG carrier sheet density n_s .

A°) Carrier sheet density in the 2DEG

In the triangular approximation of the potential well if a quasi-constant electric field is assumed, the solution of the longitudinal quantized energy can be approximated as [10]

$$E_n = \left(\frac{\hbar^2}{2m_l} \right)^{1/3} \left(\frac{3}{2} \pi q E \right)^{2/3} \left(n + \frac{3}{4} \right)^{2/3} \quad (\text{III.7})$$

where m_l is the longitudinal effective mass.

The first two sub-band energy levels in binary compound GaN are given as

$$E_0 \approx 1.83 \times 10^{-6} \xi^{2/3} \quad \text{and} \quad E_1 \approx 3.23 \times 10^{-6} \xi^{2/3} \quad (\text{III.8})$$

with $\xi = \frac{q}{\epsilon_1}$ is the electrical field.

The approximation of the energies of the sub-bands given by Eq. (III.8) over estimates the sub-bands splitting. This is because the conduction band increases sub-linearly. However, the $2/3$ power relation between E_0 , E_1 and E_f is reasonable [11]. A more accurate estimation of the band splitting can be done by improving the coefficients. This can be done by establishing a relationship between the carrier sheet density and the interface

Chapter III: *An analytical physics-based compact modeling of I-V and C-V characteristics in $\text{Al}_x\text{Ga}_{1-x}\text{N}/\text{GaN}$ HEMTs*

electric field. Figure (III.4) shows the band diagram of a hetero-junction consisted of an n -type large bandgap semiconductor and p -type semiconductor with a smaller bandgap. As the electric field in the smaller bandgap material obeys Poisson's equation, we have [12]

$$\frac{d\xi_1}{dx} = -\frac{q[n(x)+N_{A1}]}{\varepsilon_1} \quad (\text{III.9})$$

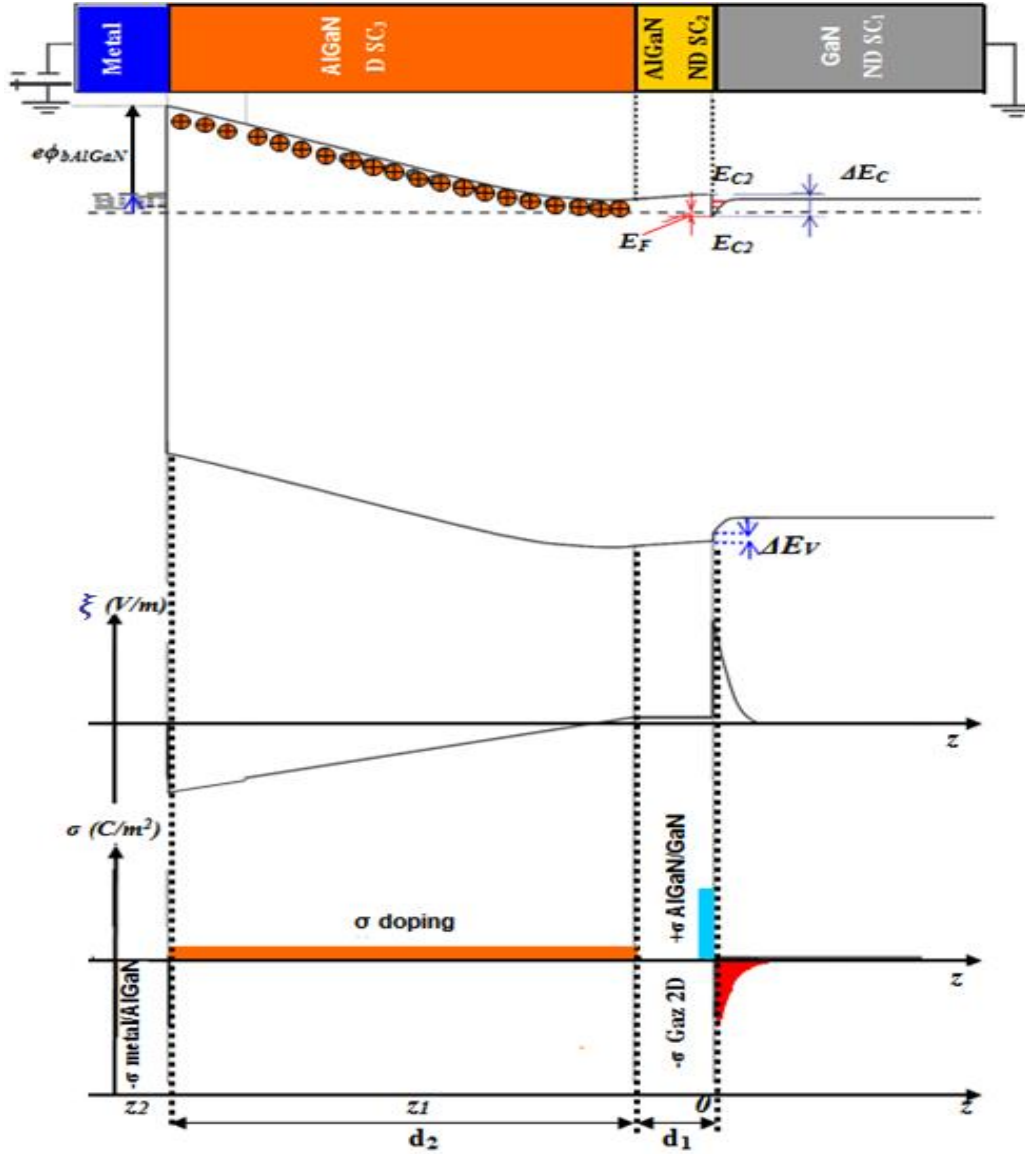


Figure III.4: Band structure diagram at a hetero-junction for $\text{Al}_x\text{Ga}_{1-x}\text{N}/\text{GaN}$ HEMT.

Chapter III: *An analytical physics-based compact modeling of I-V and C-V characteristics in $Al_xGa_{1-x}N/GaN$ HEMTs*

The electric field is integrated within the limit of the depletion region. The boundary conditions for the electric field and the depletion width are:

$\Rightarrow \xi_1$ from 0 at the end of the depletion region to ξ_{i1} at the hetero-junction interface,

$\Rightarrow x$ from 0 at the hetero-junction interface to d_1 at the end of the depletion region.

Thus, the integration of the Poisson's equation with these boundary conditions gives

$$\varepsilon_1 \xi_{i1} = qn_s + qN_{A1}d_1 \quad (\text{III.10})$$

In most cases the smaller band gap material is doped very lightly or unintentionally doped to improve mobility of charge carriers in the region. In such cases the second term in the right side of Eq. (III.10) is very small. Thus, it can be written as

$$\varepsilon_1 \xi_{i1} = qn_s \quad (\text{III.11})$$

Eq. (III.11) gives the approximated relationship between the electric field at the interface and the carrier sheet density. Substituting for the electric field from Eq. (III.11) into Eq. (III.8) gives

$$E_0 = \gamma_0 n_s^{2/3} \quad \text{and} \quad E_1 = \gamma_1 n_s^{2/3} \quad (\text{III.12})$$

where

$$\gamma_0 = 1.83 \times 10^{-6} \left(\frac{q}{\varepsilon_1} \right)^{2/3} \quad \text{and} \quad \gamma_1 = 3.23 \times 10^{-6} \left(\frac{q}{\varepsilon_1} \right)^{2/3}. \quad (\text{III.13})$$

The carrier sheet density in the potential well at the hetero-junction interface can be calculated using the Fermi-Dirac distribution and the two dimensional density of states D . For a density of states D between E_0 and E_1 and $2D$ for energy levels above the Fermi-level E_f , the carrier sheet density n_s , is given as [10]

Chapter III: *An analytical physics-based compact modeling of I-V and C-V characteristics in $Al_xGa_{1-x}N/GaN$ HEMTs*

$$n_s = D \int_{E_0}^{E_1} \frac{dE}{1 + \exp\left(\frac{E - E_f}{V_{th}}\right)} + 2D \int_{E_1}^{\infty} \frac{dE}{1 + \exp\left(\frac{E - E_f}{V_{th}}\right)} \quad (III.14)$$

where $D = \frac{4\pi m^*}{h^2}$ is the conduction band density of state of 2DEG system.

After integrating Eq. (III.14), the carrier sheet density is given as

$$n_s = DV_{th} \left\{ \ln \left[\exp\left(\frac{E_f - E_0}{V_{th}}\right) + 1 \right] + \ln \left[\exp\left(\frac{E_f - E_1}{V_{th}}\right) + 1 \right] \right\}. \quad (III.15)$$

Eq. (III.15) gives an important relation between the Fermi-level E_f , the carrier sheet density n_s , and the sub-band energy levels E_0 and E_1 . However, it is not an explicit analytical relation between the parameters. The systematically developments of analytical relationships between the important parameters, for the development of compact analytical models, are described in the following consecutive sections.

B^o) Space charge region in equilibrium

Before looking into the characteristics of the hetero-junction region while being manipulated by an additional Schottky contact, in this section a hetero-junction in thermal equilibrium is investigated. The band diagram of the hetero-junction shown in Figure (III.1) is in its equilibrium state. Assuming depletion approximation in the space charge region of the large band gap material, the potential and the electric field in the region obey the Poisson's equation [13]. Thus,

$$\frac{d^2 V_2(x)}{dx^2} = -\frac{q}{\epsilon_2} N_A(x). \quad (III.16)$$

and

$$\frac{d\xi_2}{dx} = -\frac{q}{\epsilon_2} N_A(x). \quad (III.17)$$

Chapter III: *An analytical physics-based compact modeling of I-V and C-V characteristics in $Al_xGa_{1-x}N/GaN$ HEMTs*

If the heterojunction interface is taken as origin, then the electric field is zero at the end of the space charge region of the wide bandgap semiconductor, d_2 , and it is $-\xi_{i2}$ at the interface. Thus,

$$\left(\frac{dV_2}{dx}\right)_{x=0} = -\xi_{i2} \quad \text{and} \quad \left(\frac{dV_2}{dx}\right)_{x=-d_2} = 0. \quad (\text{III.18})$$

Thus, after first integral we have

$$\frac{dV_2(x)}{dx} = -\frac{q}{\epsilon_2} \int_0^x N_A(x') dx' + \xi_{i2}. \quad (\text{III.19})$$

Integrating in the total width of the space charge region of the wide bandgap semiconductor, the potential at the end of the depletion region during the neutral state can be written as

$$V_2(-d_2) = V_{20} = \int_0^{-d_2} \left(-\frac{q}{\epsilon_2} \int_0^x N_A(x') dx' \right) dx + \int_0^{-d_2} \xi_{i2} dx. \quad (\text{III.20})$$

$$V_{20} = \xi_{i2} d_2 - \frac{q}{\epsilon_2} \int_0^{-d_2} dx \int_0^x N_A(x') dx'. \quad (\text{III.21})$$

The boundary conditions of the donor density distribution are

$$\begin{cases} N_A(x) = 0 & \text{for } -d_s < x < 0 \\ N_A(x) = N_A & \text{for } -d_2 < x < -d_s. \end{cases} \quad (\text{III.22})$$

Using these boundary conditions we have

$$V_{20} = \xi_{i2} d_2 - \frac{q}{\epsilon_2} \int_0^{-d_2} dx N_A \int_{-d_2}^x dx'. \quad (\text{III.23})$$

$$V_{20} = \xi_{i2} d_2 - \frac{q N_A}{\epsilon_2} \int_0^{-d_2} (x + d_s) dx. \quad (\text{III.24})$$

$$V_{20} = \xi_{i2} d_2 - \frac{q N_A}{\epsilon_2} \left[\frac{1}{2} (d_2^2 - d_s^2) - d_s (d_2 - d_s) \right]. \quad (\text{III.25})$$

Chapter III: *An analytical physics-based compact modeling of I-V and C-V characteristics in $Al_xGa_{1-x}N/GaN$ HEMTs*

From the Poisson's equation written for the electric field in the region, one can easily obtain

$$\varepsilon_2 \xi_{i2} = qN_A(d_2 - d_s). \quad (\text{III.26})$$

Thus, substituting for the electric field gives

$$V_{20} = \frac{qN_A(d_2 - d_s)d_2}{\varepsilon_2} - \frac{qN_A}{\varepsilon_2} \left[\frac{1}{2} (d_2^2 - d_s^2) - d_s(d_2 - d_s) \right]. \quad (\text{III.27})$$

$$V_{20} = \frac{qN_A}{\varepsilon_2} \left[(d_2 - d_s)d_2 - \frac{1}{2} (d_2^2 - d_s^2) - d_s(d_2 - d_s) \right]. \quad (\text{III.28})$$

Thus,

$$V_{20} = \frac{qN_A}{\varepsilon_2} (d_2^2 - d_s^2). \quad (\text{III.29})$$

V_{20} , the band bending, is the potential at d_2 in the space charge region in the equilibrium state.

From Eqs. (III.26) and (III.29) the product $\varepsilon_2 \xi_{i2}$ can be written as

$$\varepsilon_2 \xi_{i2} = \sqrt{2q\varepsilon_2 N_A V_{20} + q^2 N_A^2 d_s^2} - qN_A d_s. \quad (\text{III.30})$$

By applying geometrical rules on Figure (III.1), V_{20} can also be expressed as

$$V_{20} = \Delta E_c - \delta_2 - \xi_{F0}. \quad (\text{III.31})$$

Eqs. (III.29) and (III.30) express the approximated values of the potential and the electric field at the hetero-structure in its equilibrium state. Note that the depletion length in the large band-gap material, d_2 , is not necessarily the same as the total width of the material and a complete depletion of the large bandgap material is not assumed in the calculations in this case.

Chapter III: *An analytical physics-based compact modeling of I-V and C-V characteristics in $Al_xGa_{1-x}N/GaN$ HEMTs*

C°) Charge control model

Figure (III.1) shows the band structure when a metallic material is attached to the large band-gap semiconductor to form a Schottky contact.

Assuming that the region between the Schottky contact and the hetero-junction interface is fully depleted, the electrostatic potential in the region obeys Poisson's equation like that of the neutral state described in Section (III.2) [13,14]. Therefore, Eqs (III.16) and (III.17) still hold in this region. A full depletion of the large band-gap semiconductor is assumed in this case. Thus, the second integration boundary in x is now extended to d , which is the total width of the large band-gap semiconductor. Hence, the electrostatic potential is given as

$$V_2 = \frac{qN_A}{2\epsilon_2} (d_2^2 - d_s^2) - \xi_{i2}d. \quad (III.32)$$

From Eq. (III.32) one can easily obtain

$$\epsilon_2 \xi_{i2} = \frac{\epsilon_2}{d} \left(\frac{qN_A}{2\epsilon_2} (d - d_s)^2 - V_2 \right). \quad (III.33)$$

Applying basic geometry rules on Figure (III.1) also gives

$$V_2 = \phi_M - V_G + E_f - \Delta E_C. \quad (III.34)$$

Substituting for V_2 from Eq. (III.34) into Eq. (III.33) gives

$$\epsilon_2 \xi_{i2} = \frac{\epsilon_2}{d} \left(\frac{qN_A}{2\epsilon_2} (d - d_s)^2 - \phi_M + V_G - E_f + \Delta E_C \right). \quad (III.35)$$

If the interface states are neglected, the product of the dielectric constants and the electric fields at hetero-junction interface and the charge in the region can be related using Gauss's law as

$$\epsilon_2 \xi_{i1} = \epsilon_2 \xi_{i2} = qn_s. \quad (III.36)$$

Chapter III: *An analytical physics-based compact modeling of I-V and C-V characteristics in $Al_xGa_{1-x}N/GaN$ HEMTs*

Therefore, the charge Q_s of the free charge carriers at the heterojunction can be expressed as

$$Q_s = qn_s \left(V_G - \phi_M - E_f + \Delta E_C + \frac{qN_A}{2\epsilon_2} (d - d_s)^2 \right). \quad (\text{III.37})$$

D°) Simple charge control model

The expressions given by Eqs (III.15) to (III.46) are transcendental in nature. From a compact modeling point of view, analytical solutions are desirable since a solution based on numerical techniques will result in a drastic reduction of the circuit simulation speed. Analytical expressions are developed for these equations by dividing the variation of E_f with V_g into various regions. These region are physically meaningful and are based on the position of E_f with respect to the energy levels E_0 and E_1 .

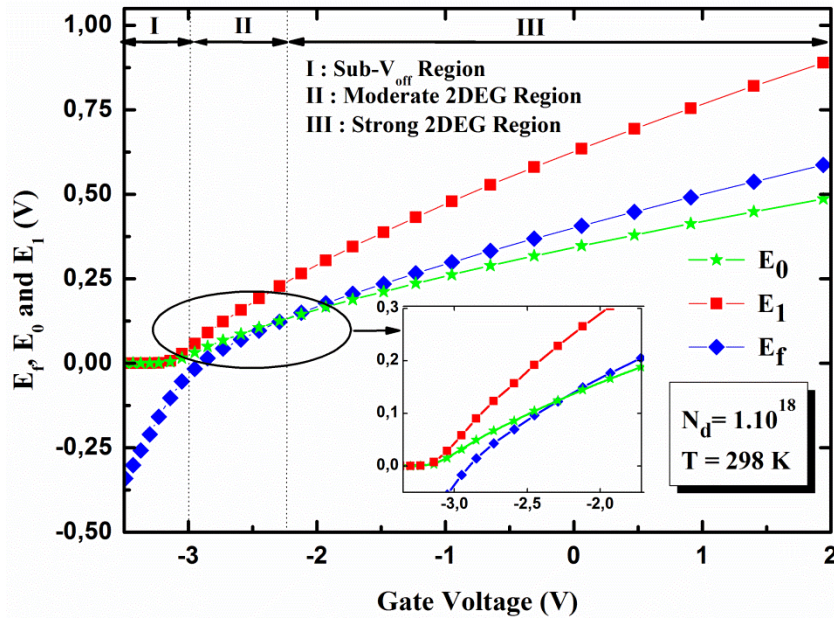


Figure III.5: E_f , E_0 and E_1 versus V_g calculated. The regions defined for modeling are marked in this figure.

Chapter III: *An analytical physics-based compact modeling of I-V and C-V characteristics in $Al_xGa_{1-x}N/GaN$ HEMTs*

These regions are shown in Figure (III-5) along with numerical solution of E_f , E_0 and E_1 . The regions are:

- I. Sub- V_{off} region with $V_g < V_{off}$ 2DEG charge carriers density is very low as E_f is well below E_0 and E_1 .
- II. Moderate 2DEG and region with $V_g > V_{off}$ and $E_0 < E_f < E_1$, since E_f cross E_0 there is considerable 2DEG.
- III. $E_f > E_1$ thus 2DEG density is very high in the channel. This is called the strong 2DEG charge carriers density region.

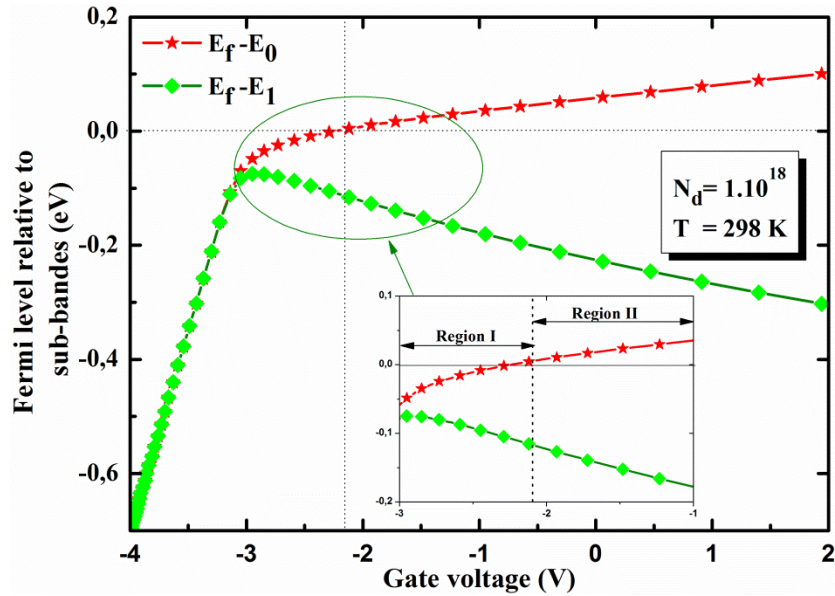


Figure III.6: Numerical calculations of $E_f - E_0$ and $E_f - E_1$ versus gate voltage regions I and II are marked in this figure.

To accentuate the observation in Figure (III.5), we plot $E_f - E_0$ and $E_f - E_1$ in Figure (III.6) and find two observations:

- 1) Lower level E_0 has two distinct regions, namely:

Chapter III: *An analytical physics-based compact modeling of I-V and C-V characteristics in $\text{Al}_x\text{Ga}_{1-x}\text{N}/\text{GaN}$ HEMTs*

- region I, where E_0 is higher than E_f corresponding to $V_{g0} < 0.9\text{V}$,
- region II, where E_0 is lower than E_f corresponding to $V_{g0} \geq 0.9\text{V}$. We also note that, in the full range of gate voltages considered, except very close to cut-off, E_f will be much smaller than V_{g0} .

2) Upper level E_1 is higher than E_f for the complete range of the gate voltages. In addition, E_1 is significantly higher than E_0 over the same range. Hence, the contribution to n_s from the second sub-band can be safely ignored.

Furthermore, we can see that the contribution of the second energy level to the carrier sheet density in the triangular potential well is negligible. Therefore, considering the contribution of only the first sub-band to the carrier sheet density, Eq. (III.15) can be rewritten as

$$n_s = DV_{th} \left\{ \ln \left[\exp \left(\frac{E_f - E_0}{V_{th}} \right) + 1 \right] \right\}. \quad (\text{III.38})$$

Eq. (III.38) gives the carrier sheet density in $\text{Al}_x\text{Ga}_{1-x}\text{N}/\text{GaN}$ hetero-structure system where the contribution of only the first energy level is considered. After rearranging Eq. (III.38) and making use of Eqs (III.12) and (III.38), a simple charge control model is derived, given as

$$V_{g0} = \frac{qdn_s}{\varepsilon} + \gamma_0 n_s^{2/3} + V_{th} \ln \left(\frac{n_s}{DV_{th}} \right). \quad (\text{III.39})$$

The derivation of Eq. (III.48) provides an explicit analytical relation between the controlling gate voltage and carrier sheet density. This can be used to derive analytical expressions for terminal characteristics of a functional device based on such hetero-structure system. It, Eq. (III.39), can be extended to include the lateral potential V , considered as the local quasi-Fermi potential, at any point along the channel [15]. Therefore,

Chapter III: *An analytical physics-based compact modeling of I-V and C-V characteristics in $Al_xGa_{1-x}N/GaN$ HEMTs*

$$V_{g0} - V = \frac{qdn_s}{\varepsilon} + \gamma_0 n_s^{2/3} + V_{th} \ln \left(\frac{n_s}{DV_{th}} \right). \quad (III.40)$$

The unified expression for n_s that covers all the operating regions from deep subthreshold to full active gate bias, is calculated as

$$n_s = \frac{2 V_{th} (C_g / q) \ln \{ 1 + \exp (V_{g0} / 2 V_{th}) \}}{1/H(V_{g0}) + (C_g / qD) \exp (-V_{g0} / 2 V_{th})} \quad (III.41)$$

where C_g is the gate capacitance. The derivation of (III.41) is shown in Appendix A.

The function $H(V_{g0})$ in the denominator, which simulates the nonlinear behaviour in the above threshold region, is given as

$$H(V_{g0}) = \frac{V_{g0} + V_{th} [1 - \ln(\beta V_{gon})] - \frac{\gamma_0}{3} \left(\frac{C_g V_{g0}}{q} \right)^{2/3}}{V_{g0} \left(1 + \frac{V_{th}}{V_{god}} \right) + \frac{2\gamma_0}{3} \left(\frac{C_g V_{g0}}{q} \right)^{2/3}}. \quad (III.42)$$

where $\beta = C_g / qDV_{th}$, and the two interpolation functions V_{gon} and V_{god} of V_{g0} are given by

$$V_{gon} = \frac{V_{g0} \alpha_n}{\sqrt{V_{g0}^2 + \alpha_n^2}} \quad \text{and} \quad V_{god} = \frac{V_{g0} \alpha_d}{\sqrt{V_{g0}^2 + \alpha_d^2}}. \quad (III.43)$$

where

$$\alpha_n = e/\beta \quad \text{and} \quad \alpha_d = 1/\beta. \quad (III.44)$$

In Figure (III-7) a comparison of developed model with numerical solution is plotted which shows that the model produced an excellent fit in all the regions of device operation. There are no fitting parameters in the n_s model, which is important to keep the parameter count for the full GaN HEMT model to a minimum, the details of the model can be found in [14,16].

Chapter III: *An analytical physics-based compact modeling of I-V and C-V characteristics in $Al_xGa_{1-x}N/GaN$ HEMTs*

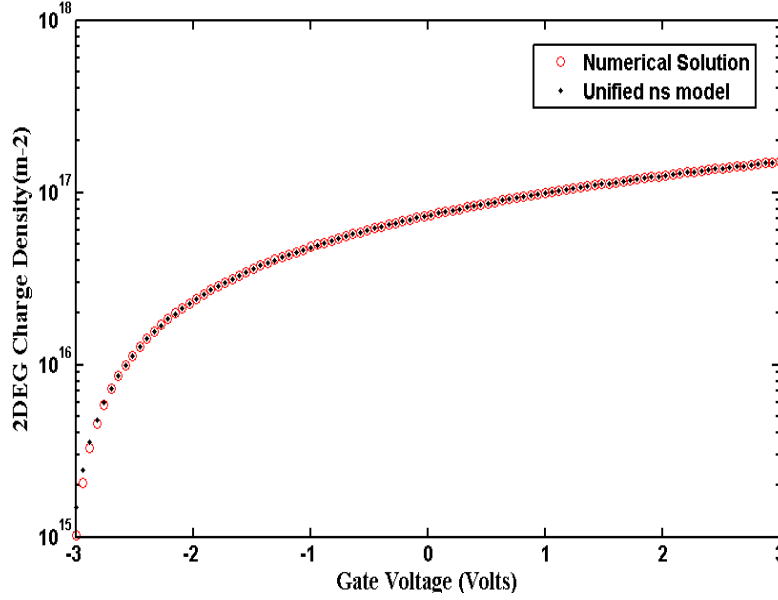


Figure III.7: Comparison of the developed model of 2DEG charge carriers density with the numerical solution, at $T = 300$ K. Typical value of $V_{off} = -3$ V is used.

III.3 Mole fraction effect

The cut-off voltage V_{off} is a very important parameter as it defines the level of external voltage that is necessary to wipe out the charge carriers in the 2DEG.

In Eq. (III.37) the Fermi-level term E_f is very small as compared to the other terms, and the rest of the terms except V_g are summed and expressed as one single term, the so-called cut-off voltage, given by [12]

$$V_{off} = \varphi_{eff}(x) - \Delta E_{C,eff}(x) - \frac{qN_d d_d^2}{2\varepsilon(x)} - \frac{\sigma_{total}}{\varepsilon(x)}(d - d_s). \quad (III.45)$$

Chapter III: *An analytical physics-based compact modeling of I-V and C-V characteristics in $\text{Al}_x\text{Ga}_{1-x}\text{N}/\text{GaN}$ HEMTs*

Where $\varphi_{eff}(x)$ is the effective Schottky barrier height in the case of $\text{Al}_x\text{Ga}_{1-x}\text{N}$ barrier layer can be expressed using the Vegard's interpolation formula

$$\varphi_{eff}(x) = 0.84 + 1.3x. \quad (\text{III.46})$$

The dielectric constant in the case of $\text{Al}_x\text{Ga}_{1-x}\text{N}$ barrier layer depends on the Al mole fraction and is given by [17]

$$\varepsilon(x) = 0.3x + 10.4 \quad (\text{III.47})$$

The conduction band offset ΔE_C can be expressed by

$$\Delta E_{C,eff}(x) = 0.7[E_g^{Al_xGa_{1-x}N} - E_g^{GaN}], \quad (\text{III.48})$$

where $E_g^{Al_xGa_{1-x}N}$ is the energy bandgap of $\text{Al}_x\text{Ga}_{1-x}\text{N}$ layer as a function of Al mole fraction, and is given by [18-19]

$$E_g^{Al_xGa_{1-x}N} = 6.13x + 3.42(1-x) - x(1-x), \quad (\text{III.49})$$

and $E_g^{GaN} = 3.42$ eV is the energy gap of GaN and $N_d = 10^{24} \text{cm}^{-3}$ is the donor concentration.

The total induced polarization density σ_{total} at the interface is given by [20]

$$\sigma_{total} = P_{pz} + P_{sp} \quad (\text{III.50})$$

where P_{pz} is the piezoelectric polarization can be weighed using the Vegard's interpolation formula [16]

$$P_{pz} = P_{pz}^{Al_xGa_{1-x}N} - P_{pz}^{GaN} \quad (\text{III.51})$$

where $P_{pz}^{Al_xGa_{1-x}N}$ and P_{pz}^{GaN} are the piezoelectric polarizations of $\text{Al}_x\text{Ga}_{1-x}\text{N}$ and GaN, respectively.

Chapter III: *An analytical physics-based compact modeling of I-V and C-V characteristics in $\text{Al}_x\text{Ga}_{1-x}\text{N}/\text{GaN}$ HEMTs*

The spontaneous polarization P_{sp} can expressed as

$$P_{sp} = P_{sp}^{\text{Al}_x\text{Ga}_{1-x}\text{N}} - P_{sp}^{\text{GaN}} \quad (\text{III.52})$$

where $P_{sp}^{\text{Al}_x\text{Ga}_{1-x}\text{N}}$ and $P_{sp}^{\text{GaN}} = -0.029$ are the spontaneous polarizations of $\text{Al}_x\text{Ga}_{1-x}\text{N}$ and GaN, respectively.

Now, Q_s can be written as

$$Q_s = qn_s = \frac{\varepsilon_2}{d} (V_G - V_{off} - E_f). \quad (\text{III.53})$$

III.4 Drain-source current model

In this section and in the next consecutive sections, the developments of analytical models for terminal current and charges by making use of Eq. (III.40) are discussed.

An analytical drain-source current model can be formulated using the definition of the drain-source current along the channel written as [21]

$$I_{ds} = Wqn_s v, \quad (\text{III.54})$$

where W is the gate width, q is the electron charge and v is the electron velocity in the channel, if a constant mobility μ , of the electrons is assumed then, the relation between v and the electric field ξ , at a certain point in the channel is given as

$$v = -\mu\xi = -\mu \frac{dV}{dx}. \quad (\text{III.55})$$

Therefore,

$$I_{ds} = W\mu qn_s \frac{dV}{dx}. \quad (\text{III.56})$$

Chapter III: *An analytical physics-based compact modeling of I-V and C-V characteristics in $Al_xGa_{1-x}N/GaN$ HEMTs*

After integrating along the total length of the channel from source to drain I_{ds} is expressed by

$$I_{ds} = \frac{W}{L} \int_{V_s}^{V_d} qn_s dV. \quad (III.57)$$

The integration variable can easily be changed to n_s , the carrier sheet density, using the relation given by Eq. (III.53). Taking the derivative of both sides of Eq. (III.53) and rearranging gives

$$dV = - \left(\frac{qd}{\epsilon} + \frac{2}{3} \gamma_0 n_s^{-\frac{1}{3}} + V_{th} n_s^{-1} \right) dn_s. \quad (III.58)$$

Substituting Eq. (III.58) into Eq. (III.57) for dV and integrating from the source to drain gives a simple analytical expression of the drain-source current that is written as

$$I_{ds} = \frac{q\mu W}{L} \left[\frac{qd}{2\epsilon} (n_D^2 - n_S^2) + \frac{2}{5} \gamma_0 (n_D^{5/3} - n_S^{5/3}) \right] + V_{th} (n_S - n_D). \quad (III.59)$$

where n_S and n_D are the carrier sheet densities at the source and drain, respectively, and d is the barrier layer thickness and all the other symbols have the standard definition. The current model in Eq. (III.59) can satisfactorily be used to reproduce the I - V characteristics of a long channel device. n_S and n_D can be obtained iteratively from Eq. (III.40). Anyway, sufficiently accurate explicit expressions would make the model computationally faster.

Here, we have used an approximate unified explicit expression that covers all the operating regions from deep subthreshold to full active gate bias to obtain the carrier sheet densities at the source and drain [15].

Chapter III: *An analytical physics-based compact modeling of I-V and C-V characteristics in $Al_xGa_{1-x}N/GaN$ HEMTs*

III.4.1 Derivative of the drain-source current

The derivative of the drain-source current model is one of the important figures of merit of a current model. They can be considered as the measures of the continuity of the current model and enable investigations of discontinuity anywhere in the operating regime of the model. The continuity of the current model is critical when it comes to applying the model for non-linearity studies which mainly involves the successive derivatives. The derivative of the drain-source model in terms of the gate voltage at a constant drain voltage, the transconductance, and the derivative in terms of the drain voltage at a constant gate voltage, the conductance, is the two main first derivatives of the current. These two parameters are defined as [22]

$$g_m = \left. \frac{\partial I_{ds}}{\partial V_g} \right| V_d \quad (\text{III.60})$$

and

$$g_d = \left. \frac{\partial I_{ds}}{\partial V_d} \right| V_g. \quad (\text{III.61})$$

Once a drain-source current model is developed, obtaining the transconductance numerically from the calculated current is a common practice. However, dedicated analytical expressions for the transconductance and conductance are developed. Having an independent transconductance expression will provide one an alternative to directly use the transconductance when it is not necessary to calculate the current for a certain applications. The partial derivative of the current, Eq. (III.55), in terms of the gate voltage is

$$g_m = \frac{\partial I_{ds}}{\partial V_g} = - \frac{q\mu W}{L} \left[\frac{qd}{2\epsilon} \left(\frac{\partial n_D^2}{\partial V_g} - \frac{\partial n_S^2}{\partial V_g} \right) + \frac{2}{5} \gamma_0 \left(\frac{\partial n_D^{5/3}}{\partial V_g} - \frac{\partial n_S^{5/3}}{\partial V_g} \right) + V_{th} \left(\frac{\partial n_D}{\partial V_g} - \frac{\partial n_S}{\partial V_g} \right) \right]. \quad (\text{III.62})$$

Chapter III: *An analytical physics-based compact modeling of I-V and C-V characteristics in $Al_xGa_{1-x}N/GaN$ HEMTs*

From Eq. (III.61) a simplified expression of the transconductance can be obtained as

$$g_m = - \frac{q\mu W}{L} \left[\left(\frac{qd}{\varepsilon} n_D + \frac{2}{5} \gamma_0 n_D^{2/3} + V_{th} \right) \frac{\partial n_D}{\partial V_g} - \left(\frac{qd}{\varepsilon} n_S + \frac{2}{5} \gamma_0 n_S^{2/3} + V_{th} \right) \frac{\partial n_S}{\partial V_g} \right] \quad (III.63)$$

where

$$\frac{\partial n_S}{\partial V_g} = \frac{1}{\frac{qd}{\varepsilon} + \frac{2}{3} \gamma_0 n_S^{-1/3} + V_{th} n_S^{-1}} \quad (III.64)$$

and

$$\frac{\partial n_D}{\partial V_g} = \frac{1}{\frac{qd}{\varepsilon} + \frac{2}{3} \gamma_0 n_D^{-1/3} + V_{th} n_D^{-1}}. \quad (III.65)$$

Eqs (III.64) and (III.65) are obtained from the differentiation of Eq. (III.40) at the source and at the drain respectively. Substituting each partial derivative of the carrier sheet densities at the source and drain given by Eqs (III.64) and (III.65) respectively into Eq. (III.63) and simplifying gives

$$g_m = - \frac{q\mu W}{L} [n_D - n_S]. \quad (III.66)$$

Similarly, the analytical expression of the conductance can be obtained by calculating the partial derivative of the current in terms of the drain voltage. Thus,

$$\frac{\partial I_{ds}}{\partial V_d} = g_d = - \frac{q\mu W}{L} \left[\frac{qd}{2\varepsilon} \left(\frac{\partial n_D^2}{\partial V_d} - \frac{\partial n_S^2}{\partial V_d} \right) + \frac{2}{5} \gamma_0 \left(\frac{\partial n_D^{5/3}}{\partial V_d} - \frac{\partial n_S^{5/3}}{\partial V_d} \right) + V_{th} \left(\frac{\partial n_D}{\partial V_d} - \frac{\partial n_S}{\partial V_d} \right) \right]. \quad (III.67)$$

Since the carrier sheet density at the source does not depend on the drain voltage, all the partial derivative terms of n_S in Eq. (III.67) result in zero. Therefore, the expression of the conductance can be written as

Chapter III: *An analytical physics-based compact modeling of I-V and C-V characteristics in $Al_xGa_{1-x}N/GaN$ HEMTs*

$$g_d = - \frac{q\mu W}{L} \left[\left(\frac{qd}{\varepsilon} n_D + \frac{2}{3} \gamma_0 n_D^{2/3} + V_{th} \right) \frac{\partial n_D}{\partial V_d} \right]. \quad (\text{III.68})$$

where

$$\frac{\partial n_D}{\partial V_d} = \frac{-1}{\frac{qd}{\varepsilon} + \frac{2}{3} \gamma_0 n_D^{-1/3} + V_{th} n_D^{-1}}. \quad (\text{III.69})$$

Eq. (III.69) obtained by the partial differentiation of Eq. (III.40) at the drain terminal. Thus, substituting Eq. (III.69) into Eq. (III.68) gives

$$g_d = - \frac{q\mu W}{L} n_D. \quad (\text{III.70})$$

III.4.2 Self-heating effects and temperature dependencies

As the operating power of GaN HEMT devices increases, it also becomes important to include the self-heating effects (*SHE*) in the compact model. The importance of self-heating in these devices has been studied in [23, 24]. The additional amount of temperature incurred due to *SHE* is given

$$\Delta T = R_{TH} P_d \quad (\text{III.71})$$

and

$$P_d = I_{ds} V_d, \quad (\text{III.72})$$

where P_d is the dissipated power and R_{TH} is the thermal resistance, that is the representative of the thermal behaviour of the device [25, 26]. Therefore, the operating temperature of the device should be modified to account for the temperature increment, ΔT , as

$$T_{actual} = T_{room} + \Delta T \quad (\text{III.73})$$

Chapter III: *An analytical physics-based compact modeling of I-V and C-V characteristics in $Al_xGa_{1-x}N/GaN$ HEMTs*

where T_{room} is the room temperature and T_{actual} is the modified operating temperature. The thermal voltage is an important device parameter, and all the other temperature dependent parameters of the model should then be calculated using the modified operating temperature.

The local temperature in the device due to self-heating may increase to well above the room temperature T_{room} . The presence of *SHE* can be seen from the output (I_d - V_d) characteristics of the device in high power operation P_d .

The drain current decrease I_d with increasing V_d is the signature of *SHE*. The effects of self-heating have been included in the model using the thermal circuit approach as is done in standard models like BSIMSOI [27]. In addition, the empirical temperature dependences of mobility [28] and cut-off voltage V_{off} [29] are included in the model.

III.5 Analytical gate charge and capacitances model

III.5.1 Gate charge model

The total gate charge can be obtained by integrating the carrier sheet density along the channel over the total gate charge area [21]. Therefore,

$$Q_g = W \int_0^L qn_s(x) dx. \quad (III.74)$$

The integration variable in Eq. (III.74), dx can be changed to dV using Eq. (III.51) as the expression of dV in terms of dn_s is already given by Eq. (III.54) and an once again be used to derive the gate charge expression in terms of carrier sheet densities at the source and the drain. Thus, using Eq. (III.52)

$$Q_g = \frac{W^2 q^2 \mu}{I_{ds}} \int_{v_s}^{v_d} n_s^2 dV. \quad (III.75)$$

Again substituting for I_{ds} into Eq. (III.75) from Eq. (III.53) gives

Chapter III: *An analytical physics-based compact modeling of I-V and C-V characteristics in $Al_xGa_{1-x}N/GaN$ HEMTs*

$$Q_g = WLq \left(\frac{\int_{V_s}^{V_d} n_s^2 dV}{\int_{V_s}^{V_d} n_s dV} \right). \quad (III.76)$$

Let the two integrals at the numerator and denominator inside the brackets in Eq. (III.76) be represented as $f(n_s)$ and $g(n_s)$, respectively. Integrating the two separately after changing the integration variable from dV to dn_s using Eq. (III.54) gives

$$f(n_s) = \frac{qd}{3\epsilon} (n_D^3 - n_S^3) + \frac{1}{4} \gamma_0 (n_D^{8/3} - n_S^{8/3}) + \frac{1}{2} V_{th} (n_D^2 - n_S^2). \quad (III.77)$$

$$g(n_s) = \frac{qd}{2\epsilon} (n_D^2 - n_S^2) + \frac{2}{5} \gamma_0 (n_D^{5/3} - n_S^{5/3}) + V_{th} (n_D - n_S). \quad (III.78)$$

Note that : $g(n_s) = -I_{ds} L / q\mu W$.

Thus, the complete gate charge expression becomes

$$Q_g = WLq \left(\frac{\frac{qd}{3\epsilon} (n_D^3 - n_S^3) + \frac{1}{4} \gamma_0 (n_D^{8/3} - n_S^{8/3}) + \frac{1}{2} V_{th} (n_D^2 - n_S^2)}{\frac{qd}{2\epsilon} (n_D^2 - n_S^2) + \frac{2}{5} \gamma_0 (n_D^{5/3} - n_S^{5/3}) + V_{th} (n_D - n_S)} \right). \quad (III.79)$$

Eq. (III.79) gives the total gate charge of the charge carriers in the whole channel region from source to drain [30].

III.5.2 Gate capacitances model

The two main intrinsic capacitances associated with the gate region, gate-source capacitance C_{gs} and gate-drain capacitance C_{gd} , can be derived using the partial differentiations of the total gate charge with respect to the corresponding source and drain terminal voltages. To come up with simplified expressions of the gate capacitances, the two functions of numerator and denominator n_s given by Eqs (III.77) and (III.78) have been used. In addition, the letter x is also used to refer to a point along the channel so that one can determine the derivative of the gate charge not only at the source and drain but

Chapter III: *An analytical physics-based compact modeling of I-V and C-V characteristics in $Al_xGa_{1-x}N/GaN$ HEMTs*

also at any point along the channel as long as the potential at that point is identified. Thus, the general gate capacitances are given by [30].

$$C_{gx} = WLq \frac{\partial n_D}{\partial V_d} \left(\frac{g(n_s) \frac{\partial f(n_s)}{\partial V_x} - f(n_s) \frac{\partial g(n_s)}{\partial V_x}}{(g(n_s))^2} \right). \quad (\text{III.80})$$

where, for example, $V_x = V_s$ at the source terminal and $V_x = V_d$ at the drain terminal and similarly $C_{gx} = C_{gs}$ at the source and $C_{gx} = C_{gd}$ at the drain. To simplify the partial differentiations of $f(n_s)$ and $g(n_s)$, they can be written as the differences of two functions calculated at the source and the drain terminals as follows

$$f(n_s) = f_{main}(n_D) - f_{main}(n_s). \quad (\text{III.81})$$

$$g(n_s) = g_{main}(n_D) - g_{main}(n_s). \quad (\text{III.82})$$

where

$$f_{main}(n_x) = \frac{qd}{3\epsilon} n_x^3 + \frac{1}{4} \gamma_0 n_x^{8/3} + \frac{1}{2} V_{th} n_x^2. \quad (\text{III.83})$$

$$g_{main}(n_x) = \frac{qd}{3\epsilon} n_x^2 + \frac{2}{5} \gamma_0 n_x^{5/3} + \frac{1}{2} V_{th} n_x. \quad (\text{III.84})$$

where $n_x = n_D$ at the drain and $n_x = n_s$ at the source. The main advantage of expressing $f(n_s)$ and $g(n_s)$ as given by Eqs (III.81) and (III.82) using the functions given in Eqs (III.83) and (III.84) is that the partial derivatives of $f(n_s)$ and $g(n_s)$ in V_s and V_d will be simplified into direct derivatives of $f_{main}(n_x)$ and $g_{main}(n_x)$ at the respective terminals as they can be calculated independently at each terminal. These derivatives of $f_{main}(n_x)$ and $g_{main}(n_x)$ are given as

$$\frac{df_{main}(n_x)}{dV_x} = \left(\frac{qd}{\epsilon} n_x^2 + \frac{2}{3} \gamma_0 n_x^{5/3} + \frac{1}{2} V_{th} n_x \right) \frac{dn_x}{dV_x} \quad (\text{III.85})$$

and

Chapter III: *An analytical physics-based compact modeling of I-V and C-V characteristics in $Al_xGa_{1-x}N/GaN$ HEMTs*

$$\frac{dg_{main}(n_x)}{dV_x} = \left(\frac{qd}{\varepsilon} n_x + \frac{2}{3} \gamma_0 n_x^{2/3} + \frac{1}{2} V_{th} \right) \frac{dn_x}{dV_x}. \quad (III.86)$$

Therefore, the general gate capacitances can be expressed as

$$C_{gx} = WLq \left(\frac{g(n_s) \frac{df_{main}(n_x)}{dV_x} - f(n_s) \frac{dg_{main}(n_x)}{dV_x}}{(g(n_s))^2} \right). \quad (III.87)$$

The gate to source and gate to drain capacitances term in Eq. (III.87) can be calculated using the partial differentiations of the gate charge to calculate the capacitances, C_{gs} and C_{gd} .

III.5.3 Cut-off frequency f_T

The cut-off frequency of a transistor is a figure of merit used to characterize the switching speed of the transistor. A simplified method can be used to calculate the cutoff frequency. As shown in [31], dividing the intrinsic transconductance of the device by the total of the parasitic gate capacitance (C_{gs} plus C_{gd}), the cut-off frequency f_T can be expressed as

$$f_T = \frac{g_m}{2\pi(C_{gs} + C_{gd})}, \quad (III.88)$$

The " 2π " is included in the denominator to yield a result in terms of hertz and not radians. Often C_{gd} can be excluded from the expression altogether since it is usually orders of magnitudes less than C_{gs} .

The maximum oscillation frequency f_{max} is given by

$$f_{max} = \frac{g_m}{2 \sqrt{4 \frac{(R_s + R_g + R_{gs})}{R_{ds}} + 2 \frac{C_{gd}}{C_{gs}} \left(\frac{C_{gd}}{C_{gs}} + g_m (R_s + R_{gs}) \right)}}. \quad (III.89)$$

Chapter III: *An analytical physics-based compact modeling of I-V and C-V characteristics in $\text{Al}_x\text{Ga}_{1-x}\text{N}/\text{GaN}$ HEMTs*

where R_s, R_g, R_{gs} and R_{ds} are the resistances of: source, gate, gate-to-source and drain-to-source respectively. C_{gs} and C_{gd} are the gate-source and gate-to-drain capacitances. Figure (III.8) shows the small-signal equivalent circuit for GaN HEMT.

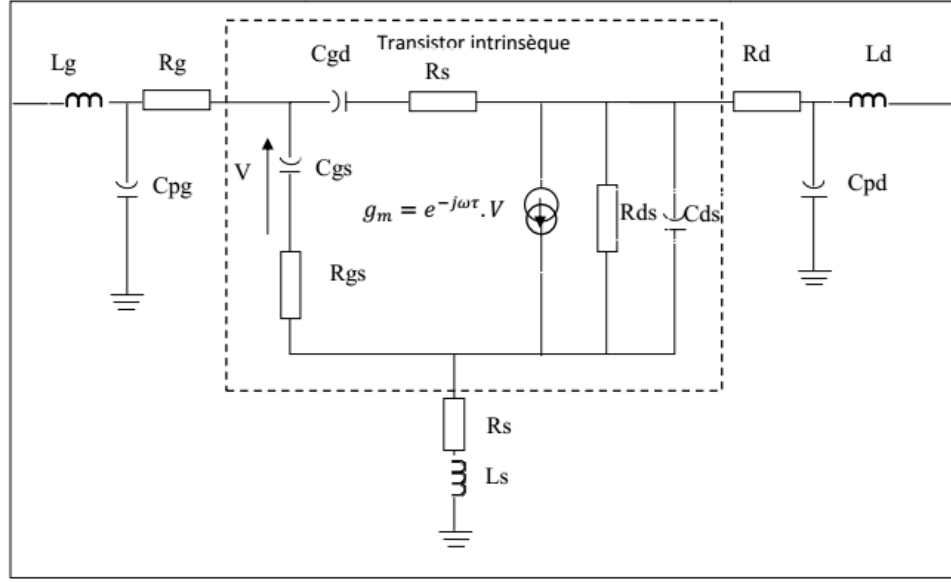


Figure III.8: GaN high electron mobility transistor small-signal equivalent circuit model [32].

III.6 Summary

In this chapter, a physics-based compact model of current, charge and capacitances has been developed based on the fundamental electrostatic consideration of the heterojunction interface of $\text{Al}_x\text{Ga}_{1-x}\text{N}/\text{GaN}$ HEMT. The Schrodinger's equation was used to generate an equation relating the carrier sheet density n_s to the Fermi level E_f and the first two energy sub-bands E_0, E_1 . The special case of $\text{Al}_x\text{Ga}_{1-x}\text{N}/\text{GaN}$ heterojunction has been considered, the relative positions of the first two energy sub-bands and the Fermi-level have shown that the second energy level is significantly higher than the first energy level and the

Chapter III: *An analytical physics-based compact modeling of I-V and C-V characteristics in $Al_xGa_{1-x}N/GaN$ HEMTs*


Fermi-level. Therefore, the contribution of the second energy level to the carrier sheet density has been neglected.

We have incorporated the effect of the mole fraction in this compact model for $Al_xGa_{1-x}N/GaN$ HEMT, by means of the threshold voltage expression. The carrier sheet density expression depends on V_{off} , where the mole fraction effect is accounted for. This leads to mole fraction dependent expressions of the drain current and capacitances. This allows a better understanding of the ways to achieve higher performance levels for GaN based high speed devices.


References

- [1] B.J. Sheu, D.L. Scharfetter, P.K. Ko and Min Chie Jeng, "BSIM : Berkeley short-channel IGFET model for MOS transistor", *IEEE J. Solid State Circuits*, vol. **22**, n°.4, pp.558-566, 1987.
- [2] "BSIM3 Users Manual", *BSIM Group*, Technical report No. UCB/ERL M98/51, *University of California, Berkeley*.
- [3] M. Bucher, C. Lalleement, C. Enz, and F. Krummenacher, "Accurate MOS modeling for analogue circuit simulation using the EKV model", *Proc. Inc. Conf. on Circuit and Systems*, vol. **4**, pp.703-706, 1996.
- [4] G. Gildenblat, X. Li, W. Wu Wang, A. Jha, Rvan Langevelde, G. D. J. Smit, A. J. Scholten, and D. B. M. Klaseen, "PSP: An advance surface-potential-based MOSFET model for circuit simulation", *IEEE Trans. Electron Devices*, vol. **53**, n°.9, pp.1979-1993, 2006.

Chapter III: *An analytical physics-based compact modeling of I-V and C-V characteristics in $Al_xGa_{1-x}N/GaN$ HEMTs*

- 
- [5] X. Cheng and Y. Wang, "A surface-potential-based compact model for algan/gan modfets", *Electron Devices, IEEE Transactions on*, vol. **58**, n°.2, pp.448–454, 2011.
- [6] S. Khandelwal, C. Yadav, S. Agnihotri, Y. S. Chauhan, A. Curutchet, T. Zimmer, J-C De Jaeger, N. Defrance, and T. A. Fjeldly, "Robust surface-potential-based compact model for gan hemt ic design", *Electron Devices, IEEE Transactions on*, vol. **60**, n°.10, pp.3216–3222, 2013.
- [7] P. Martin and R. Hahe, "Hsp: A surface-potential-based compact model of algan/gan hemts power transistors", *MOS-AK, Bordeaux, France*, 2012.
- [8] M. Shur, "Physics of semiconductor devices", *Engelwood Clifs, NJ, Prentice-Hall, Inc.* 1990.
- [9] F. Robert. Pierret, "Modulator Series on Solid State devices", *Addison Wesley Publishing Company*, vol. **VI**, 1999.
- [10] D. Delagebeaudeuf and N. T. Linh, "Metal-(n) AlGaAs-GaAs two-dimensional electron gas Fet", *Electron Devices, IEEE Transactions on*, vol. **29**, n°.6, pp.955-960, 1982.
- [11] K. Lee, M. Shur, T. Drummond, and H. Morkoc, "Current-voltage and capacitance voltage characteristics of modulation-doped field-effect transistors", *Electron Devices, IEEE Transactions on*, vol. **30**, n°.3, pp.207-212, 1983.
- [12] O. Ambacher, B. Foutz, J. Smart, J.R. Shealy, N. G. Weimann, K. Chu, M. Murphy, A.J. Sierakowski, W.J. Schaff, and L.F. Eastman "Two dimensional electron gases induced by spontaneous and piezoelectric polarization in undoped and doped AlGaN/GaN heterostructures", *Journal of Applied Physics*, vol. **87**, n°.1, 2000.

Chapter III: *An analytical physics-based compact modeling of I–V and C–V characteristics in $\text{Al}_x\text{Ga}_{1-x}\text{N}/\text{GaN}$ HEMTs*

- 
- [13] S.M. Sze and K.K. Ng, "Physics of Semiconductor Devices", 3rd Ed. *John Wiley & Sons*, Inc. 2007.
- [14] S. Khandelwal and T. A. Fjeldly, "A physics based compact model for I–V and C–V characteristics in AlGaIn/GaN HEMT devices", *Solid State Electron*, vol. **76**, pp.60–66, 2012.
- [15] F. Yigletu, B. Iniguez, S. Khandelwal, and T. Fjeldly, "A compact charge-based physical model for AlGaIn/GaN HEMTs", *In Radio and Wireless Symposium (RWS), IEEE*, pp.274-276, 2013.
- [16] S. Khandelwal, N. Goyal, and T. Fjeldly, "A physics-based analytical model for 2DEG charge density in AlGaIn/GaN HEMT devices", *Electron Devices, IEEE Transactions on*, vol. **58**, n°.10, pp.3622-3625, 2011.
- [17] Z. Lin, W. Lu, J. Lee, and D. Liu, "Barrier heights of Schottky contacts on strained AlGaIn/GaN heterostructures: Determination and effect of metal work functions", *Appl. Phys. Lett*, vol. **82**, n°.24, 2003.
- [18] A.J. Ekpunobi, A.O.E. Animalu, "Band offsets and properties of $\text{AlGaAs}/\text{GaAs}$ and AlGaIn/GaN material systems", *Superlattices and Microstructures*, vol. **31**, n°.5, 2002.
- [19] X. Cheng, Y. Wang, "A surface-potential-based compact model for AlGaIn/GaN MODFETs", *IEEE Transactions on Electron Devices*, vol. **58**, n°.2, pp.448 – 454, 2011.
- [20] V. Fiorentini, F. Bernardini, O. Ambacher, "Evidence for nonlinear macroscopic polarization in III–V nitride alloy heterostructures", *Appl. Phys. Lett*. vol. **80**, n°.7, 2002.
- [21] Y.C. Trond Ytterdal and T.A. Fjeldly, "Device modeling for analog and RF CMOS circuit design", *John Wiley & Sons*, Inc, 2003.

Chapter III: *An analytical physics-based compact modeling of I-V and C-V characteristics in $Al_xGa_{1-x}N/GaN$ HEMTs*

- [22] F. Mulugeta Yigletu, S. Khandelwal, A. Fjeldly, B. Iñiguez, "Compact Charge-Based Physical Models for Current and Capacitances in AlGaN/GaN HEMTs", *IEEE transactions on electron devices*, vol. **60**, n°.11, 2013.
- [23] T. Sadi, R.W. Kelsall, N.J. Pilgrim, "Investigation of self-heating effects in submicrometer GaN/AlGaN HEMTs using an electrothermal Monte Carlo method", *IEEE Trans Electron Dev*, vol. **53**, n°.12, pp.2892–900, 2006.
- [24] V. O. Turin, A. A. Balandin, "Electrothermal simulation of the self-heating effects in GaN based field-effect transistors", *J Appl Phys*, vol. **100**, n°.5, pp.054–501, 2006.
- [25] A. Santarelli, V. Di Giacomo, R. Cignani, S. D'Angelo, D. Niessen, and F. Filicori, "Nonlinear thermal resistance characterization for compact electrothermal GaN HEMT modelling", *In Microwave Integrated Circuits Conference (EuMIC), European*, pp.82-85, 2010.
- [26] S. Dahmani, E. Mengistu, and G. Kompa, "Thermal model extraction of GaN HEMTs for large-signal modelling", *In Microwave Integrated Circuit Conference, EuMIC. European*, pp.226-229, 2008.
- [27] "BSIMSOI4.3 User's Manual", *BSIM Group*, <http://wwwdevice.eecs.berkeley.edu/~bsimsoi/archive>, 2009.
- [28] W.S. Tan, M.J. Uren, P.W. Fry, P.A. Houston, R.S. Balmer, T. Martin, "High temperature performance of AlGaN/GaN HEMT on Si substrates", *J Solid State Electron*, vol. **50**, n°.3, pp.511-513, 2006.
- [29] M. Shur, "GaAs devices and circuits", *New York: Plenum Press*, pp.518–521, 1987.

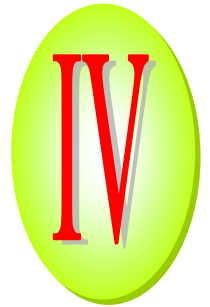
Chapter III: *An analytical physics-based compact modeling of I-V and C-V characteristics in $Al_xGa_{1-x}N$ /GaN HEMTs*

[30] F. Yigletu, B. Iniguez, S. Khandelwal, and T. Fjeldly, "Compact physical models for gate charge and gate capacitances of AlGa_N/Ga_N HEMTs", *International Conference on Simulation of Semiconductor Processes and Devices (SISPAD)*, pp.268-271, 2013.

[31] W. Liu, "Fundamentals of III-V Devices: HBTs, MESFETs, and HFETs/HEMTs", *John Wiley and Sons, New York, NY*, 1999.

[32] Z. Wen, Y. Xu, C. Wang, X. Zhao and R. Xu, "An efficient parameter extraction method for Ga_N HEMT small-signal equivalent circuit model", *Int. J. Numer. Model.*, 2015.

Chapter



Simulation results and discussion

Chapter IV

Simulation results and discussion


IV.1 Introduction

In this chapter, we calculate the different electrical properties based on the compact analytical model derived in chapter III and implemented in Matlab software. The calculated properties are compared to those obtained with the commercial Silvaco software and with experimental data if available.

Simulation results to be compared with our analytical model are generated using Silvaco software package. An input deck was generated in the DECKBUILD™ VWF interactive tool, solved through the ATLAS™ routine, and analyzed using the TONYPLOT™ tool. Additionally, the BLAZE™ routine, a routine specifically designed for group III-V materials and devices with position dependent band structures was utilized to simulate the AlGaIn/GaN HEMTs.

First of all, we calculate the I - V characteristics and their dependence on the mole fraction of the AlGaIn barrier layer, and then we calculate the C - V characteristics taking the mole fraction as a parameter. The self-heating effect on the HEMT devices is also simulated and studied. In the following section we present briefly the Silvaco software.

Chapter IV: *Simulation results and discussion*



IV.2 Silvaco simulation software

IV.2.1 Overview

The Silvaco software suite is powerful simulation software that uses physics based simulations. Physically-based device simulators predict the electrical characteristics that are associated with specified physical structures and bias conditions. ATLAS™ achieves this simulation by applying a two or three dimensional grid that forms nodes throughout the structure. The nodes are solved in a matrix with charge transport equations from Maxwell's continuity and drift-diffusion equations [1].

The ATLAS™ simulator is a command driven simulator that requires an input in a specific sequence. The order in which the statements occur is important to the proper simulation of a device. There are five groups of statements, and if not correctly stated will result in errors or erroneous simulations. The required groups and statements are as follows [1]:

- **Structure specification**
 - o Mesh
 - o Region
 - o Electrode
 - o Doping
- **Material Models Specification**
 - o Material
 - o Models
 - o Contact Interface
- **Numerical Method Selection**
 - o Method
- **Solution Specification**

Chapter IV: *Simulation results and discussion*

- o Log
- o Solve
- o Load
- o Save
- **Results Analysis**
 - o Extract
 - o TONYPLOT

The above commands represent the entire structure definition and solution method. It is critical to have a firm understanding of the simulation variables prior to defining a structure. A small change in one variable or solution method can have undesirable consequences on device performance. Figure (IV.1) depicts a flowchart of the device simulation utilizing Silvaco International's simulators and modules.

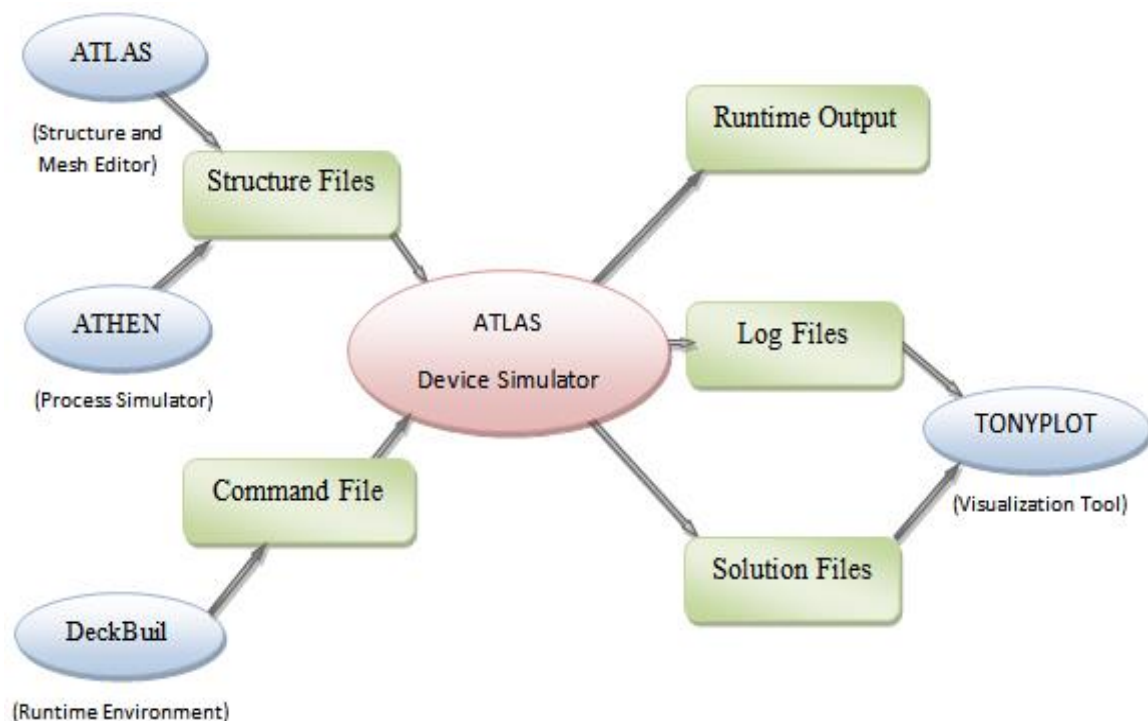


Figure IV.1: Silvaco simulation flowchart [1].

Chapter IV: *Simulation results and discussion*

IV.2.2 Silvaco semiconductor modeling equations

The models developed to simulate the operation of semiconductor devices consist of equations derived from Maxwell's laws, Poisson's equation. The continuity equations and the drift-diffusion transport equations. The method in which the above equations will be solved is a prime consideration when developing a device model in ATLAS™. Several different numerical methods can be used for calculating the solutions to various device structures. Different solution methods are employed depending on the situation [1].

IV.3 Model definition

To define the HEMTs model, ATLAS™ requires an input of the geometric parameters corresponding to the dimensions of the device to be modeled. The second step is to assign a mesh to enclose the structure. The purpose of the mesh is to define solution points throughout the structure. Defining the mesh correctly is one of the most important factors in the model development. If the mesh is too coarse, the solutions will not be correct, and if the mesh is too finely defined, the computation time can be prohibitive. The rest of the program file is defines to modifying statements and output parameters that will be discussed individually when necessary. (The entire model definition file, referred to as a *.in file is provided in Appendix B). The structure definition is saved in ATLAS™ as a *.str file. The structure file view in TONYPLOT™ provides a visual representation of the device. There are drop down menus that allow for a selection of the desired plot [2].

IV.4 AlGa_xGa_{1-x}N HEMTs structure

Figure (IV.2) shows the Al_xGa_{1-x}N/GaN HEMTs device consisting of 150 nm GaN buffer layer, where deposited on the SiC substrate in (0001) direction. The SiC

Chapter IV: *Simulation results and discussion*

substrate is insulating. On top 50 nm of the GaN buffer layer, followed by the growth of a 3 nm of $\text{Al}_x\text{Ga}_{1-x}\text{N}$ spacer layer with 9 nm of $\text{Al}_x\text{Ga}_{1-x}\text{N}$ barrier, It can be seen here that the barrier layer AlGa_N under the gate is doped, while the GaN buffer layer is undoped. The source and drain contacts are ohmic, while the gate is a Schottky barrier of (Ni and Ti) [3] with Si_3N_4 Oxide layer is deployed in both sides of the gate.

For low values of drain-to-source bias, a current flows from drain to source through the electron channel. The carrier sheet density and consequently the conductivity of the channel are controlled by the gate bias. The gate width is a physical device dimension that is of primary importance to the determination of device behavior. The device current is directly proportional to the gate width because the cross-section area available for the channel current is proportional to Z . For low-noise, low-current applications relatively small-gate-width devices are utilized. In contrast, large-gate-width devices are typically used for power applications [4].

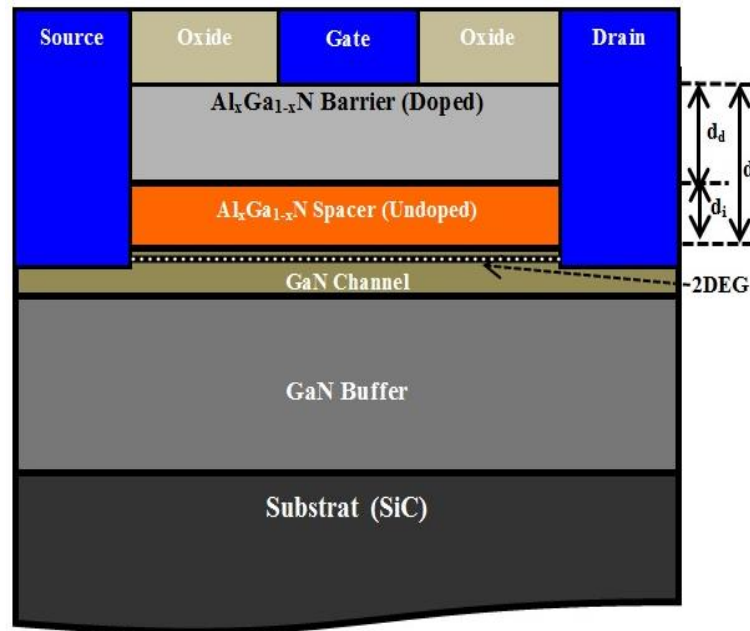


Figure IV.2: Cross sectional view of $\text{Al}_x\text{Ga}_{1-x}\text{N}/\text{GaN}$ nanostructures HEMTs using for simulation.

Chapter IV: *Simulation results and discussion*

To define a device through the ATLAS command language, we must first define a mesh. This mesh or grid covers the physical simulation domain. The mesh is defined by a series of horizontal and vertical lines and the spacing between them (see Figure (IV.3a)) Then, regions within this mesh are allocated to different materials as required to construct the device. Figure (IV.3b) show the mesh structure use for the simulation, the mesh is refined at the surface under the gate contact and at the AlGaIn/GaN heterointerface (2DEG channel region).

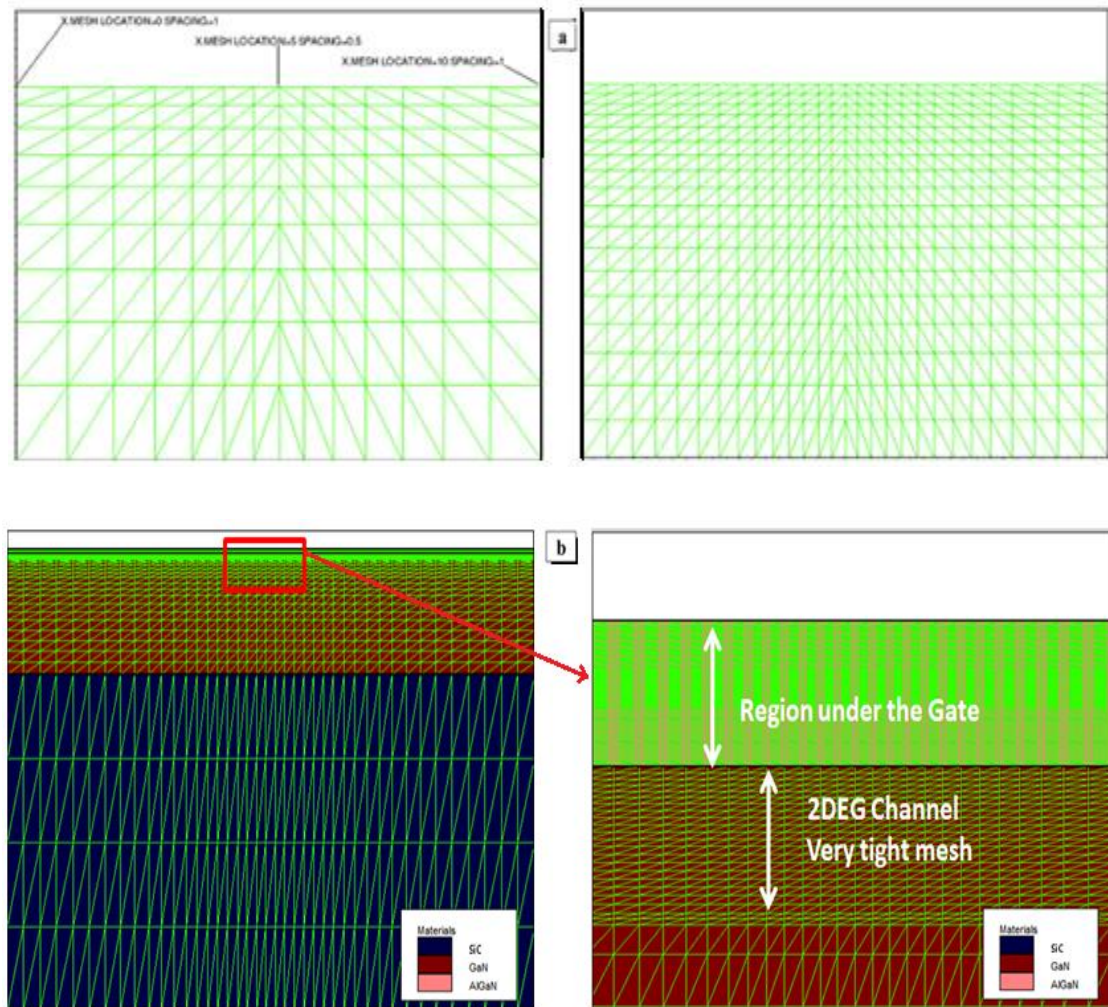


Figure IV.3: (a) Example of non-uniform mesh creation using ATLAS [1], (b) structure and mesh of $\text{Al}_x\text{Ga}_{1-x}\text{N}/\text{GaN}$ nanostructures HEMTs using for simulation.

Chapter IV: *Simulation results and discussion*

IV.5 Mole fraction, gate length and self-heating effects

IV.5.1 Mole fraction effect

The current-voltage (I - V) and capacitance-voltage (C - V) characteristics of devices with different mole fractions (see Table IV.1) have been simulated and compared with data exported from Atlas TCAD results.

Table IV.1: Parameters used to plot the I - V and C - V characteristics for three different samples in relation with molar fraction.

Parameter	Description	Sample 1 $\text{Al}_{0.25}\text{Ga}_{0.75}\text{N}$	Sample 2 $\text{Al}_{0.30}\text{Ga}_{0.70}\text{N}$	Sample 3 $\text{Al}_{0.35}\text{Ga}_{0.65}\text{N}$
V_{off} (V)	Cut-off voltage	-1.16	-1.61	-2.10
d_i (nm)	Thickness of barrier	9	9	9
d_d (nm)	Thickness of spacer	3	3	3
W_g (μm)	Gate width	100	100	100
L_g (μm)	Gate length	0.4	0.4	0.4

In order to validate our theoretical results against available experimental data, we compare some of the important parameters listed in Table (IV.1) with results obtained by Herwig Hahn *et al.* [5]. The highlighted part in Table (IV.2) show that for the 8.8 nm $\text{Al}_{0.26}\text{Ga}_{0.74}\text{N}$ barrier sample, the threshold voltage $V_{th} = -1.22$ Volts which is comparable to our theoretical value $V_{th} = -1.16$ for $\text{Al}_{0.25}\text{Ga}_{0.75}\text{N}$ sample with a barrier layer thickness of 9 nm.

Chapter IV: *Simulation results and discussion*

Table IV.2: Extracted DC values for four different samples of $\text{Al}_{0.26}\text{Ga}_{0.74}\text{N}/\text{GaN}$ HEMT [5]

Sample	V_{th} (V)	$I_{d,max}$ (A/mm)	$g_{m,max}$ (mS/mm)
22 nm	-3.83	1.36	215
8.8 nm	-1.22	1.16	260
5.1 nm	+0.00	1.27	342
2.1 nm	+0.82	1.35	366

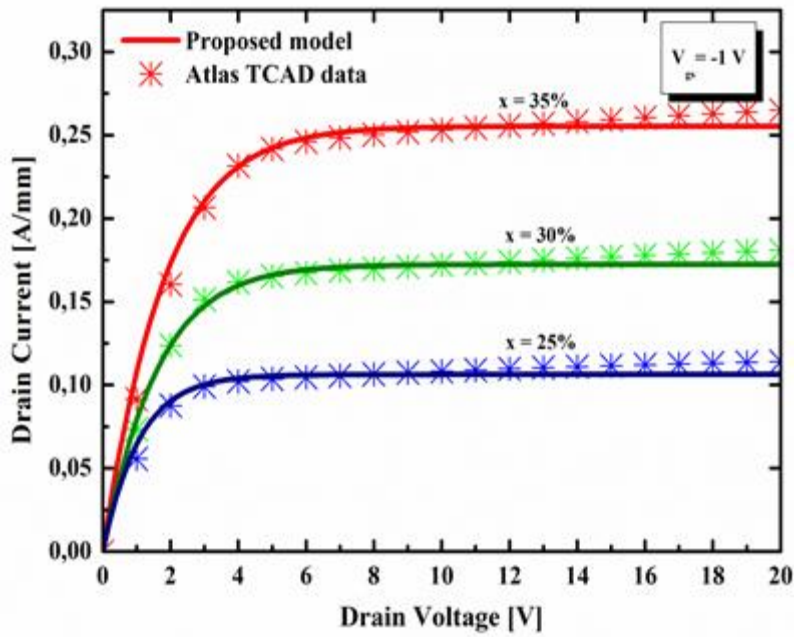


Figure IV.4: Comparison of modeled I_d - V_d characteristics (solid line) with Atlas TCAD data (symbols) Curves were plotted for mole fraction x values of (25, 30, and 35) %. At gate-to-source voltage $V_{gs} = -1$ V.

Figure (IV.4) shows the calculations of the electrical output characteristics of $\text{Al}_x\text{Ga}_{1-x}\text{N}/\text{GaN}$ HEMTs with a gate length of $0.4 \mu\text{m}$ for different mole fractions x in $\text{Al}_x\text{Ga}_{1-x}\text{N}/\text{GaN}$ HEMTs at $V_{gs} = -1$ V. The simulation results show that for $x = 35\%$ the

Chapter IV: *Simulation results and discussion*

HEMT reaches the maximum drain-to-source saturation current $I_{ds,sat} = 0.25$ A/mm compared with those obtained with $x = (25 \text{ and } 30) \%$.

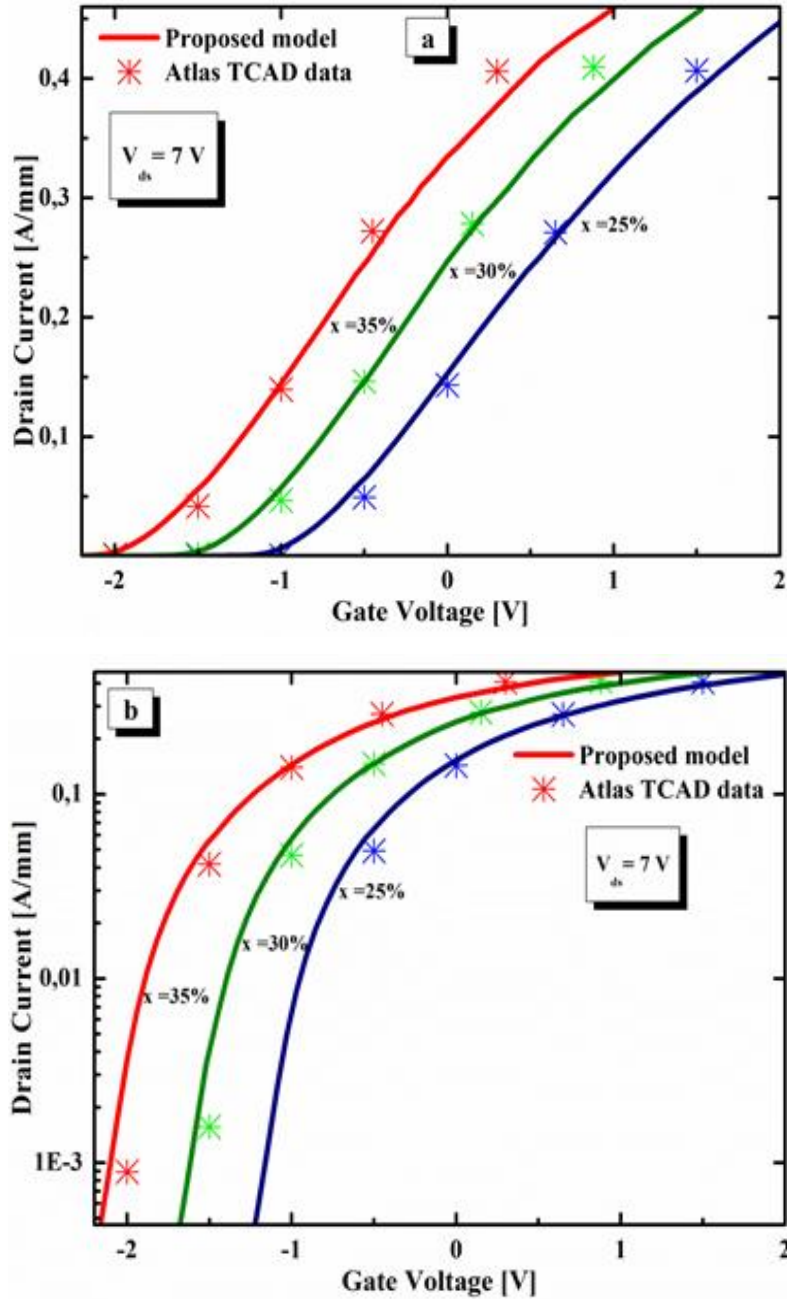


Figure IV.5: The I_d - V_g characteristics plotted from the model simulation results (solid line) is validated by comparison against Atlas TCAD data (symbols), (a) in linear and (b) in logarithmic scale for different mole fractions x in $\text{Al}_x\text{Ga}_{1-x}\text{N}/\text{GaN}$ HEMTs. Drain voltage was kept fixed at 7 V.

Chapter IV: *Simulation results and discussion*

The electrical transfer characteristics of $\text{Al}_x\text{Ga}_{1-x}\text{N}/\text{GaN}$ HEMTs for different mole fractions are shown in Figures (IV.5) (a) and (b) in linear and logarithmic scales, respectively. The measurement direction was from negative to positive voltages, with $V_{ds} = 7\text{V}$, where the HEMT reaches a low value of threshold voltage at $x = 35\%$. Thus, the current flowing in the device depends strongly on the mole fraction of the top layers. This is essentially due to an increase in the current drain saturation. Our results indicate that an improvement of the performance of HEMTs can be reached by varying mole fraction in the $\text{Al}_x\text{Ga}_{1-x}\text{N}$ layer.

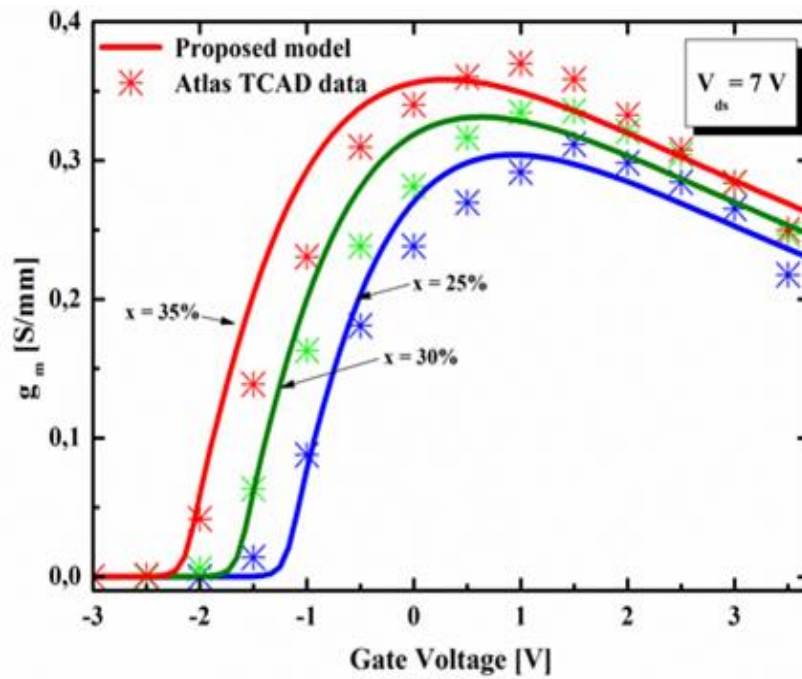


Figure IV.6: Transconductance plots for different mole fractions x of our HEMT devices, with drain-to-source voltage $V_{ds} = 7\text{V}$. Good agreement is achieved between the model (line) and Atlas TCAD data (symbols).

On the other hand, Figure (IV.6) shows the transconductance (the electrical characteristics relating the current through the output of a device to the voltage across the input of a device) as function of gate-to-source voltage V_{gs} . The maximum transconductance g_m at $V_{ds} = 7\text{V}$ is around 0.36 S/mm for $W_g = 100\text{ }\mu\text{m}$, this value is

Chapter IV: *Simulation results and discussion*

reached for 35% aluminum mole fraction in AlGa_N barrier layer. Similar results were obtained for both the model and Atlas TCAD data.

Once again, in order to verify the simulation results and calibration of the model parameters are compared with experimental values taken from [5], we can see in Table (IV.2) and Figure (IV.7) that for device width of 100 μm at $V_{\text{ds}} = 8\text{ V}$, The transconductance g_m (at $V_{\text{ds}} = 8\text{ V}$) for $V_{\text{gs}} = (-2, -1\text{ and } 0)\text{ V}$ were (0, 0.13 and 0.26) S/mm, respectively. We can see that these experimental results are in good agreement with the one obtained by our model and Atlas TCAD data.

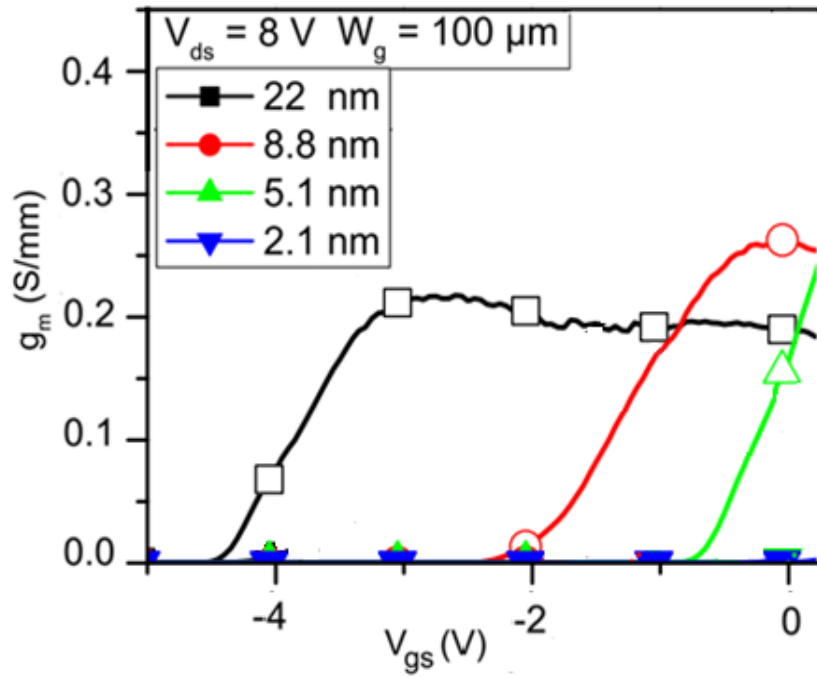


Figure IV.7: Transfer characteristics for four samples of Al_{0.25}Ga_{0.75}/GaN HEMT with gate width $W_g = 100\text{ }\mu\text{m}$ at $V_{\text{ds}} = 8\text{ V}$. The measurement direction was from negative to positive voltages [5].

Simulation results of the C – V characteristics have been carried out and compared with data obtained from Atlas TCAD. In Figure (IV.8) we show a plot of the gate-source capacitance C_{gs} in terms of the gate voltage V_g at drain voltage $V_d = 7\text{ V}$.

Chapter IV: *Simulation results and discussion*

Our results show the dependence of threshold voltage on the mole fraction. C_{gs} is small when V_g is below or close to V_{off} and it is equal to the fringing capacitance. The value of the fringing capacitance is found to be 0.78 pF/mm. As V_g increases C_{gs} rises due to the increase of the depth of the electron channel and the sheet carrier density increases thereby increasing the channel charge, and thus affects the gate-source capacitance. It is clear that the simulated model and the C_{gs} values obtained from Atlas TCAD software agrees quite well. Unfortunately, experimental data could not be obtained for comparison to the other results.

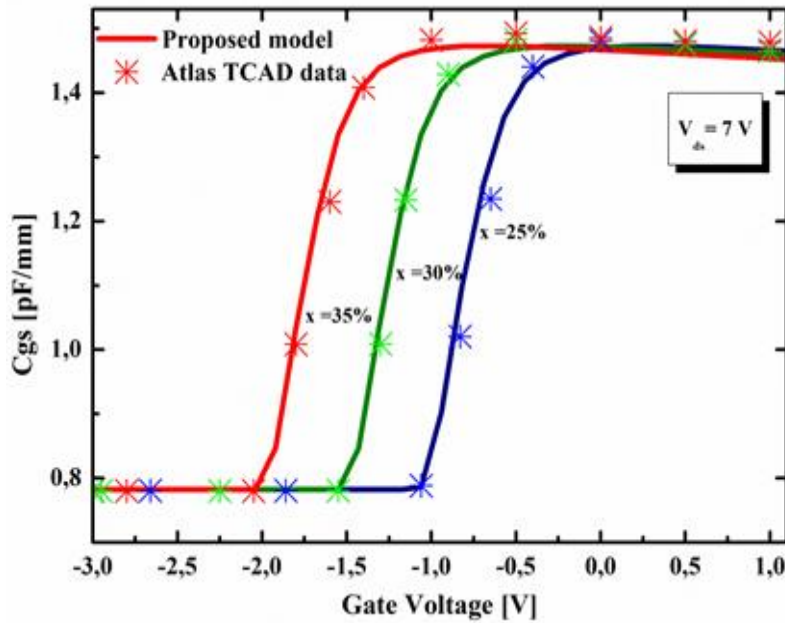


Figure IV.8: Atlas TCAD data (symbols) and modeled (solid lines) gate-source capacitance, C_{gs} , of a device with a mole fraction value varies between (25 and 35)%. Drain voltage was kept fixed at 7 V.

The gate-drain capacitance C_{gd} plotted against the drain voltage is shown in Figure (IV.9). This indicates a steady decrease in C_{gd} as the drain bias increases from (0 to 10) V and then maintained almost constant. Moreover, we observe that as mole fraction increases the capacitance decreases and we can see again that there is a good agreement between the model and exported Atlas TCAD data.

Chapter IV: Simulation results and discussion

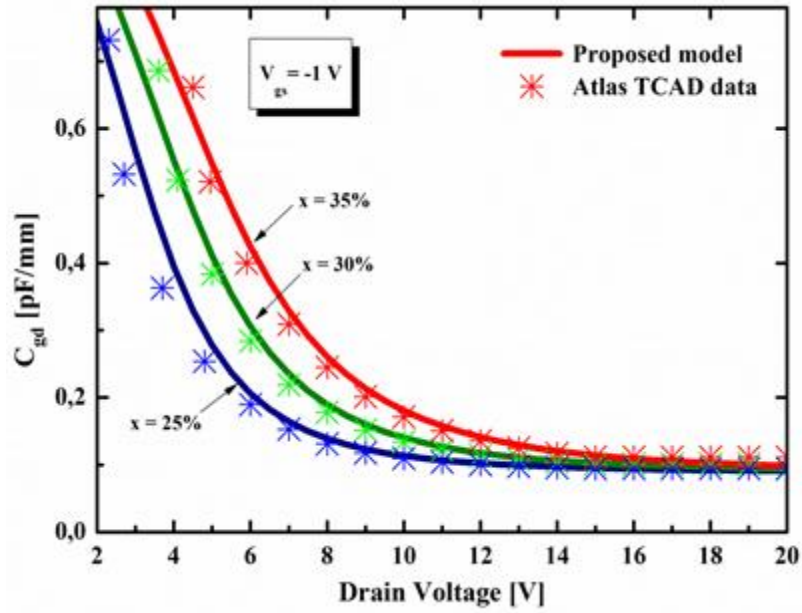


Figure IV.9: Comparison of modeled (solid line) with Atlas TCAD data (symbols) C_{gs} - V_d , for different mole fractions x in $\text{Al}_x\text{Ga}_{1-x}\text{N}/\text{GaN}$ HEMTs at $V_g = -1 \text{ V}$.

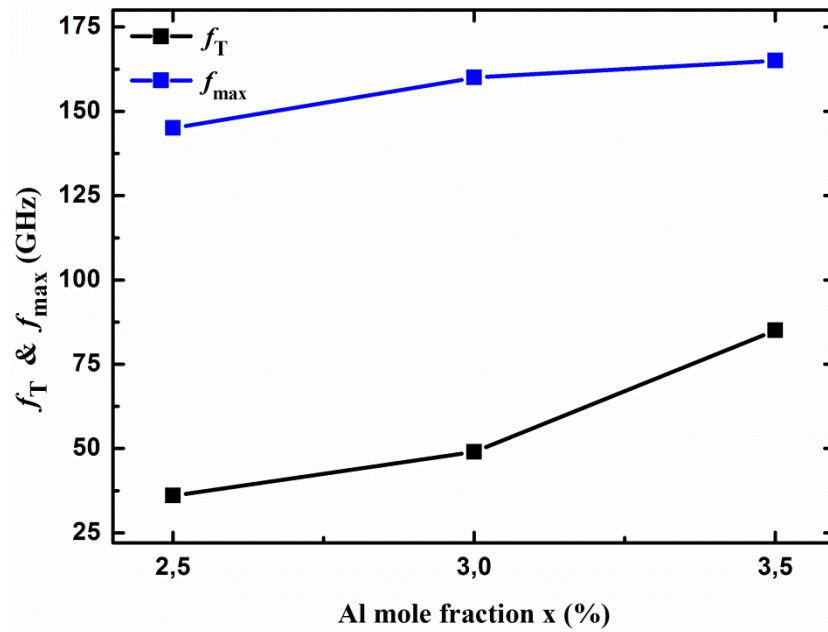


Figure IV.10: Influence of variation of the mole fraction (x) on the two frequencies: the cut-off frequency f_T (black) and the maximum oscillation frequency f_{max} (blue).

Chapter IV: *Simulation results and discussion*

The influence of variation of the mole fraction (x) on the cut-off frequency f_T and the maximum oscillation frequency f_{max} is shown in Figure (IV.10). We see that the frequency increases with the Al mole fraction. This can be explained by the fact that the increase of the Al molar fraction leads to a higher electric field of induced polarization. As a result, the electron confinement increase which cause a reduction of electron scattering in the channel. This leads to a decrease in the short channel effect, and consequently a higher output resistance, R_{ds} . Since f_T is directly proportional to R_{ds} (see Eq. (III-88) in chapter III), this leads to a higher f_{max} frequency.

IV.5.2 Gate length effect

The gate length is one of the important geometric parameters that affect the device performances. In this part, the impact of gate length variation on HEMTs parameter such as the output characteristics and the threshold voltage were investigated.

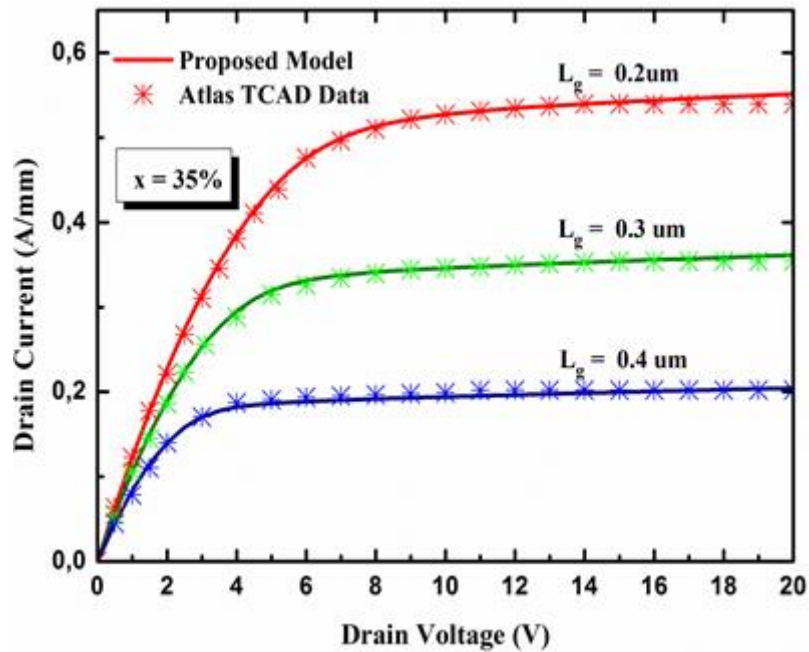


Figure IV.11: Drain current plotted as a function of drain voltage. Plot used to show the gate length variation effect on the HEMT devices transfer characteristics of in both linear and saturation regions of operation.

Chapter IV: *Simulation results and discussion*

The output characteristics for different gate lengths L_g in $\text{Al}_x\text{Ga}_{1-x}\text{N}/\text{GaN}$ HEMTs is shown in Figure (IV.11), with mole fraction $x = 35\%$ and gate voltage $V_g = -1$ V. Our results show remarkable improvement due to the gate length reduction and a good match between the model and Atlas TCAD exported data.

The knee voltage signifies the voltage where saturation occurs in the graph. Also, maximum drain current is the intersection of the linear and saturation regions. Pinch-off voltage V_{off} is where the drain current is almost zero.

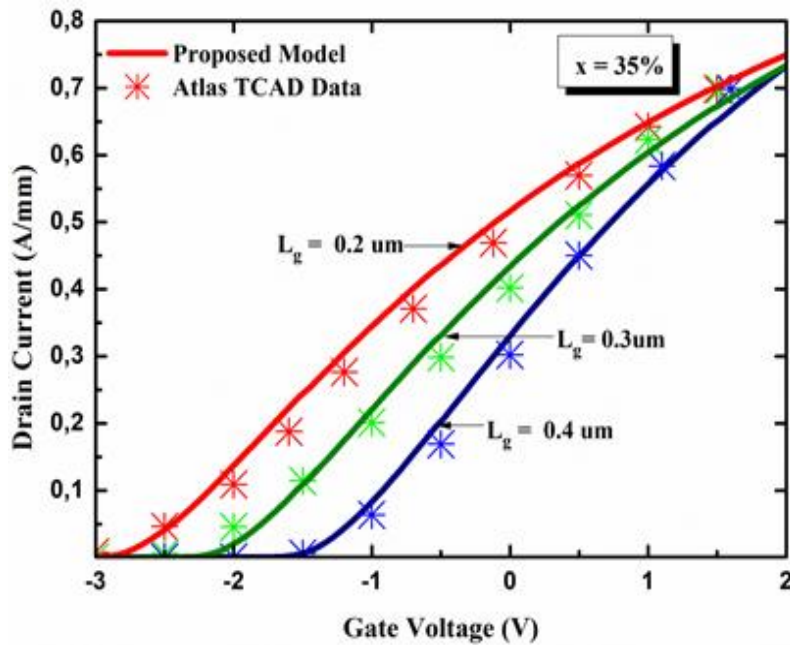


Figure IV.12: modeled drain current plotted as a function of gate voltage and compare against Atlas TCAD data in linear scale, for gate length L_g varies between (0.2 and 0.4) μm at $x = 35\%$.

Typical transfer characteristics I_d - V_g curve show some important parameters of the device, threshold voltage V_{th} is one of this important parameters that reveal the device. The transfer characteristics in (linear and logarithm) scale of $\text{Al}_x\text{Ga}_{1-x}\text{N}/\text{GaN}$ HEMTs with different gate lengths L_g varying from (0.4 to 0.2) μm , with step of 0.1 μm , when

Chapter IV: Simulation results and discussion

the mole fraction x is equal to 35%, which are shown in Figures (IV.12) and (IV.13), respectively. The simulation results show significant increasing in drain current I_d by scaling down the gate length, we can see here that the results of our proposed model are in good agreement with the Atlas TCAD simulation data.

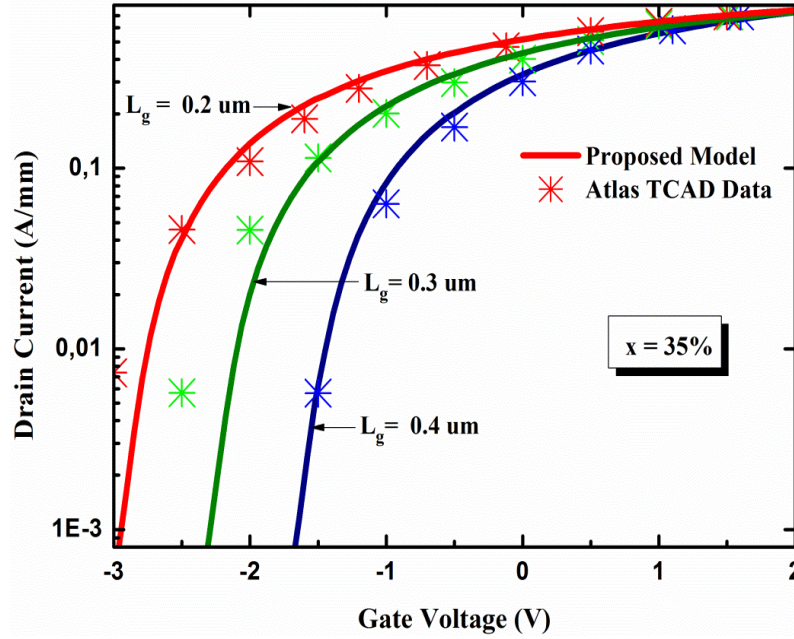


Figure IV.13: I_d - V_g characteristics of $Al_xGa_{1-x}N/GaN$ HEMTs for different gate lengths L_g at $x = 35\%$. The model simulation result (line) is validated by comparison against Atlas TCAD data (symbols).

In Figure (IV.14), modeled (solid line) and Atlas TCAD (symbols) C - V curves are shown from negative to positive gate bias for different gate length. The mole fraction x is fixed at 35% with drain-to-source voltage $V_{ds} = 5V$. The simulation results shows that as V_g increases C_{gs} rises because of the increase of the sheet carrier density due to the increases of the depth of the electron channel and thereby increasing the channel charge. A good matching between the Atlas TCAD data and modeled simulation results is obtained.

Chapter IV: Simulation results and discussion

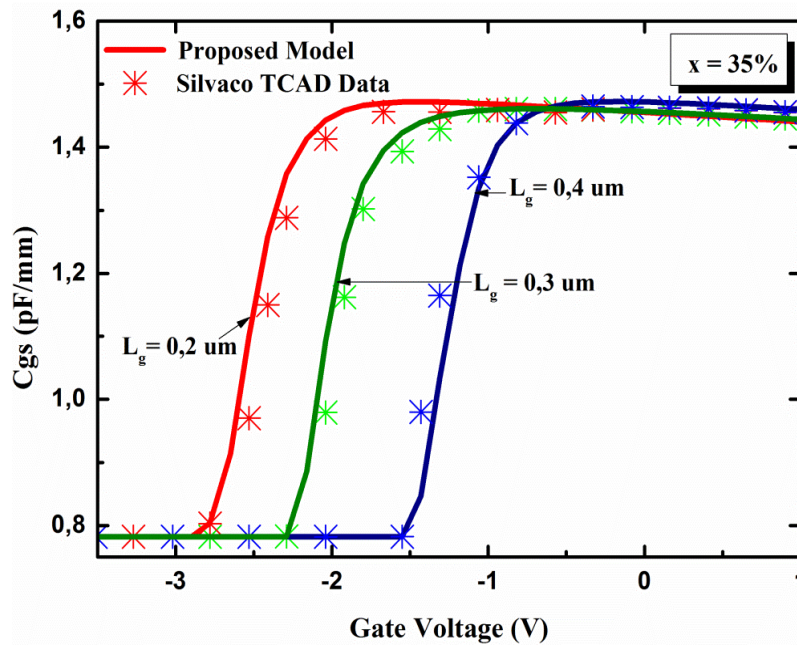


Figure IV.14: Comparison of modeled (solid line) with Atlas TCAD data (symbols) C_{gs} - V_g , for different gate lengths L_g in $\text{Al}_x\text{Ga}_{1-x}\text{N}/\text{GaN}$ HEMTs at $x = 35\%$.

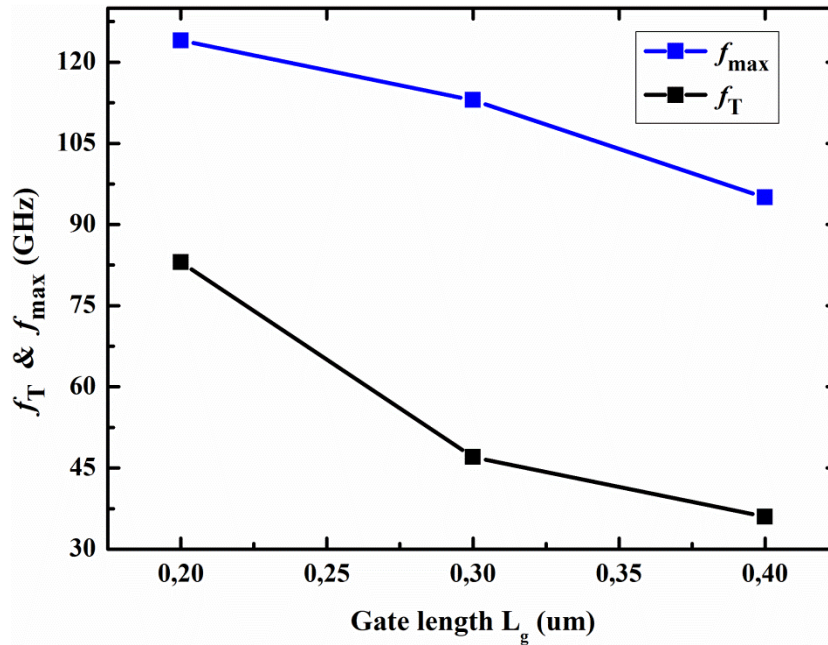


Figure IV.15: Gate length variation effect on the cut-off frequency f_T (black color) and the maximum oscillation frequency f_{max} (blue color).

Chapter IV: Simulation results and discussion

Since f_T and f_{max} are inversely proportional to C_{gs} and C_{gd} (see Eqs. (III.88) and (III.89) in chapter III), the decrease of the gate length leads to a noticeable improvement in AC characteristics as we can see in Figure (IV.15). But after a certain gate length, the AC characteristics of the device will be reduced due to the occurrence of short channel effects. The increase of the cut-off frequency f_T can therefore be obtained by decreasing the values of the C_{gs} and C_{gd} capacitances.

IV.5.3 Self-heating effect

Figure (IV.16) shows the output characteristics of the HEMTs with mole fraction of 35% are plotted for different gate biases ($V_{gs} = -3$ to 0 V, in -1 V steps). In this part, we have done a comparison to see the self-heating effect (SHE) on the drain current, we notice that at the high drain voltage values the drain-source current have started to reduce compare to the normal case.

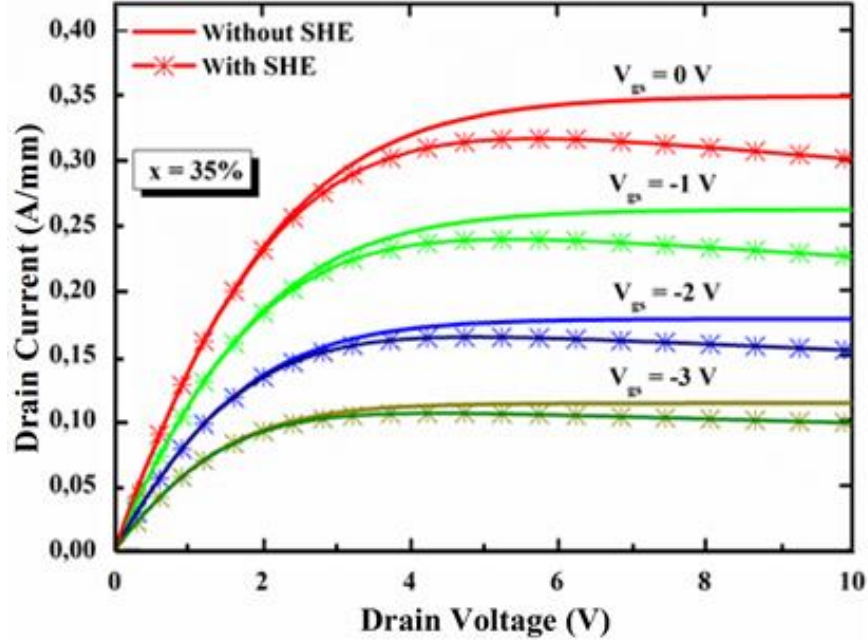


Figure IV.16: Drain current as a function of drain voltage (with and without self-heating effect). Gate voltages of $(-3, -2, -1$ and $0)$ V, were used for the curves. At mole fraction of the $\text{Al}_x\text{Ga}_{1-x}\text{N}$ layer $x = 35\%$.

Chapter IV: Simulation results and discussion

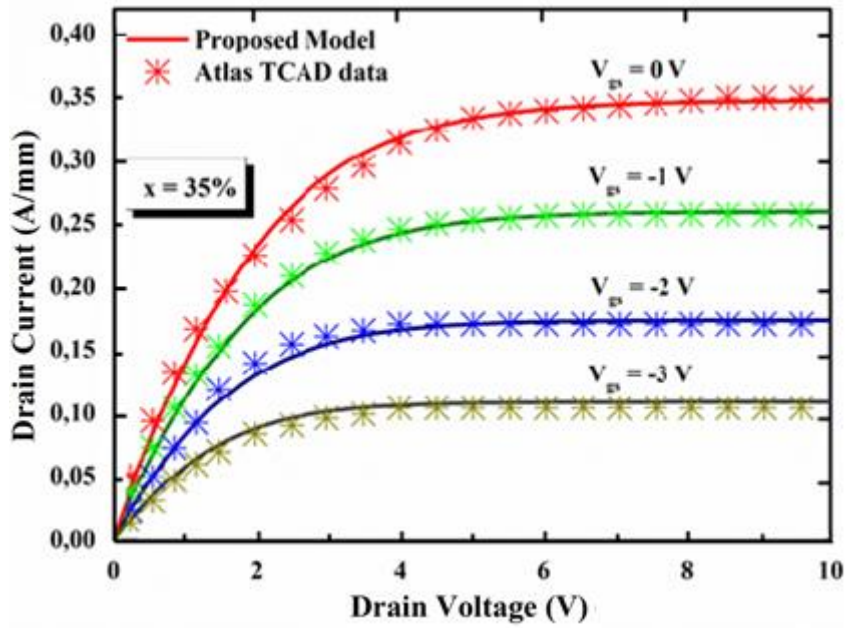



Figure IV.17: $\text{Al}_x\text{Ga}_{1-x}\text{N}/\text{GaN}$ HEMTs drain current as a function of drain voltage with gate voltage as a parameter. Solid lines correspond to model simulations; symbols correspond to Atlas TCAD data.

Moreover, to reproduce the current reduction at higher voltage that is caused by high power dissipation, we have to include the *SHE* in the model and we were able to reduce the drain current at higher voltage as we can see in Figure (IV.17) Current curves plotted for V_{gs} values of (-3, -2, -1, and 0) V. Maximum current results was for $V_{gs} = 0$ V with an I_d of 0.35 A/mm. Once again the model and Atlas TCAD data show an excellent agreement.

IV.6 Summary

In this chapter, we have incorporated the mole fraction effect in a compact model for $\text{Al}_x\text{Ga}_{1-x}\text{N}/\text{GaN}$ HEMTs, by means of the threshold voltage expression. The carrier sheet density expression depends on V_{off} , where the mole fraction effect is accounted for. Moreover, the simulation results shown significant increasing in drain current I_d by scaling the down the gate length and also we have done a comparison to see the self-heating effect on the drain current, we notice that at the high drain voltage values

Chapter IV: *Simulation results and discussion*



of the drain-source current have started to reduce compare to the normal case. Our results show that an excellent agreement obtained between Atlas TCAD data and modeled I - V and C - V characteristics of different mole fractions and gate lengths for $\text{Al}_x\text{Ga}_{1-x}\text{N}/\text{GaN}$ HEMTs. This leads to mole fraction dependent expressions of the drain current and capacitances. This allows a better understanding of the ways to achieve higher performance levels for GaN based high speed devices.

References

- [1] Silvaco International, *Silvaco International, ATLAS User's Manual*, 2000.
- [2] N. Wesley Scott, "Development of AlGa_N/Ga_N High Electron Mobility Transistors (HEMTs) on diamond substrates", *The NPS Institutional Archive*, 2006.
- [3] L. Yuan, H.C. Kevin. J. Chen, "Normally Off AlGa_N/Ga_N Metal-2DEG Tunnel-Junction Field-Effect Transistors", *IEEE electron device letters.*, vol. **32**, n°.3, pp.303-305, 2011.
- [4] H. Mathieu, "Physique des semiconducteurs et des composants électroniques". 6^{ème} Edition, pp.639-653, 2009.
- [5] H. Hahn, F. Benkhelifa, O. Ambacher, A. Alam, M. Heuken, H. Yacoub, A. Noculak, H. Kalisch, and A. Vescan, "GaN-on-Si enhancement mode metal insulator semiconductor heterostructure field effect transistor with on-current of 1.35 A/mm", *Japanese Journal of Applied Physics*, vol. **52**, pp.090204_1-090204_2, 2013.

Conclusion and future work prospects



Conclusion and future work prospects



V.1 General conclusion

In conclusion, this thesis is devoted to the study of the impact of different parameters on the performance of AlGaIn/GaN HEMTs. This task is accomplished through the development of a physics based compact model of the dependence of the 2DEG charge density on gate bias in AlGaIn/GaN HEMTs. The model includes important effects like velocity saturation, channel length modulation, short channel effect and self-heating effect. The model is developed by simplifying the basic device equations in different regions of operation and combining them in order to derive the terminal characteristics of the device. Analytical equations of drain current, gate charge and drain or gate capacitance dependence on mole fraction are derived. In addition, several geometrical and physical effects are investigated. The parameters used in this model are clearly linked to physical effects and does not have any empirical or fitting parameters.

By using our compact model combined with ATLAS SILVACO commercial software, we have carried out simulation of electrical characteristics of AlGaIn HEMTs. Regarding the electrical behavior, the distribution electron density, etc., were simulated, for better understanding the device operation principle. The device electrical characteristics as the drain current, drain and gate capacitance and thermal behavior have been investigated.

Several models are activated in the TCAD simulation in order to obtain realistic device characteristics, including: Shockley–Read–Hall recombination (SRH model), Auger recombination (Auger model), concentration and temperature dependent mobility (Analytic model), parallel electric-field-dependent mobility (Fldmob model). The spontaneous and piezoelectric polarizations are taken into account as fixed sheet charges

Conclusion and future work prospects



at the AlGa_N surface and AlGa_N/Ga_N interface. The proposed model is in excellent agreement with simulated data of I - V and C - V characteristics of the device obtained using Atlas Silvaco TCAD.

V.2 Future work prospects

As a device model is never complete, all the core and non-ideal effect modeling approaches used should be put under constant revision and improvement in consistence with the dynamic device fabrication. The possible future extensions of the research work fall into five themes:

- ☑ To develop an analytical expressions of the total drain charge using the charge control model.
- ☑ To derive the drain-gate and drain-source capacitance expressions from the analytical drain charge model.
- ☑ To study the influence the doping of AlGa_N barrier and of the temperature on the electrical properties of HEMT devices.
- ☑ To study the impact of geometrical parameters on the performance of the HEMT transistor.
- ☑ To explore the use of novel materials like high dielectrics to improve performance of the transistor.

Appendix



Appendix

A) Unified charge density model derivation

In chapter III, the Schrodinger's equation was used in conjunction with Fermi-Dirac statistics to generate an equation relating the sheet carrier density n_s , to the Fermi level, E_f . The unified expression for n_s that covers all the operating regions from deep subthreshold to full active gate bias can be derivate as explain in the follow.

Considering only the first energy level E_0 , we have

$$n_s = DV_{th} \ln \left[\exp \left(\frac{E_f - E_0}{V_{th}} \right) + 1 \right], \quad (A.1)$$

This can be simplified as

$$\ln \left[\exp \left(\frac{E_f - E_0}{V_{th}} \right) + 1 \right] \approx \exp \left(\frac{E_f - E_0}{V_{th}} \right), \quad (A.2)$$

Therefore, we have

$$\frac{n_s}{DV_{th}} = \exp \left(\frac{E_f - E_0}{V_{th}} \right), \quad (A.3)$$

$$V_{th} \ln \left(\frac{n_s}{DV_{th}} \right) = E_f - E_0, \quad (A.4)$$

From Eq. (A.4), E_f can be written as

$$E_f = E_0 + V_{th} \ln \left(\frac{n_s}{DV_{th}} \right), \quad (A.5)$$

Substituting for E_0 from the follow expression

$$E_0 = \gamma_0 n_s^{2/3}, \quad (A.6)$$

gives

Appendix

$$E_f = \gamma_0 n_s^{2/3} + V_{th} \ln \left(\frac{n_s}{DV_{th}} \right), \quad (A.7)$$

$$E_f = \gamma_0 n_s^{2/3} + V_{th} \ln(n_s) - \ln(DV_{th}), \quad (A.8)$$

Replacing n_s in Eq. (A.8) by

$$n_s = \frac{\varepsilon}{q_d} (V_{g0} - E_f) \quad (A.9)$$

We have

$$E_f = \gamma_0 \left(\frac{\varepsilon}{q_d} (V_{g0} - E_f) \right)^{2/3} + V_{th} \ln \left(\frac{\varepsilon}{q_d} (V_{g0} - E_f) \right) - \ln(DV_{th}), \quad (A.10)$$

$$E_f = \gamma_0 \left(\frac{\varepsilon}{q_d} \right)^{2/3} (V_{g0})^{2/3} \left(1 - \frac{E_f}{V_{g0}} \right)^{2/3} + V_{th} \ln \left(\frac{\varepsilon}{q_d} (V_{g0} - E_f) \right) - V_{th} \ln(DV_{th}), \quad (A.11)$$

$$E_f = \gamma_0 \left(\frac{\varepsilon}{q_d} \right)^{2/3} (V_{g0})^{2/3} \left(1 - \frac{E_f}{V_{g0}} \right)^{2/3} + V_{th} \ln \left(\frac{\varepsilon}{q_d} V_{g0} \left(1 - \frac{E_f}{V_{g0}} \right) \right) - V_{th} \ln(DV_{th}), \quad (A.12)$$

$$E_f = \gamma_0 \left(\frac{\varepsilon}{q_d} \right)^{2/3} (V_{g0})^{2/3} \left(1 - \frac{E_f}{V_{g0}} \right)^{2/3} + V_{th} \ln \frac{\varepsilon V_{g0}}{q_d} + V_{th} \ln \left(1 - \frac{E_f}{V_{g0}} \right) - V_{th} \ln(DV_{th}), \quad (A.13)$$

$$E_f = \gamma_0 \left(\frac{\varepsilon}{q_d} \right)^{2/3} (V_{g0})^{2/3} \left(1 - \frac{2}{3} \frac{E_f}{V_{g0}} \right) + V_{th} \ln \frac{\varepsilon V_{g0}}{q_d} - V_{th} \frac{E_f}{V_{g0}} - V_{th} \ln(DV_{th}), \quad (A.14)$$

We can simplify Eq. (A.14) as

Appendix

$$\frac{V_{g0}}{V_{g0}} E_f + \frac{2}{3} \gamma_0 \left(\frac{\varepsilon}{q d} \right)^{2/3} (V_{g0})^{2/3} + V_{th} \frac{E_f}{V_{g0}} = \gamma_0 \left(\frac{\varepsilon}{q d} \right)^{2/3} (V_{g0})^{2/3} + V_{th} \ln \frac{\varepsilon V_{g0}}{q d} - V_{th} \ln(DV_{th}), \quad (A.15)$$

Thus, E_f can be expressed as

$$E_f = V_{g0} \frac{\gamma_0 \left(\frac{\varepsilon}{q d} \right)^{2/3} (V_{g0})^{2/3} + V_{th} \ln \frac{\varepsilon V_{g0}}{q d} - V_{th} \ln(DV_{th})}{V_{g0} + \frac{2}{3} \gamma_0 \left(\frac{\varepsilon}{q d} \right)^{2/3} (V_{g0})^{2/3} + V_{th}} \quad (A.16)$$

The gate capacitance is given by

$$C_g = \frac{\varepsilon}{d} \quad (A.17)$$

Substituting for C_g into Eq. (A.16) gives

$$E_f = V_{g0} \frac{\gamma_0 \left(\frac{C_g V_{g0}}{q} \right)^{2/3} + V_{th} \ln \left(\frac{C_g V_{g0}}{q D V_{th}} \right)}{V_{g0} + V_{th} + \frac{2}{3} \gamma_0 \left(\frac{C_g V_{g0}}{q} \right)^{2/3}}, \quad (A.18)$$

When the gate depletion and channel depletion overlap to give a fully depleted barrier layer, the carrier density is given by

$$n_s = \frac{\varepsilon}{q d} (V_{g0} - E_f), \quad (A.19)$$

Substituting Eq. (A.17) and (A.18) into Eq. (A.19) we have

$$n_s = \frac{C_g}{q} (V_{g0} - E_f) = \frac{C_g V_{g0}}{q} - \frac{C_g E_f}{q}, \quad (A.20)$$

$$n_s = \frac{C_g V_{g0}}{q} - \frac{C_g V_{g0}}{q} \frac{V_{th} \ln(\beta V_{g0}) + \gamma_0 \left(\frac{C_g V_{g0}}{q} \right)^{2/3}}{V_{g0} + V_{th} + \frac{2}{3} \gamma_0 \left(\frac{C_g V_{g0}}{q} \right)^{2/3}}, \quad (A.21)$$

where $\beta = \frac{C_g}{q D V_{th}}$.

Appendix

$$n_s = \frac{C_g V_{g0}}{q} \frac{V_{g0} + V_{th} (1 - \ln(\beta V_{g0})) - \frac{\gamma_0}{3} \left(\frac{C_g V_{g0}}{q} \right)^{2/3}}{V_{g0} + V_{th} + \frac{2}{3} \gamma_0 \left(\frac{C_g V_{g0}}{q} \right)^{2/3}}, \quad (\text{A.22})$$

The unified expression for n_s is expressed as

$$n_s = \frac{2 V_{th} (C_g / q) \ln \{ 1 + \exp (V_{g0} / 2 V_{th}) \}}{1/H(V_{g0}) + (C_g / qD) \exp (-V_{g0} / 2 V_{th})}, \quad (\text{A.23})$$

The function $H(V_{g0})$ in the denominator, which simulates the nonlinear behaviour in the above threshold region, is given as

$$H(V_{g0}) = \frac{V_{g0} + V_{th} [1 - \ln(\beta V_{g0n})] - \frac{\gamma_0}{3} \left(\frac{C_g V_{g0}}{q} \right)^{2/3}}{V_{g0} \left(1 + \frac{V_{th}}{V_{g0d}} \right) + \frac{2\gamma_0}{3} \left(\frac{C_g V_{g0}}{q} \right)^{2/3}}. \quad (\text{A.24})$$

Appendix

B) ATLAS model for simulation

```
# (c) Silvaco Inc., 2013
go atlas

# Sweep increment
set vstart = 0
set vstop = 20
set vinc = .5

mesh width=100

# x plane meshing
x.m l=0.0 s=0.25
x.m l=0.05 s=0.25
x.m l=0.1 s=0.25
x.m l=0.35 s=0.15
x.m l=0.55 s=0.15
x.m l=2.8 s=0.15
x.m l=2.85 s=0.25
x.m l=2.9 s=0.25

# y plane meshing
y.m l=0 s=0.25
y.m l=0.02 s=0.001
y.m l=0.029 s=0.001
y.m l=0.032 s=0.005
y.m l=0.04 s=0.5
y.m l=0.100 s=0.1
y.m l=0.7 s=1

#-----Region-----

region num=1 x.min=0 x.max=2.9 y.min=0.020 y.max=0.029
mat=AlGaIn x.comp=0.35
region num=2 x.min=0 x.max=2.9 y.min=0.029 y.max=0.032
mat=AlGaIn x.comp=0.35
region num=3 x.min=0 x.max=2.9 y.min=0.00 y.max=0.02
mat=oxide
region num=4 x.min=0 x.max=2.9 y.min=0.032 y.max=0.20 mat=GaN
region num=5 x.min=0 x.max=2.9 y.min=0.20 y.max=0.70 mat=GaN
substrate
```

Appendix

```
#-----Electrod-----

elec num=1 name=source  x.min=0      x.max=0.05  y.min=0.02
y.max=0.04
elec num=2 name=drain   x.min=2.85  x.max=2.90  y.min=0.02
y.max=0.04
elec num=3 name=gate    x.min=0.25  x.max=2.60  y.min=0.00
y.max=0.02
elec num=4 substrate

#-----Doping-----

doping      uniform y.min=0.020 y.max=0.029 n.type conc=1.e19
doping      uniform y.min=0.029 y.max=0.032 n.type conc=1.e16
doping      uniform y.min=0.032 y.max=0.20  n.type conc=2.e16

doping      uniform x.min=0.0  x.max=0.05 y.min=0.02
y.max=0.035 n.type conc=1.e20
doping      uniform x.min=2.85 x.max=2.90 y.min=0.02
y.max=0.035 n.type conc=1.e20

#-----Contact-----

contact name=gate    work=5
contact name=source  work=3.93
contact name=drain   work=3.93

models print srh
mobility albrct.n
model polarization calc.strain polar.scale=1

output con.band val.band charge  polar.charge band.par
method gummel  newton itlim=20 trap  maxtrap=20
vsatmod.inc=0.01  carriers=1 elect #carriers=2
#method newton trap maxtrap=20

solve init
save outf=IdVg_0.str

solve vdrain=5
solve name=gate vfinal=-5 vstep=-0.5
log outf=IdVgX25-01_0.log
solve name=gate vfinal=2.0 vstep=0.5 ac freq=1e6
```

Appendix



```
log off
```

```
solve vdrain=7
solve name=gate vfinal=-5 vstep=-0.5
log outf=IdVgX25-01_0.log
solve name=gate vfinal=2.0 vstep=0.5 ac freq=1e6
log off
```

```
solve init
save outf=IdVd_0.str
```

```
solve init
solve vgate=-2
log outf=IdVd_1.log
solve name=drain vdrain=$vstart vfinal=$vstop vstep=$vinc
log off
```

```
solve init
solve vgate=-1
log outf=IdVd_2.log
solve name=drain vdrain=$vstart vfinal=$vstop vstep=$vinc
log off
```

```
solve init
solve vgate=0
log outf=IdVd_3.log
solve name=drain vdrain=$vstart vfinal=$vstop vstep=$vinc
log off
```

```
solve init
solve vgate=1
log outf=IdVd_4.log
solve name=drain vdrain=$vstart vfinal=$vstop vstep=$vinc
log off
```

```
solve init
solve vgate=2
log outf=IdVd_5.log
solve name=drain vdrain=$vstart vfinal=$vstop vstep=$vinc
log off
```

```
quit
```

Appendix



C) Abbreviations

HEMT	H igh E lectron M obility T ransistor
2DEG	T wo D imensional E lectron G as
GaN	G allium N itride
AlN	A luminium N itride
AlGaN	A luminium G allium N itride
AlGaAs	A luminium G allium A rsenide
InGaN	I ndium G allium N itride
InGaAs	I ndium G allium A rsenide
MOCVD	M etal O rganic C hemical V apour D eposition
FET	F ield E ffect T ransistor
MOSFET	M etal- O xide-Semiconductor F ield E ffect T ransistor
JFET	J unction F ield E ffect T ransistor
TCAD	T echnology C AD
CAD	C omputer-Aided D esign
SCE	S hort C hannel E ffect parameter
SHE	S elf- H eating E ffect

Appendix



D) Physical constants

Constant Name	Symbol	Constant Value (units)
Plank's constant	h	$6.626 \times 10^{-34} \text{ J.s}$
Reduced Planck's constant	\hbar	$1.055 \times 10^{-34} \text{ J.s}$
Speed of light	c	$2.997 \times 10^8 \text{ m/s}$
Charge of electron	e	$1.602 \times 10^{-19} \text{ C}$
Mass of electron	m_e	$9.109 \times 10^{-31} \text{ K}$

Appendix



E) Symbols

Symbol	Description
μ	Mobility
μ_0	Low-field mobility
ε	Dielectric constant
E_g	Bandgap
E_b	Breakdown field
T_{max}	Maximum temperature
X	Mole fraction
b	Bandgap bowing parameter
q	Electron charge
E_C	Conduction band energy
E_V	Valance band energy
ΔE_g	Energy gap difference
ΔE_C	Conduction band offset
ΔE_V	Valance band offset
E_f	Fermi-level position in non-equilibrium state
D	Two-dimensional density of states
d	Thickness of barrier layer

Appendix



ξ	Electric field
c	Speed of light
h	Plank's constant
\hbar	Reduced Plank's constant
E_0	First sub-band energy level
E_1	Second sub-band energy level
P_{pz}	Piezoelectric polarization
P_{sp}	Spontaneous polarization
P_{total}	The total polarization
V_{th}	Threshold voltage
V_{off}	Cut-off voltage
n_s	Sheet carrier density in the 2DEG
L	Device length
W	Device width
V_s	Applied source voltage
V_g	Applied gate voltage
V_d	Applied drain voltage
V_{sat}	Saturation voltage
ϕ_M	Metal Schottky-barrier height
∇^2	Laplacian operator
φ	Electric potential

Appendix



ρ	The charge density
ψ_s	The surface-potential
m	The mass of the particle
J_{drift}	The drift current density
m_l	The longitudinal effective mass
V_{20}	Conduction band bending in neutral state
V_2	Conduction band bending in non-equilibrium state
δ_1	Conduction band and Fermi level difference
φ_{eff}	The effective Schottky barrier height
n_s	The charge carrier concentrations at the source
n_D	The charge carrier concentrations at the drain
C_g	The gate capacitance
d_1	Depletion region in the small bandgap semiconductor
d_2	Depletion region in the large bandgap semiconductor
d_s	Spacer layer width
Q_g	Total gate charge
R_{TH}	Thermal resistance
f_T	Cut-off frequency
f_{max}	The maximum oscillation frequency

Compact mole fraction-dependent modeling of I-V and C-V characteristics in $\text{Al}_x\text{Ga}_{1-x}\text{N}/\text{GaN}$ HEMTs

Nawel Kermas¹ · Bouaza Djellouli¹ · Driss Bouguenna² · Wondwosen Eshetu³ · Oana Moldovan³ · Benjamin Iñiguez³

Published online: 19 September 2017
© Springer Science+Business Media, LLC 2017

Abstract In this paper we present a compact mole fraction-dependent modeling of the I-V and C-V characteristics in $\text{Al}_x\text{Ga}_{1-x}\text{N}/\text{GaN}$ HEMTs using Atlas TCAD. The C-V characteristics of the $\text{Al}_x\text{Ga}_{1-x}\text{N}/\text{GaN}$ HEMTs are obtained using a charge conserving model. Based on this modeling, we have developed an analytical model for the threshold voltage, the carrier sheet density, the drain current, and the capacitance. The model covers all the different operating regimes of the device. The model includes the Al mole fraction of the barrier layer effects and was incorporated into our previously developed charge based on I-V and C-V characteristics, and we also simulated the device transconductance of $\text{Al}_x\text{Ga}_{1-x}\text{N}/\text{GaN}$ HEMTs. The results of the modeled I-V and C-V characteristics are in excellent agreement with the simulated data obtained by the Atlas TCAD simulator, which demonstrates the validity of the proposed model.

Keywords I-V and C-V characteristics · Transconductance · $\text{Al}_x\text{Ga}_{1-x}\text{N}/\text{GaN}$ · HEMTs · Mole fraction · Threshold voltage · Numerical simulation · Atlas TCAD simulator

1 Introduction

Recently, high performance $\text{Al}_x\text{Ga}_{1-x}\text{N}/\text{GaN}$ HEMT devices have been successfully used for various applications [1,2]. This is motivated by their potential in commercial and military applications, e.g., in the area of telecommunication systems, base stations market, as well as radar, W-CDMA mobile-phone applications [3,4], high temperature electronics, high power solid state switching, and hard radiation in space electronics. In fact, $\text{Al}_x\text{Ga}_{1-x}\text{N}/\text{GaN}$ HEMTs exploit the advantages of the wide band gap GaN materials, namely high mobility and high carriers density reached by the two dimensional electron gas (2-DEG) formed at the hetero-interface, which is the main principle of the HEMTs operation [5–7].

An analysis of the unified 2-DEG charge density n_s for all regimes of the device operation is a primary requirement for the development of a physics based compact model for these devices [8]. The models proposed in [9] and [10] presented the I-V and the C-V characteristics of $\text{Al}_x\text{Ga}_{1-x}\text{N}/\text{GaN}$ HEMTs based on the device physics. However, the effect of the mole fraction was not taken into consideration.

The maximum sheet charge caused by piezoelectric polarization can be reached by increasing the Al concentration of the barrier in HEMTs, but increasing it into a critical limit causes a strain relaxation and, therefore, reduction in piezoelectric polarization. For example, for a barrier thickness of 300 Å macroscopic strain relaxation was first observed for mole fraction of $x = 38\%$ [11]. The degree of relaxation increased linearly with increasing mole fraction for higher values of x .

In this work, we describe the target $\text{Al}_x\text{Ga}_{1-x}\text{N}/\text{GaN}$ HEMTs structure in Sect. 2. In Sect. 3 we derive the mole fraction dependent threshold voltage model and incorporate it in the I-V and C-V model presented in [10]. In Sect. 4, the

✉ Driss Bouguenna
dbouguenna.um@gmail.com

¹ Laboratory of Modelization and Calculation Methods,
Department of Electronics, University of Saida, 20000 Saida,
Algeria

² Laboratory of Materials, Applications and Environment,
Department of Technical Science ST, Faculty of Science and
Technology, University Mustapha Stambouli of Mascara,
29000 Mascara, Algeria

³ ETSE DEEEA, University Rovira i Virgili (URV), Avda.
Països Catalans 26, 43007 Tarragona, Spain